

NEDO-22139  
DRF E21-0065—  
82NED060  
Class I  
May 1982

CORE SPRAY SPARGER CRACK ANALYSIS  
AT  
PEACH BOTTOM ATOMIC POWER STATION  
UNIT 2

Approved:

*R. J. Brandon*  
R. J. Brandon, Manager  
Nuclear Services Engineering  
Operation

Approved:

*E. Kiss*  
E. Kiss, Manager  
Plant Materials and  
Mechanics Section  
Nuclear Power Systems  
Engineering Department

Approved:

*R. L. Gridley* *fn*  
R. L. Gridley, Manager  
Fuel and Services Licensing  
Safety and Licensing Operation

8206100183 820604  
PDR ADOCK 05000277  
P PDR

NUCLEAR POWER SYSTEMS DIVISION • GENERAL ELECTRIC COMPANY  
SAN JOSE, CALIFORNIA 95125

GENERAL  ELECTRIC

IMPORTANT NOTICE REGARDING  
CONTENTS OF THIS REPORT  
PLEASE READ CAREFULLY

This report was prepared by General Electric solely for Philadelphia Electric Company (PECo) for PECo's use with the U.S. Nuclear Regulatory Commission (USNRC) for the Peach Bottom Atomic Power Station Unit 2. The information contained in this report is believed by General Electric to be an accurate and true representation of the facts known, obtained or provided to General Electric at the time this report was prepared.

The only undertakings of the General Electric Company respecting information in this document are contained in the General Electric Company Proposal No. 424-TY727-HE2 ("Core Spray Sparger Crack Analysis for Philadelphia Electric Co., Peach Bottom Atomic Power Station Unit 2", dated April 1982), and PECo P.O. No. PB306903, Change Order No. 3. The use of this information except as defined by said contract or for any purpose other than that for which it is intended, is not authorized; and with respect to any such unauthorized use, neither General Electric Company nor any of the contributors to this document makes any representation or warranty (express or implied) as to the completeness, accuracy or usefulness of the information contained in this document or that such use of such information may not infringe privately owned rights; nor do they assume any responsibility for liability of damage of any kind which may result from such use of such information.

## CONTENTS

	<u>Page</u>
1. INTRODUCTION AND SUMMARY	1-1
1.1 Structural	1-1
1.2 Lost Parts	1-1
1.3 Effect on LOCA Analysis	1-1
1.4 Reference	
2. CORE SPRAY SPARGER STRUCTURAL INTEGRITY	2-1
2.1 Sparger Configuration	2-1
2.2 Fabrication Sequence	2-2
2.3 Installation Sequence	2-3
2.4 Performance History	2-3
2.5 Potential Sources of Stress	2-3
2.5.1 Fabrication Stresses	2-7
2.5.2 Installation Stresses	2-9
2.5.3 Stresses During Normal Operation	2-9
2.5.4 Stresses During Core Spray Injection	2-12
2.6 Materials Aspects of Cracking	2-12
2.6.1 Potential Causes of Cracking	
2.6.2 Effects of Cold Work on IGSCC of Stainless Steel	2-14
2.6.3 Conclusions of Sparger Cracking	2-16
2.7 Crack Arrest Assessment	2-17
2.7.1 Stresses Due to Bracket Restraint	2-17
2.7.2 Fabrication Residual Stress	2-19
2.7.3 Conclusions on Crack Arrest	2-19
2.8 Structural Integrity with Cracks	2-20
2.9 References	
3. LOST PARTS ANALYSIS	3-1
3.1 Introduction	3-1
3.2 Loose Piece Description	3-1
3.3 Safety Concern	3-1
3.4 Safety Evaluation	3-1
3.4.1 General Description	3-2
3.4.2 Postulated Loose Pieces	3-5
3.5 Conclusion	3-6
3.6 Reference	
4. LOSS-OF-COOLANT ACCIDENT ANALYSIS WITH NONUNIFORM SPRAY IN ONE SPRAY SPARGER	4-1
4.1 Introduction	4-1
4.2 Input to the LOCA Analysis	4-3
4.3 Sensitivity of LOCA Analysis to Non Uniform Spray	4-4
4.4 Analysis Results	4-5
4.5 Conclusions	4-5
4.6 References	

CONTENTS (Continued)

Page

APPENDICES

A. STRUCTURAL ANALYSIS OF THE PEACH BOTTOM 2 CORE SPRAY SPARGER	A-1
B. SPARGER TEMPERATURE CALCULATIONS	B-1
C. FLOW VELOCITY CALCULATIONS	C-1

## ILLUSTRATIONS

<u>Figure</u>	<u>Title</u>	<u>Page</u>
2-1	Core Spray Sparger - Elevation View	2-22
2-2	Core Spray Sparger - Plan View	2-23
2-3	Sparger to Shroud Attachment Method	2-24
2-4	Sparger Nozzles	2-25
2-5	Sparger Support Method	2-26
2-6	Pipe Bending Method	2-27
2-7	Sequence of Events Leading to the Residual Stress Distribution	2-28
2-8	Bilinear Stress-Strain Curves for Type-304 Stainless Steel	2-29
2-9	Stress and Strain Distribution in the Pipe Under Applied Moment	2-30
2-10	Moment Versus Outer Fiber Strain	2-31
2-11	Resultant Residual Stress Distribution After Fabrication	2-32
2-12	Postulated Installation Stresses	2-33
2-13	Effects of Cold Work on IGSCC of Type-304 Stainless Steel	2-34
2-14	Effects of Cold Work on IGSCC	2-35
2-15	Effects of Cold Work on IGSCC	2-36
2-16	Effects of Cold Work on IGSCC	2-37
2-17	Stress Versus Cold Work	2-38
2-18	Compliance Change, Cracked Pipe	2-39
2-19	Assumed Stress Distribution on the Crack Face	2-40
3-1	Reactor Vessel	3-7
3-2	Steam Separator	3-8

## ILLUSTRATIONS (Continued)

<u>Figure</u>	<u>Title</u>	<u>Page</u>
3-3	Largest Piece That Can Fit Through the Turning Vane with the Long Dimension in a Horizontal Plane	3-9
3-4	Orificed Fuel Support	3-10
3-5	Fuel Assemblies and Control Rod Module	3-11
A-1	Flow Paths	A-6

## 1. INTRODUCTION AND SUMMARY

One of the scheduled tasks during the Reload 5 refueling and maintenance outage in March 1982 at the Peach Bottom-2 Atomic Power Station was the performance of a visual inspection of the core spray spargers using underwater television cameras. This inspection was conducted as required by IE Bulletin No. 80-13 (Reference 1-1).

During this inspection, a 180 degree, circumferentially oriented crack in the header to T-box weld heat-affected zone of the lower core spray sparger was found.

General Electric reviewed this condition and is providing justification for continued operation without the installation of additional hardware by addressing the following items.

### 1.1 STRUCTURAL

A structural analysis is presented in Section 2, which describes the potential sources of stress in the spargers resulting from fabrication, installation, normal operation, and operation during postulated loss-of-coolant accidents (LOCAs). Potential causes of cracking are also discussed, and it is concluded that the structural integrity of the sparger will be maintained for all conditions of operation.

### 1.2 LOST PARTS

If breakage of the sparger is postulated, the lost parts evaluation presented in Section 3 concludes that the potential for unacceptable flow blockage of a fuel assembly, or for unacceptable control rod interference, is essentially zero. It is also shown that loose pieces are not expected to cause damage to the other reactor pressure vessel internals.

### 1.3 EFFECT ON LOCA ANALYSIS

Section 4 presents the results of LOCA analyses assuming no core spray heat transfer credit from the cracked sparger in the calculations. This corresponds

to a postulated worst-case core spray sparger break in which the water flowing through the cracked sparger does not spray uniformly onto the core. The resulting increase in peak cladding temperature (PCT) was calculated at the request of Philadelphia Electric Company assuming no clamping repair of the sparger is implemented. The analysis is considered to be conservative by General Electric based on the calculations which support the continued structural integrity of the sparger and large conservatisms in the LOCA analysis as demonstrated by large-scale tests. The analysis nevertheless justifies continued operation with no change in MAPLHGR limits.

#### 1.4 REFERENCE

1-1 USNRC Cracking in Core Spray Spargers, IE Bulletin 80-13.

## 2. CORE SPRAY SPARGER STRUCTURAL INTEGRITY

### 2.1 SPARGER CONFIGURATION

The core spray sparger configuration is shown in Figure 2-1 through 2-5.

The spargers are mounted in the upper shroud, as shown in Figure 2-1. Vertical spacing is 12 inches between header pipe centerlines. The upper sparger has bottom-mounted nozzles and the lower sparger has top-mounted elbows. The plan view (Figure 2-2) shows that the spargers are asymmetric. The shorter header pipe has an arc length of  $82.5^\circ$ , and the longer header pipe has an arc length of  $97.5^\circ$ . The T-boxes for the spargers are located  $\pm 7.5^\circ$  from the vessel  $0^\circ$  and  $180^\circ$  azimuths.

Figure 2-3 shows the attachment of the T-box to the shroud. The T-box is a 6-in. Schedule 40 section of pipe with an end plate toward the vessel centerline. The 6-in. pipe extends through the shroud wall and is butt-welded to external piping. The T-box pipe is attached to the shroud by the seal ring with the attachment welds to the 6-in. pipe and the exterior surface of the shroud wall.

The sparger flow nozzles are depicted in Figure 2-4. The Peach Bottom-2 upper core spray sparger header uses 1-in. shielded VNC nozzles alternating with SPRACO 3101 nozzles. The lower header uses 1-in. shielded VNC nozzles alternating with 3/4-in. open elbows.

The  $97.5^\circ$  header pipe is supported at three locations and the  $82.5^\circ$  header pipe is supported at two locations. Figure 2-5 shows the support arrangement at locations other than at T-box locations. The brackets are 3/8-in. thick and are welded to the shroud. The pipe-to-bracket mating surfaces are not welded to allow circumferential relative motion between the header pipe and the shroud during a core spray injection of cold water into a system at reactor operating temperature. The header pipe is 4-in. Schedule 40 Type-304 stainless steel.

The street elbows, 90° elbows, half-couplings and the close nipples (used to connect the elbows and orifice the elbows) are all Type-304 stainless steel.

## 2.2 FABRICATION SEQUENCE

Fabrication records show that the Peach Bottom-2 spargers were fabricated as follows:

1. The pipe was bent using a four-roll bending process as shown in Figure 2-6. The rollers have 2-1/4 in. radius grooves, and rollers 3 and 4 are adjustable to accommodate the pipe size and to bend the pipe to the required radius. In this case, the design radius is  $R = 105.75$  inches. The maximum strain in the pipe is calculated to be 2.1%.
2. After the pipe is bent to the proper radius, it is placed in the shroud to verify that the pipe fits the shroud as-built conditions. During this fit-up process, the T-box 6-in. pipe is marked for drilling the header pipe holes.
3. After removing the pipe from the shroud, the headers are welded to the T-box.
4. The holes for each nozzle are drilled in the header pipes.
5. Stainless steel half-couplings are bevel welded at each nozzle opening.
6. The elbows are screwed into the assembly and roughly aimed.

## 2.3 INSTALLATION SEQUENCE

The sparger is installed in the shroud in the following manner:

1. The brackets are welded to the shroud, thereby positioning and holding the spargers. It also includes attaching the T-box to the shroud by welding the seal ring to the T-box and the shroud. It is assumed that, because of interference between sparger ends, one or more of the spargers would be cold sprung during installation. This operation was not addressed in the fabrication records.
2. The next operation was to aim the nozzles as required by the sparger drawing.
3. The elbows were then tack welded to assure that the threaded connections remain intact.

## 2.4 PERFORMANCE HISTORY

Peach Bottom-2 Station first went critical in September 1973. There have been no inadvertent core spray injections. Peach Bottom-2 does flush the core spray spargers during refueling outages. Water is pumped from condensate storage at a temperature of approximately 70°F. The maximum  $\Delta T$  that has occurred is 120°F. This  $\Delta T$  is sufficiently low that fatigue is not a concern.

## 2.5 POTENTIAL SOURCES OF STRESS

The potential sources of stress in the core spray sparger which could result from fabrication, installation, normal plant operation, and operation of the core spray system during postulated loss-of-coolant accidents are presented in this section.

### 2.5.1 Fabrication Stresses

Residual stresses are developed when an initially straight pipe is subjected to a moment sufficient to cause yielding and later unloaded, as would occur

during the fabrication of the core spray spargers. The fabrication operation is idealized in Figure 2-7. The steps involved in the calculation of the residual stresses are:

1. Determine the moment-curvature curve for the pipe assuming simple beam theory.
2. Calculate the applied moment,  $M_t$ , corresponding to the final unloaded radius of curvature. Determine the stress distribution associated with this moment.
3. Calculate the elastic stress distribution corresponding to the applied moment ( $-M_t$ ) to describe the unloading.
4. Determine the residual stress in the pipe which is the algebraic sum of the elastic-plastic stresses due to  $M_t$  and the elastic stresses due to ( $-M_t$ ).

In calculating the moment-curvature curve for the pipe, thin shell theory was applied and a representative bilinear stress-strain curve (Figure 2-8) was used.

As shown in Figure 2-9, the strain varies linearly through the section, while the stress follows the bilinear curve for angles greater than  $\theta$ .

The applied moment ( $M_t$ ) is given by:

$$M_t = 2 \int_0^{\theta} (E \epsilon_o \sin \phi) (a \sin \phi) (2at d\phi) \\ + 2 \int_{\theta}^{\pi/2} \{ (\epsilon_o \sin \phi - \epsilon_y) E_t + E \epsilon_y \} (a \sin \phi) (2at d\phi) \quad (2-1)$$

where

- $\epsilon_o$  =  $a/R$  = outside strain  
 $a$  = radius of pipe

$R$  = radius of curvature

$\epsilon_y, \sigma_y$  = yield strain and stress

$E, E_t$  = elastic and plastic modulus

The first term in Equation 2-1 is the contribution from the elastic part of the stress distribution, and the second term corresponds to the plastic portion of the stress distribution.

After integration and rearrangement, Equation 2-1 becomes:

$$M_t = M_o \left[ \frac{(1 - E_t/E)}{\pi} \left\{ \frac{(2\theta - \sin 2\theta)}{\sin \theta} + 4 \cos \theta \right\} + \frac{E_t}{E \sin \theta} \right]$$

$$\text{and } \sin \theta = \epsilon_y / \epsilon_o = \frac{\epsilon_y R}{a}$$

$M_o$  = moment corresponding to the first onset of yielding on the outside surface =  $\sigma_y \pi a^2 t$ .

Clearly, for fully elastic behavior,  $\theta = \pi/2$ , and  $M_t = M_o$ .

Figure 2-10 shows the variation of the applied moment with the outside fiber strain and also the bend radius  $R$ . As shown in the figure, in order to get a final radius of 105.75 inches, the outer fiber strain during bending is 2.33%. The corresponding moment is  $1.43 \sigma_y \pi a^2 t$ .

The residual stress distribution can now be determined by combining the elastic stress corresponding to  $(-M_t)$  and the elastic-plastic stress during bending. Figure 2-11 shows the resulting stress distribution. A correction for the thin shell theory assumption is included in the results.

Figure 2-11 shows that the pipe is subjected to high residual stresses (approaching the yield stress), and that the stress distribution varies around the circumference of the pipe. In particular, it shows tensile stresses

on the surface facing the centerline of the vessel. It should be noted that the actual stresses could be higher due to local yielding at locations where Hertzian contact stresses (between the roller and the pipe) occur during bending. Since this would be most likely to occur on the surface of the sparger facing the center of curvature, higher stresses could be expected at this location.

The residual stresses shown here were calculated for room temperature conditions. However, for reactor operating temperatures  $\approx 550^\circ\text{F}$ , the residual stresses are expected to relax to the yield value at that temperature (18.8 ksi at  $550^\circ\text{F}$ ).

Knowing the applied stress, one can calculate the minimum crack size that could propagate intergranular stress corrosion cracking (IGSCC) under sustained load. Using the following worst-case assumptions:

1.  $K_{\text{IGSCC}} = 6 \text{ ksi } \sqrt{\text{in.}}$ ,
2. A long continuous crack,
3. Sustained stress up to yield = 18.8 ksi,

the minimum crack depth for crack growth is given by:

$$K_{\text{IGSCC}} = 1.12\sigma \sqrt{\pi a_{\text{min}}}$$

or

$$a_{\text{min}} = \frac{1}{\pi} \left( \frac{6}{18.8 \times 1.12} \right)^2 = 0.026 \text{ inches}$$

This shows that under worst-case conditions, a 26-mil crack could propagate due to stress corrosion cracking.

The conclusions from the evaluation of fabrication stresses presented in this section are summarized below:

1. Stresses due to fabrication could be significant and would exist throughout plant operation.
2. A possible synergistic combination of adverse metallurgical conditions (e.g., sensitization, cold work) and high residual stresses may explain the observed cracking.
3. Since the stresses change sign (become compressive) around the circumference, a crack that initiates in the tensile region can be expected to arrest in the compressive regions.

#### 2.5.2 Installation Stresses

Stresses sufficient and necessary to cause initiation and propagation of cracks by intergranular stress corrosion cracking (IGSCC) can be identified by postulating certain installation variables. Figure 2-12 shows two cases which might be postulated.

In Case 1, it is postulated that differential weld shrinkage occurred during welding of the header pipes to the T-box. The outer bracket would provide a force to cause the header to contact the shroud wall. For simplicity, the arm is assumed to have an arc length of 90°. A 1/8-in. differential weld shrinkage is assumed. The deflection resulting at the header end would be approximately:

$$\frac{1/8}{4.5} = \frac{\Delta}{105.75} ; \Delta = 2.94 \text{ inch .}$$

Then, from Reference 2-1, Table 13.4, Case 1:

$$\Delta = \frac{WR^3}{4EI} (2\phi - \sin 2\phi) , \quad \text{where } \phi = 90^\circ .$$

Solving  $W = 648$  lb, assuming:

$$R = 105.75 \text{ in.}$$

$$E = 28.3 \times 10^6 \text{ ksi}$$

$$I = 7.23 \text{ in.}^4$$

Since  $M = WR$

$$\sigma = \frac{WRC}{I} = \frac{648 \times 105.75 \times 2.25}{7.23}$$

$$\sigma = 21300 \text{ psi}$$

$$\sigma \approx 21000 \text{ psi (elastic)}$$

For Case 2, it is assumed that  $R$  is incorrectly fabricated to a radius of 104.75 inches. It is further assumed that the vessel brackets cause a uniform moment on the pipe, thus increasing the radius to 105.75 inches.

The initial inner length is  $\pi/2 \times 102.5 = 161.01$ . After forming, the inner length is  $\pi/2 \times 103.5 = 162.58$ :

$$\text{Strain} = \epsilon = \frac{\Delta l_{\text{inner}}}{l_{\text{inner}}} = \frac{162.58 - 161.01}{161.01} = 0.010$$

$$= 1.0\%$$

Using a stress strain curve for Type-304 stainless steel, the resulting secondary stress is found to be 38,000 psi for 1.0% strain.

For the postulated conditions, these two examples show that high deflection limited tensile stresses can occur during installation. These stresses have not been confirmed. In addition, the welding process produces residual stresses in the pipe near the weld. The magnitude and sign of the stresses vary with distance from the weld and depend on pipe size and welding speed. These stresses are likely to vary circumferentially. Maximum tensile residual stresses in the range of 18 ksi to 40 ksi have been measured in weld pipe tests (Reference 2-2).

Installation stresses considered in conjunction with the material consideration discussed later (Section 2.6) may explain the cracks that have been observed. It should be emphasized that the installation stresses postulated above are all deflection-limited secondary stresses that will relax to the elevated temperature yield strength of the material during normal plant operation.

### 2.5.3 Stresses During Normal Operation

All identified stresses during normal operation were found to be negligible. Loadings that were considered include impingement loads (i.e., flow past the spargers), seismic, pressure, thermal mismatch, stagnant line top-to-bottom temperature gradients, stagnant line throughwall temperature gradients and weight. Stress calculations are given in Appendices A and B.

It should be noted that, during normal plant operation, there is no core spray flow. The sparger  $\Delta P = 0$  and  $\Delta T = 0$ . Impingement loads are 4.45 lbf/in. on the header arm, resulting in negligible stresses. Weight of the spargers and water is only 1.36 lbf/in., again resulting in negligible stresses. Stagnant line temperature gradient calculations are not provided since the maximum  $\Delta T$  for top-to-bottom gradients and for through wall gradients were found to be less than  $10^\circ\text{F}$ , which would result in insignificant stresses. It should be noted, however, that the  $\Delta T$  for core spray injection is addressed in Section 2.5.4.

It is concluded that the normal operating loadings do not result in stresses that could explain the crack observed in the Peach Bottom-2 core spray sparger.

### 2.5.4 Stresses During Core Spray Injection

Stresses during core spray injection are the design stresses for the spargers. Design loadings include all those discussed in Section 2.5.3 plus those that occur because the system is no longer a passive system. The pressure differential in the sparger at rated flow is approximately 25 psid. The hoop stress in the pipe is about 210 psi. Impingement load stresses are less during spray injection than during normal operation. Thermal stresses due to the throughwall temperature gradient are high and are known to be:

$$= \frac{E \cdot \alpha \cdot \Delta T}{2(1 - \nu)}$$

These stresses are not a concern for one or a few cycles. The radius of the sparger shrinks when the sparger is cooled, resulting in secondary bending stresses of approximately 3000 psi. The axial stress in the pipe due to  $\Delta P$  and bracket friction is low--only 420 psi. Flow through the nozzles results in a torsional stress which is low--less than 100 psi. Weight stresses are negligible. Water hammer is not expected because the pipe is essentially an open pipe, and the nozzle opening areas are approximately equal to the pipe internal area, even for the short leg. However, water hammer is addressed in the following section.

#### 2.5.4.1 Water Hammer Loads

Water hammer loads as discussed herein are those loads associated with injection of core spray water into a core spray system, where the system piping downstream of the check valve in primary containment is assumed empty (or filled with steam) because of the draining of water from the spargers and/or the flashing of water to steam during depressurization prior to core spray injection.

For the purpose of maximizing injection loads, primarily on the core spray spargers, it is assumed that reactor pressure is essentially atmospheric (as for a large LOCA), enabling system flow to increase to runout controlled only by the injection valve-opening characteristic. Upon valve opening, the head (H) is available to accelerate the flow, but as the velocity increases, the acceleration head is reduced by friction and local losses. If  $L_e$  is the equivalent length of the pipe system, the final velocity  $V_f$  is given by application of the energy equation:

$$H = f \frac{L_e}{D} \frac{V_f^2}{2g}$$

The maximum velocity attainable is limited to that at system runout flow (8000 gpm), which produces a velocity of 55 ft/sec in the sparger (at the entrance to the long sparger arm to be more concise; the velocity at the ends is zero).

Actually, the velocity of the water first entering the sparger will be less than runout velocity because of the relatively slow opening characteristics of the injection valve. The injected water fills the pipe line between the injection valve and the sparger at a time prior to full valve opening and, therefore, before the final runout velocity is attained.

Assuming the maximum velocity attainable, the resulting momentum load in the sparger is:

$$P_m = \frac{V^2}{144 gv} = \frac{(55)^2}{144(32.2)(0.0160)} = 40.8 \text{ psi}$$

or

$$F_m = P_m A_p = 40.8(12.73) = 519 \text{ lb.}$$

where

$P_m$  = momentum pressure (psi);

$F_m$  = momentum load (lb);

$V$  = velocity (ft/sec);

$g$  = gravitational acceleration (32.2 ft/sec<sup>2</sup>);

$v$  = specific volume (0.0160 ft<sup>3</sup>/lb) (~80°F water); and

$A_p$  = pipe flow area (12.73 in.<sup>2</sup>) (4-in. Schedule 40 pipe).

If the end plates at the ends of the spargers were removed, it is obvious there would be no impact load. Now cap the ends and also plug the sparger nozzles. Again, there would be no water impact load because the trapped gas in the line acts as a surge tank.

The actual end condition of the spargers is somewhere in between these two extremes. It is much closer to the open end condition, except that there are several "ends" instead of one end, and they are located along the length of the sparger arms.

The exit flow area of the sparger nozzles is computed as follows:

	<u>Number</u>	<u>Area (in.<sup>2</sup>)</u>	<u>Total Area (in.<sup>2</sup>)</u>
1-in. VNC Nozzle	32	1.018	32.6
3101 Nozzle	33	0.307	<u>10.1</u>
Total Open Flow Area Per Sparger =			42.7

The exit flow area of the nozzles and elbows is actually 68% greater than the flow area of the two sparger arms ( $2 \times 12.73 = 25.46 \text{ in.}^2$ ).

An estimate of pressures induced in the sparger at the end of the filling time of the spargers and piping can be made by considering a sparger with only one open elbow located at the end of each arm. Steam would be pushed ahead of the oncoming front of water, exiting the sparger through the assumed single nozzle. The developed differential pressure to expel the steam would be approximately 7 psid. Adding all sparger elbows and nozzles to this logic clearly demonstrates that the sparger indeed behaves like an open-ended pipe, and conventional water hammer loads of any significant magnitude would not be present. Injection conditions at higher reactor pressure would clearly be bounded by the runout case presented here.

## 2.6 MATERIALS ASPECTS OF CRACKING

The potential causes of Peach Bottom-2 core spray sparger cracking are discussed in this section. A general discussion of the effects of cold work on the IGSCC susceptibility of Type-304 stainless steel is also presented.

### 2.6.1 Potential Causes of Cracking

The potential causes of core spray sparger cracking which are considered to be most probable are indicated in Table 2-1. The table addresses cracking near the heat-affected zone (HAZ) of the T-box to sparger arm weld, as well as cracking in the sparger arm remote from the weld. The crack in the Peach Bottom-2 core spray sparger is located within the HAZ of the weld. The evidence of each possible cause is also indicated.

Near the T-box, four possible causes of sparger cracking have been identified. First, sensitization by welding the sparger arms to the tee is supported by the patterns of cracking near the HAZ of this weld. IGSCC may result if stresses are sufficiently high in this area. Such cracking has been observed in piping incidents in the past.

Second, cold work inherent in arm forming followed by weld sensitization may increase the susceptibility of IGSCC in the spargers. As discussed below, sufficient cold work is present for enhancement of cracking tendencies.

Third, fatigue induced by thermal variations in the environment may be the cause of the sparger indications. However, the variations in temperature during operation of the reactor (10°F, see Section 2.5.3) are expected to be small. No evidence of a driving force for thermal fatigue has been identified.

Finally, fatigue resulting from flow-induced vibrations could be hypothesized. However, the natural frequencies of the sparger are high relative to any flow-induced excitation sources, and the sparger brackets restrain the amplitudes of any vibrations.

In the arms remote from the T-box by distances greater than 2 inches, welding cannot be considered a major influence on cracking. Sensitization may still be present if the original solution heat treatment was inadequate, either in temperature or quench rates. No direct evidence exists of this condition. Secondly, if cold work from arm bending were followed by local heating, a susceptible condition would more readily exist. Again, no direct evidence exists. Thirdly, surface cold work resulting from arm bending or straightening could hasten crack initiation and subsequent growth could occur from residual or installation stresses. No documentation exists to support this possible cause. Finally, fatigue by either of the sources cited above for the T-box area could induce cracking, although there is no confirmed source of fatigue loading.

The most probable cause of cracking adjacent to the T-box area is currently considered to be cold work followed by weld sensitization leading to IGSCC in a region of weld residual stress. Approximately 5% cold work could result from sparger arm fabrication and installation.

Stresses in excess of the yield stress may be present, and weld sensitization could occur during arm to T-box joining. Sufficient conditions for cracking may therefore be present.

### 2.6.2 Effects of Cold Work on IGSCC of Stainless Steel

The mechanisms of cold work enhanced cracking are complex but can be visualized through the illustration in Figure 2-13. In this illustration, factors influencing susceptibility to cracking are shown as increasing or decreasing susceptibility by lying to the left or right of the diagram, respectively.

Cold work serves to increase the material yield strength. This enhances susceptibility if stresses in the material result from imposed strains because the resulting stress state of the material would also be higher, consistent with the increased yield stress. If stresses are fixed as the result of imposed loads, susceptibility may decrease because the stress state of the hardened material is a lower fraction of the yield stress.

Cold work serves to promote chromium activity in the material matrix, which reduces susceptibility through the more rapid recovery of chromium-depleted regions. However, sufficient time at higher temperatures ( $>500^{\circ}\text{F}$ ) is necessary for the recovery phenomenon, and such thermal treatment was not practical for the spargers, nor deemed necessary.

The most significant influence of cold work is in the transformation of austenite to martensite phases through deformation. Martensite, if present in sufficient quantity, can assist in recrystallization of the material upon subsequent thermal treatment. The strain energy induced in the lattice promotes recrystallization. The result of recrystallization is migration of grain boundaries away from chromium depleted regions, with attendant benefits in reducing sensitization. However, the presence of martensite increases the tendency for carbide precipitation and local chromium depletion during subsequent weld sensitization. A wider HAZ can result from welding stainless steel with prior cold work-induced martensite. If sufficient cold work is

present, transgranular cracking can occur in oxygenated water environments with or without subsequent sensitization.

Environmental tests conducted on tensile, bent beam and pressurized tube specimens are illustrated in Figures 2-14 through 2-17 (which are based on information from References 2-3 and 2-4).

In Figure 2-14 it can be seen that the time to failure in 0.2 ppm  $O_2$  water for sensitized and cold-worked and sensitized material varies with stress. Specimens tested at cold-worked-plus-sensitized conditions (at higher stresses) produced failure times (by IGSCC) comparable to samples which contained no work prior to sensitization. Cold-worked samples without subsequent sensitization, tested at comparable stresses, did not fail. IGSCC failures could be induced at very high stresses in cold-work/no-sensitization samples, as illustrated in Figure 2-15.

If the data from Figures 2-14 and 2-15 are plotted on a basis normalized by the material yield strength, a more clear picture is formed of the results of deflection-induced stresses in stainless steel (Figure 2-16). Material cold worked to various levels and subsequently sensitized can undergo stress corrosion at substantially lower percentages of the material yield strength, with cracking as low as 80%  $\sigma_{ys}$  in quarter-hard stainless steel (furnace sensitized).

An equivalence must be established between plastic strain during sparger arm forming and the cold-work condition of the test specimens. The yield strengths of specimens receiving 5, 8, and 15% cold work are illustrated in Figure 2-17. The stress-strain curves for the same heat of material without prior cold work indicate the amount of plastic strain necessary to create a comparable yield stress to the uniformly cold-worked specimens. Thus, 2.1% plastic strain calculated for arm bending corresponds to approximately 1% cold work and stresses near yield may or may not result in cracking (data are insufficiently clear). The strain concentration from localized bending, if a factor of 4 is considered, would be comparable to 5% cold work. A reduction of the cracking threshold to 0.8  $\sigma_y$  and cracking under residual and installation stresses could occur.

### 2.6.3 Conclusions of Sparger Cracking

Core spray sparger cracking at the Peach Bottom-2 plant can be hypothesized by the influence of weld sensitization or prior sensitization of the arm material and subsequent cold work of the arms during forming and installation. Sources of stress for IGSCC are dependent on residual stresses from arm bending, weld residual stresses, and deflection during installation.

The principal factors suspected of causing cracking are considered to be highly variable from one plant to another. The absence of one or several key factors may explain the lack of reported indications in the majority of the BWR operating plants inspected to date (May 1982).

### 2.7 CRACK ARREST ASSESSMENT

In assessing the possibility of crack arrest, the following sources of stress are considered:

1. Stress due to pressure, mechanical loads and thermal gradients. These stresses have been shown to be negligible and are not considered in the crack growth assessment.
2. Stresses due to bracket restraint: these are displacement controlled (secondary) stresses and would be expected to relax as the crack propagates.
3. Residual stress due to fabrication: as the crack propagates into a region of compression, the stress intensity factor can be expected to decrease, thereby resulting in arrest.
4. Weld residual stress: weld residual stresses at the T-box - sparger welds would influence crack propagation. These stresses are likely to vary circumferentially and also relax as the cracks become larger.
5. Stresses due to vibration are assumed to be negligible.

In considering crack arrest, the stresses due to bracket restraint and the fabrication residual stress are significant and are evaluated in detail.

### 2.7.1 Stresses Due to Bracket Restraint

Stresses due to bracket restraint are governed by the applied displacement and the compliance of the pipe. Since the displacement is fixed, the compliance change with crack growth could lead to crack arrest. This is comparable to crack arrest in a bolt-loaded wedge-opening-loading (WOL) specimen in stress corrosion tests. Figure 2-18 shows the variation of compliance with crack length for a pipe subjected to bending. The compliance was determined using the relationship between the strain energy release rate  $G$  and the compliance change per unit area of crack extension  $dc/dA$  (Reference 2-5). For the cracks in the sparger,  $L/d$  is expected to be in the range of  $0 < L/D < 40$ . Figure 2-18 shows that, when more than 30% of the pipe is cracked, the compliance of the pipe increases by a factor of 10. Therefore, for the given initial displacement, the stress in the sparger and the applied stress intensity factor would decrease by a factor of 10 when more than 30% of the pipe circumference is cracked. Clearly, when the crack length exceeds this value, the restraint stresses become negligible and crack arrest is expected.

### 2.7.2 Fabrication Residual Stress

The residual stresses due to fabrication vary around the circumference, and a precise calculation of the stress intensity is not possible. Nevertheless, a conservative representation of the stress is used to calculate the stress intensity factor. The assumptions made are as follows:

1. The crack in the sparger is modeled as a through crack in an infinite plate.

2. It is assumed that the tensile stress ( $\sigma$ ) is uniform and is applied on the crack face over a length ( $2b$ ). (Later this will be conservatively taken as 25% of the circumference.)
3. The remaining portion of the crack is assumed to be subjected to a compressive stress, which is half the tensile stress (Figure 2-19).
4. The crack length ( $2a$ ) for which the combined stress intensity factor reduces to zero is calculated.

The stress intensity factor due to the tensile stress can be shown to be:

$$K_I^{\text{tension}} = \frac{2\sigma a}{\sqrt{\pi a}} \sin^{-1} \left( \frac{b}{a} \right)$$

The stress intensity factor due to the compressive stress  $\sigma/2$  is given by:

$$K_I^{\text{compression}} = \frac{-2(\sigma/2) a}{\sqrt{\pi a}} \left\{ \frac{\pi}{2} - \sin^{-1} \left( \frac{b}{a} \right) \right\}$$

Setting  $K_I^{\text{tens}} + K_I^{\text{comp}} = 0$ , we get

$$\sin^{-1} \left( \frac{b}{a} \right) = \frac{1}{2} \left\{ \frac{\pi}{2} - \sin^{-1} \left( \frac{b}{a} \right) \right\}$$

$$\text{or, } \sin^{-1} \left( \frac{b}{a} \right) = \frac{\pi}{6}$$

$$\text{or, } b = 0.5a$$

If we assume  $b = 25\%$  of the circumference is under tension  $\sigma_y$  and the remaining portion of the crack is under compressive stress (equal to half the tensile stress), the applied stress intensity factor becomes zero when the crack length is equal to 50% of the circumference. Thus, even under extremely conservative assumptions, crack arrest is expected.

### 2.7.3 Conclusions on Crack Arrest

Based on the above material, the following conclusions may be drawn:

1. Since the applied loading is predominantly displacement controlled, the stresses can be expected to relax as the cracks grow. Crack arrest is therefore expected.
2. The residual stresses due to fabrication vary from tension to compression. As the cracks propagate into regions of compressive stress, the K value reduces to zero. Even for extremely conservative assumptions, crack arrest can be shown for a 50% circumferential crack.
3. The above conclusions are valid as long as there is no stress cycling due to vibration (e.g., flow-induced vibration).

### 2.8 STRUCTURAL INTEGRITY WITH CRACKS

From the discussion of the potential stresses in the core spray sparger (Sections 2.5 and 2.6), it is concluded that only deflection limited secondary stresses approach 25% of the material yield strength (except for self equilibrating thermal stresses). If a 360° throughwall crack is postulated at any location on any sparger arm, the remaining stresses will not produce a failure at any other location on the sparger. The  $\Delta P$  stress and the stress resulting from an axial load in the pipe due to bracket friction are proportional to the cross-sectional area of the pipe. The load from  $\Delta P$  and friction was found to be <1000 lbs. Assuming a yield strength of 30,000 psi at core spray flow temperature, an area of less than 0.033 in.<sup>2</sup> is required to maintain continuity. This area is much less than the original pipe metal area of 3.17 in.<sup>2</sup>. The bending type stresses are all deflection limited secondary stresses. The discussion in Section 2.7 shows that cracks are expected to arrest, since the driving stress will be relieved. The bending loads may, however, in a worst case, cause an existing crack to open up by an additional 0.005 in., assuming the existing crack has progressed 360°. This is a geometry limited condition.

It is concluded that no loadings have been identified which could result in stresses that would cause the spargers to break during normal plant operation, transients, or postulated loss-of-coolant accidents.

## 2.9 REFERENCES

- 2-1. Hopkins, Design Analysis of Shafts and Beams, McGraw-Hill Book Company.
- 2-2. H. H. Klepfer, et al, "Investigation of Cause of Cracking in Austenitic Stainless Steel Piping," NEDO-21000-1, July 1978.
- 2-3. A. E. Pickett and R. G. Sim, "The Effect of Stress and Cold Work on Intergranular Stress Corrosion", Materials Protection and Performance, Vol. 12, No. 6, June 1973.
- 2-4. G. M. Gordon and R. E. Blood, "Reactor Structural Materials Environmental Exposure Program", Symposium on Materials Performance in Operating Nuclear Systems, Ames Laboratory, Ames, Iowa, August 28-30, 1973.
- 2-5. E. Kiss, J. D. Heald, D. A. Hale, "Low Cycle Fatigue of Prototype Piping", GEAP-10135, January 1970.

Table 2-1  
POSSIBLE CAUSES OF CRACKING

<u>Location</u>	<u>Possible Cause</u>	<u>Evidence</u>
1. Sparger Arm Near T-Box	Sensitization by Welding.	Location of cracks
	Cold Work Followed by Weld Sensitization	Approximate 5% Cold Work Near T-Box
	Weld Residual Stresses	Location of cracks
	Fatigue (thermally Induced)	RT's are Low
	Fatigue (Flow-Induced Vibration)	Amplitudes are Limited
2. Sparger Arms  Away from T-Box	Sensitization from Fabrication	None*
	Cold Work Followed by Sensitization	Pipe Bend Forming*, No Evidence of Sensitization
	Local Heavy Cold Work	None*
	Fatigue	Same as in 1. Above

\*Sensitization and cold work state of spargers not yet known.

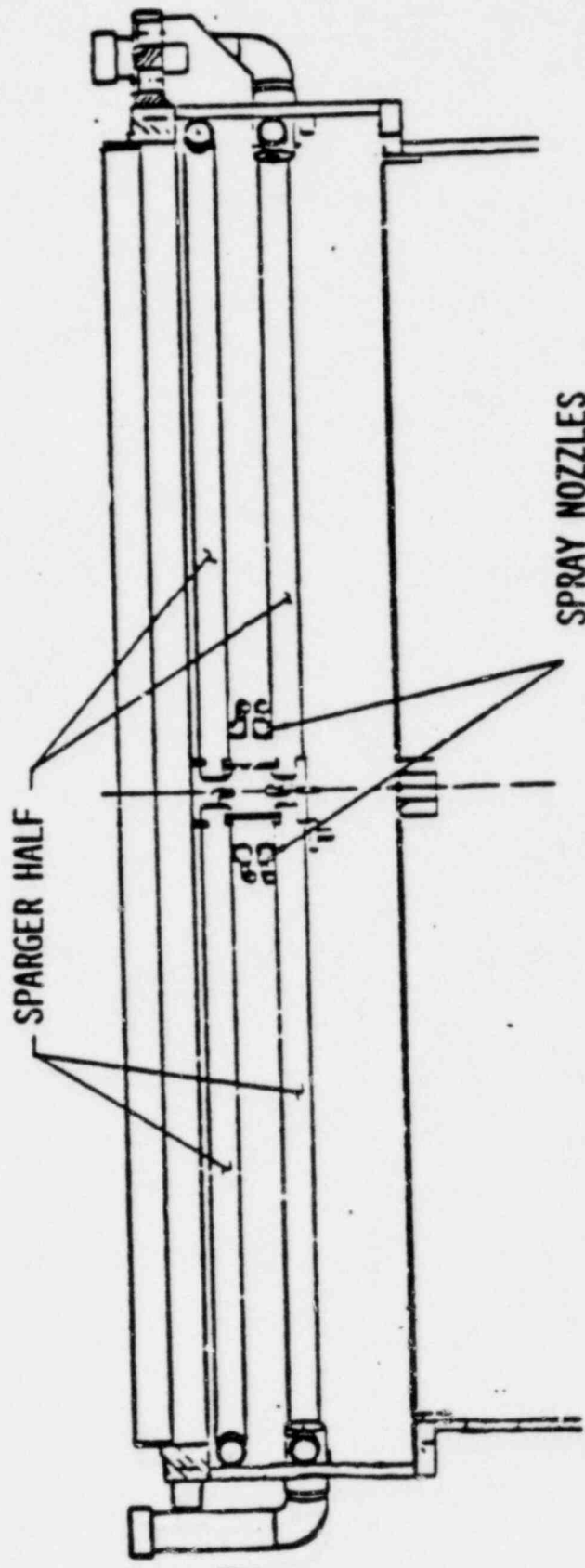


Figure 2-1. Core Spray Sparger - Elevation View

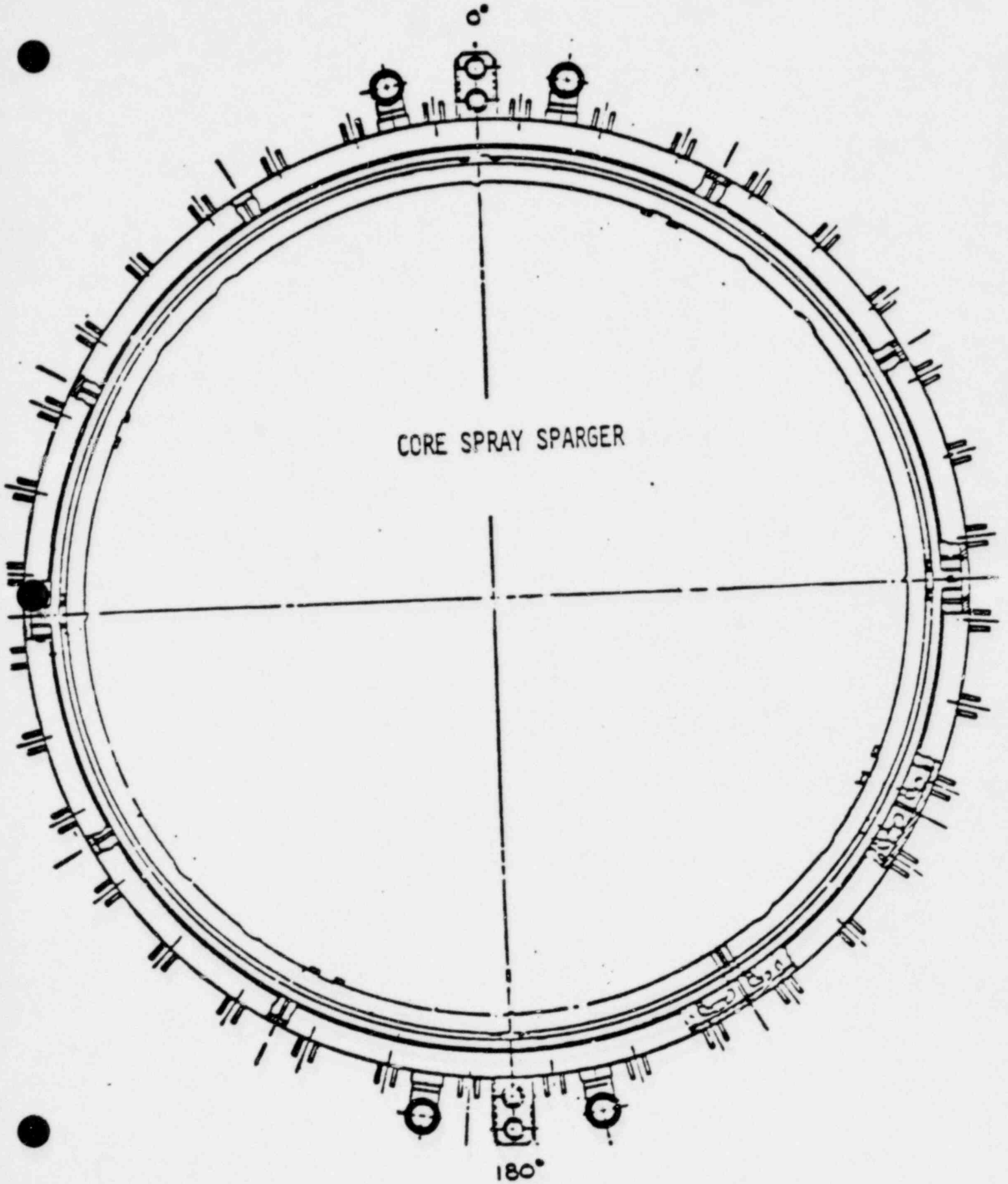


Figure 2-2. Core Spray Sparger - Plan View  
2-23

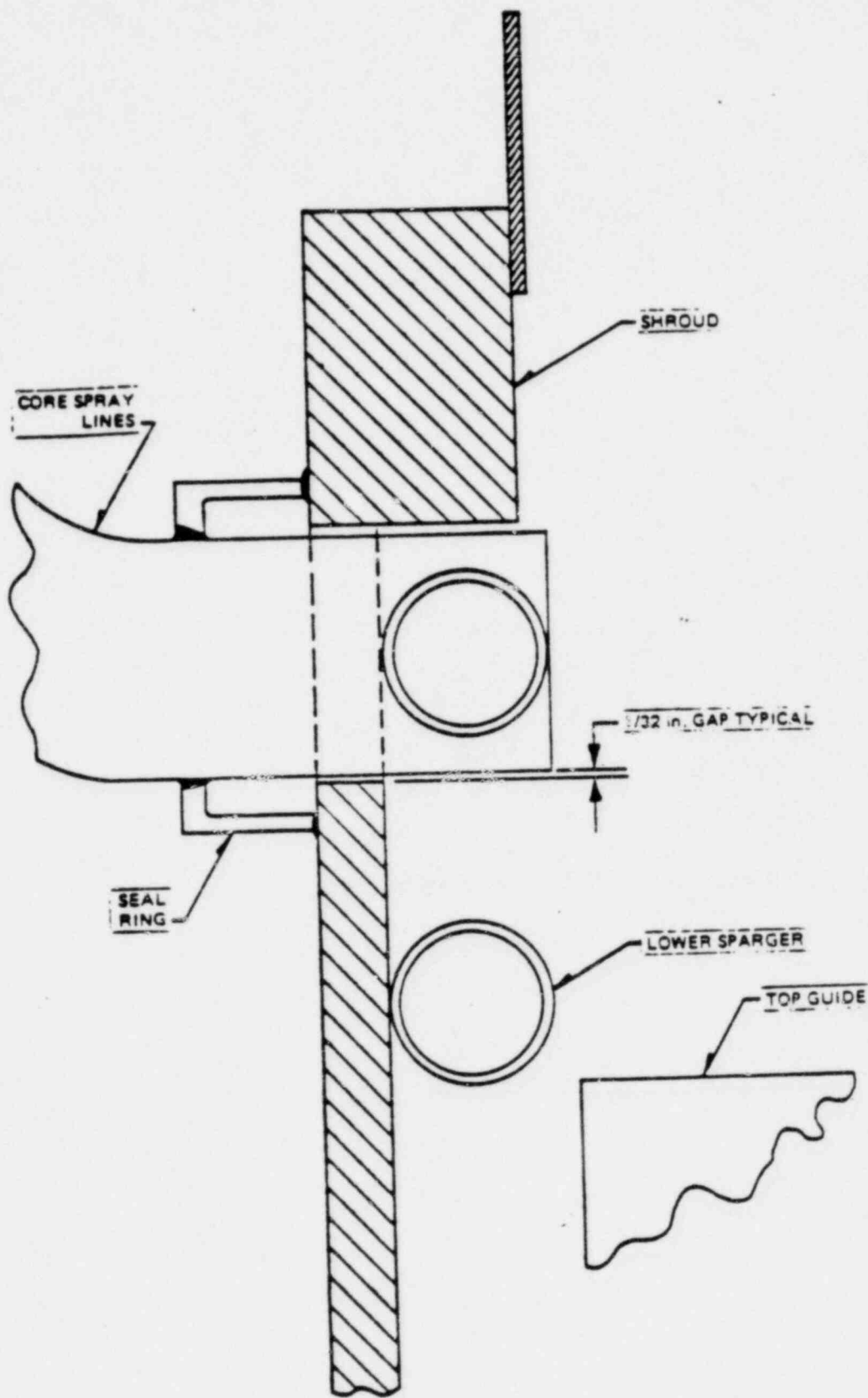


Figure 2-3. Sparger to Shroud Attachment Method

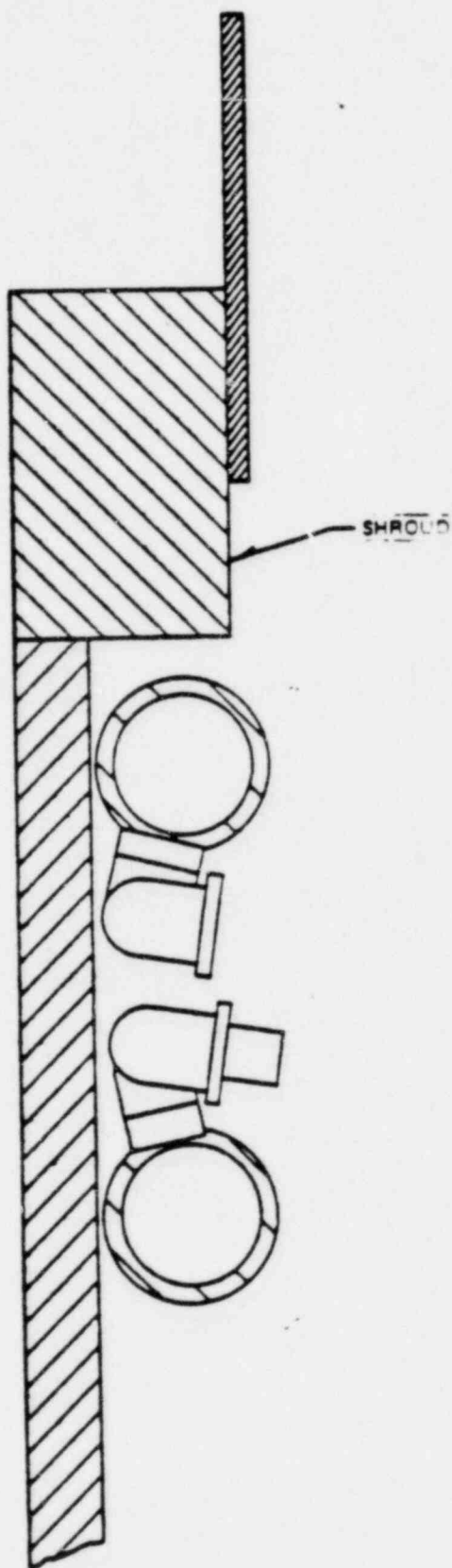


Figure 2-4. Sparger Nozzles

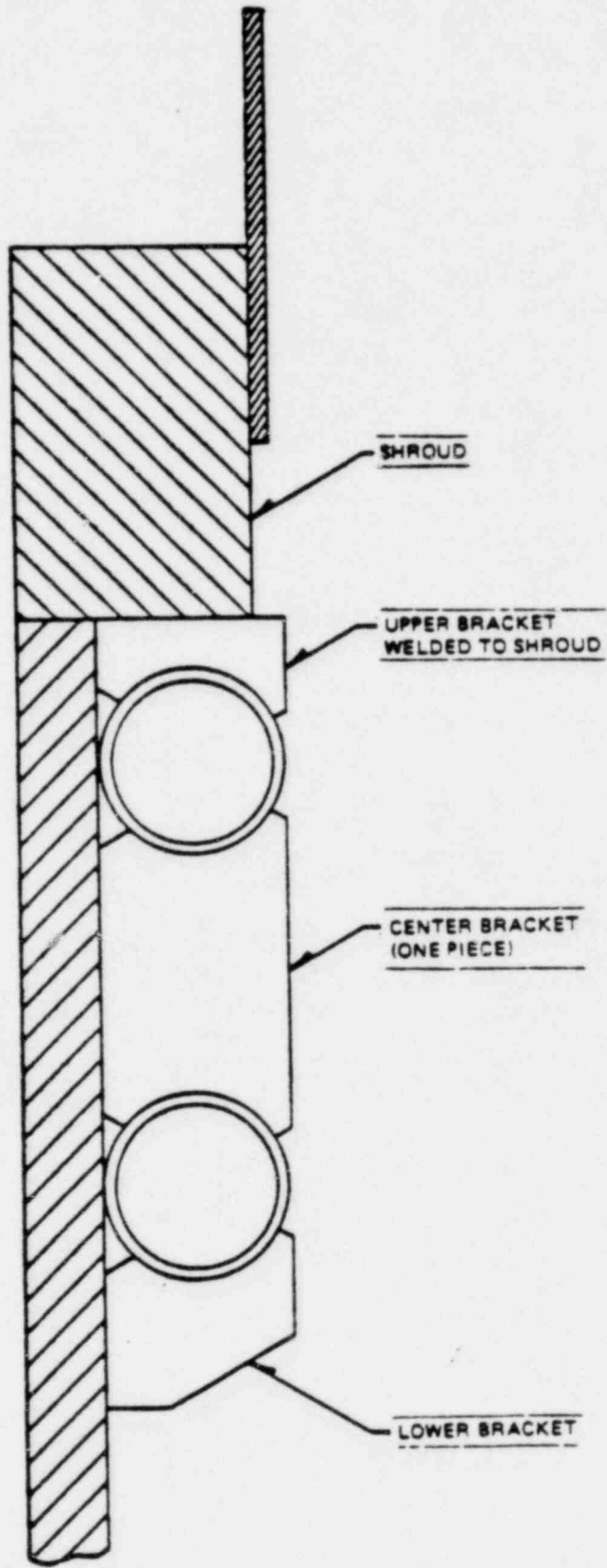


Figure 2-5. Sparger Support Method

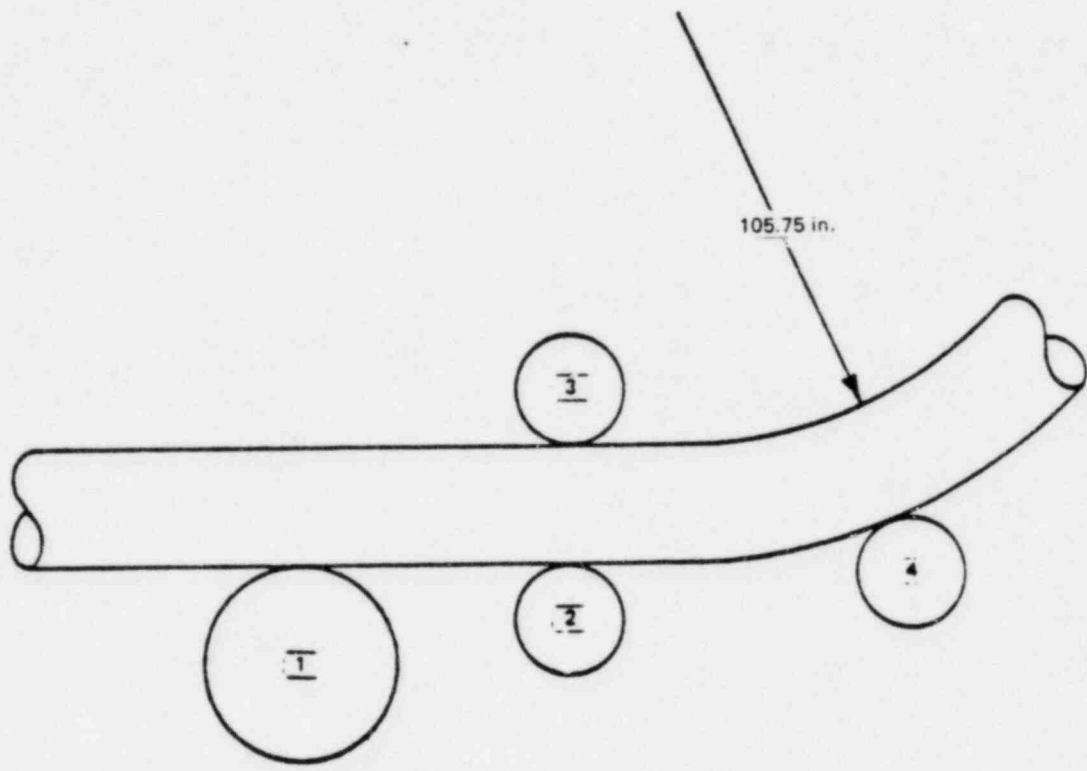
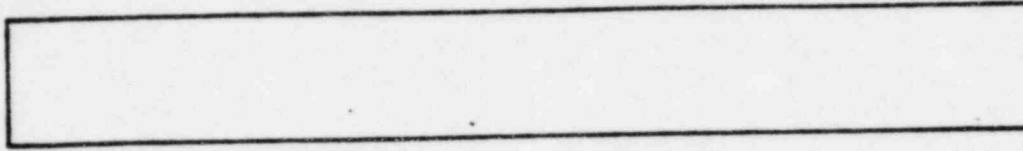


Figure 2-6. Pipe Bending Method



INITIAL CONFIGURATION

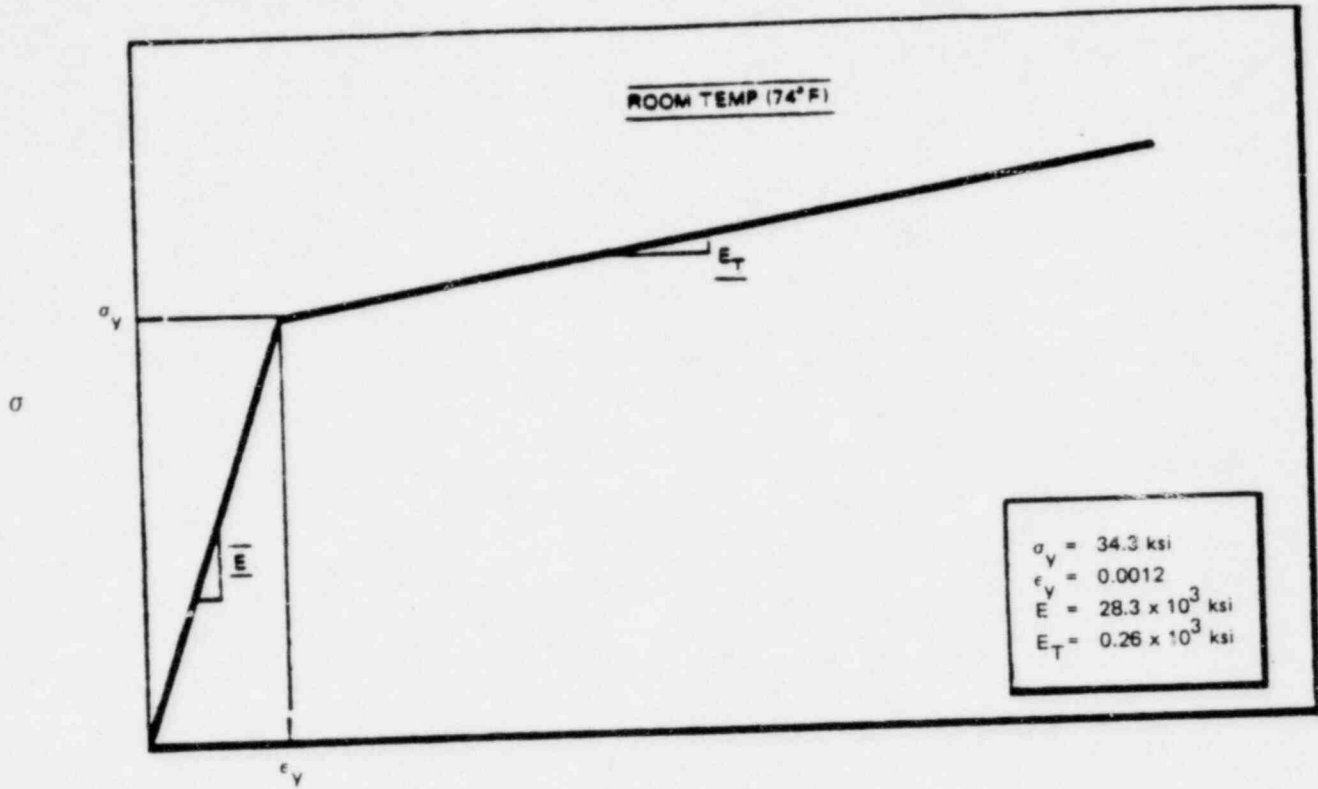


LOAD APPLICATION DURING FABRICATION

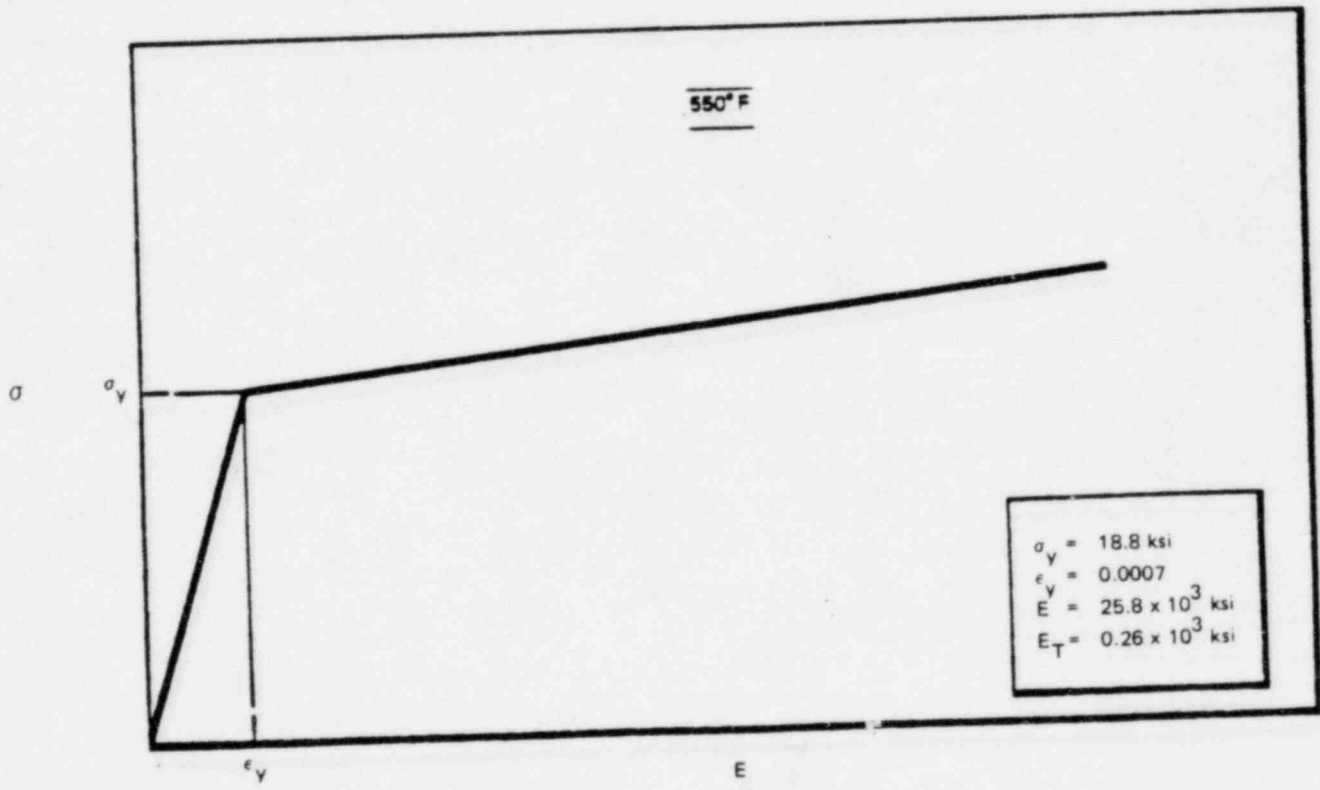


FINAL DEFORMED SHAPE AFTER LOAD REMOVAL

Figure 2-7. Sequence of Events Leading to the Residual Stress Distribution



(a)



(b)

Figure 2-8. Bilinear Stress-Strain Curves for Type-304 Stainless Steel

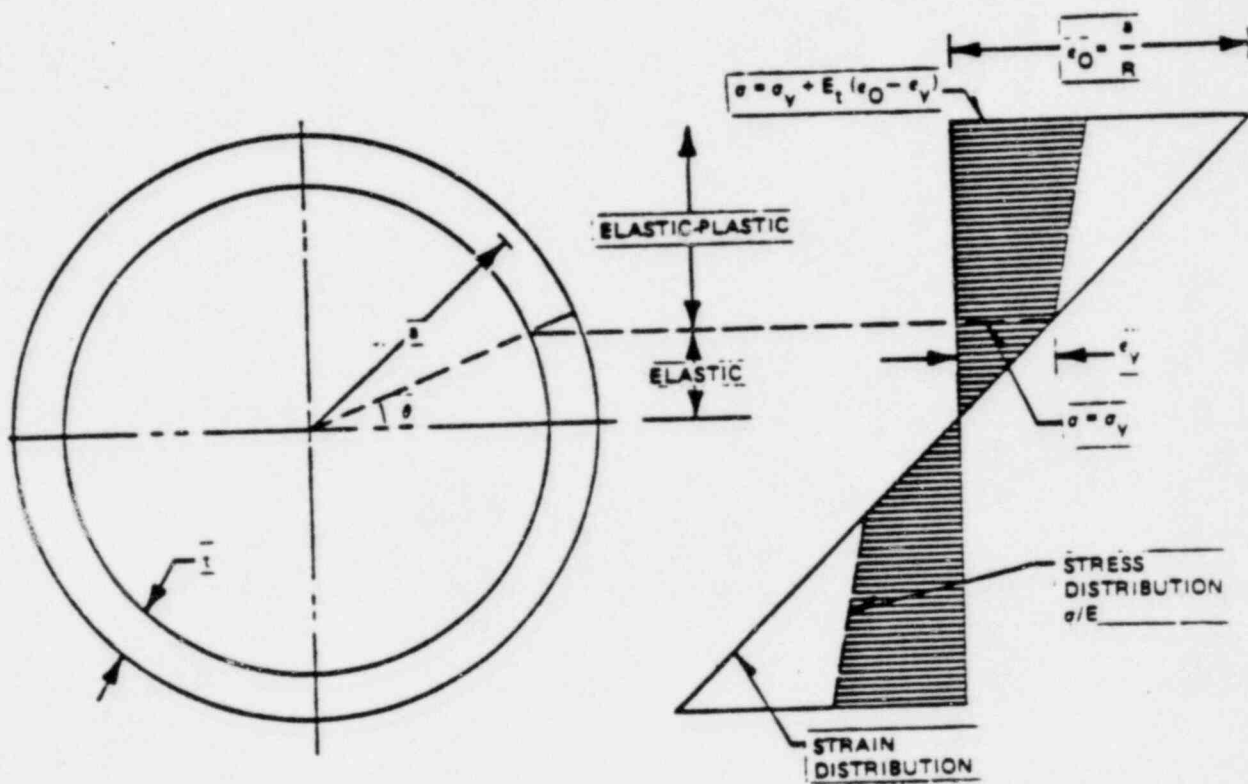


Figure 2-9. Stress and Strain Distribution in the Pipe Under Applied Moment

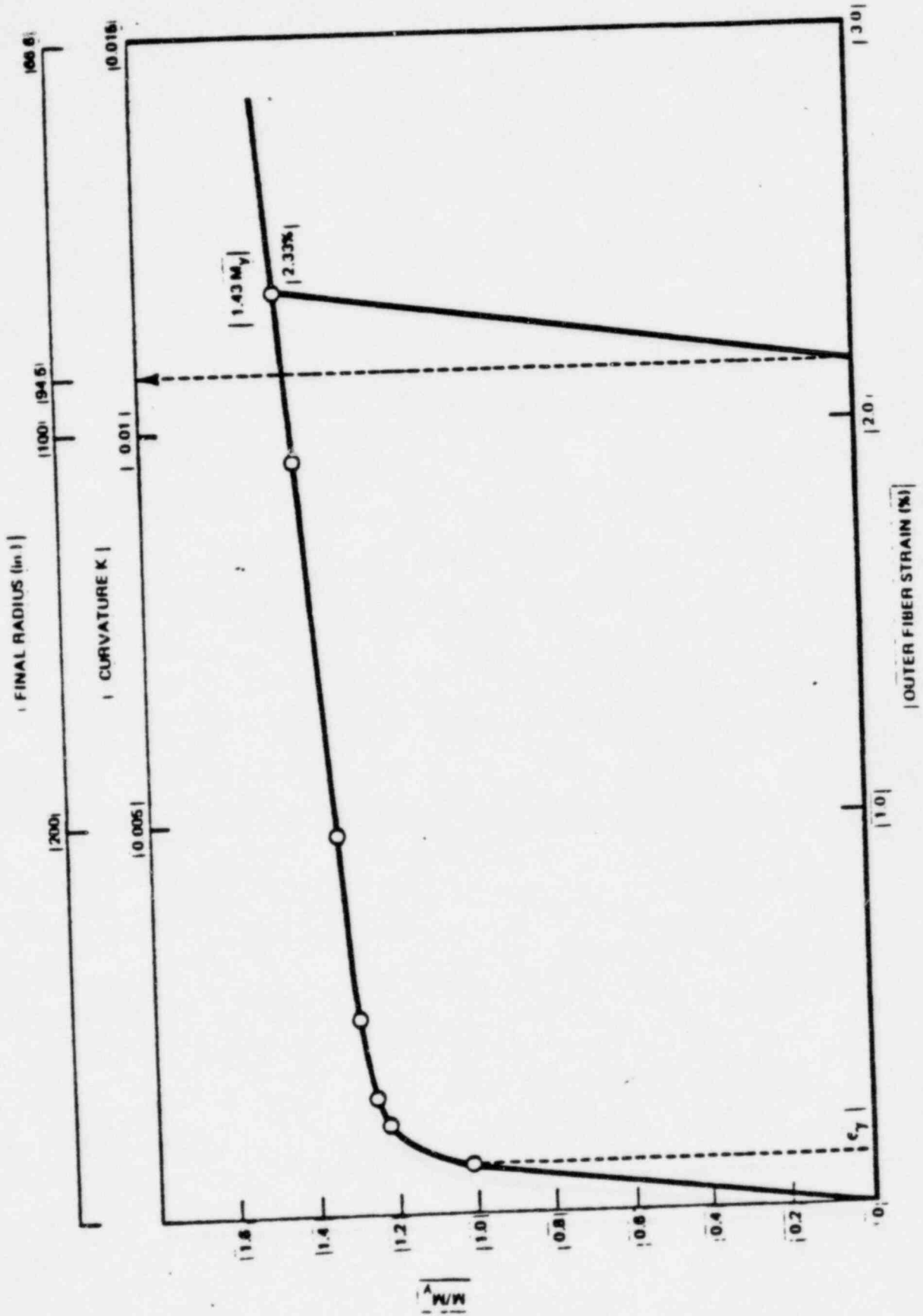


Figure 2-10. Moment Versus Outer Fiber Strain

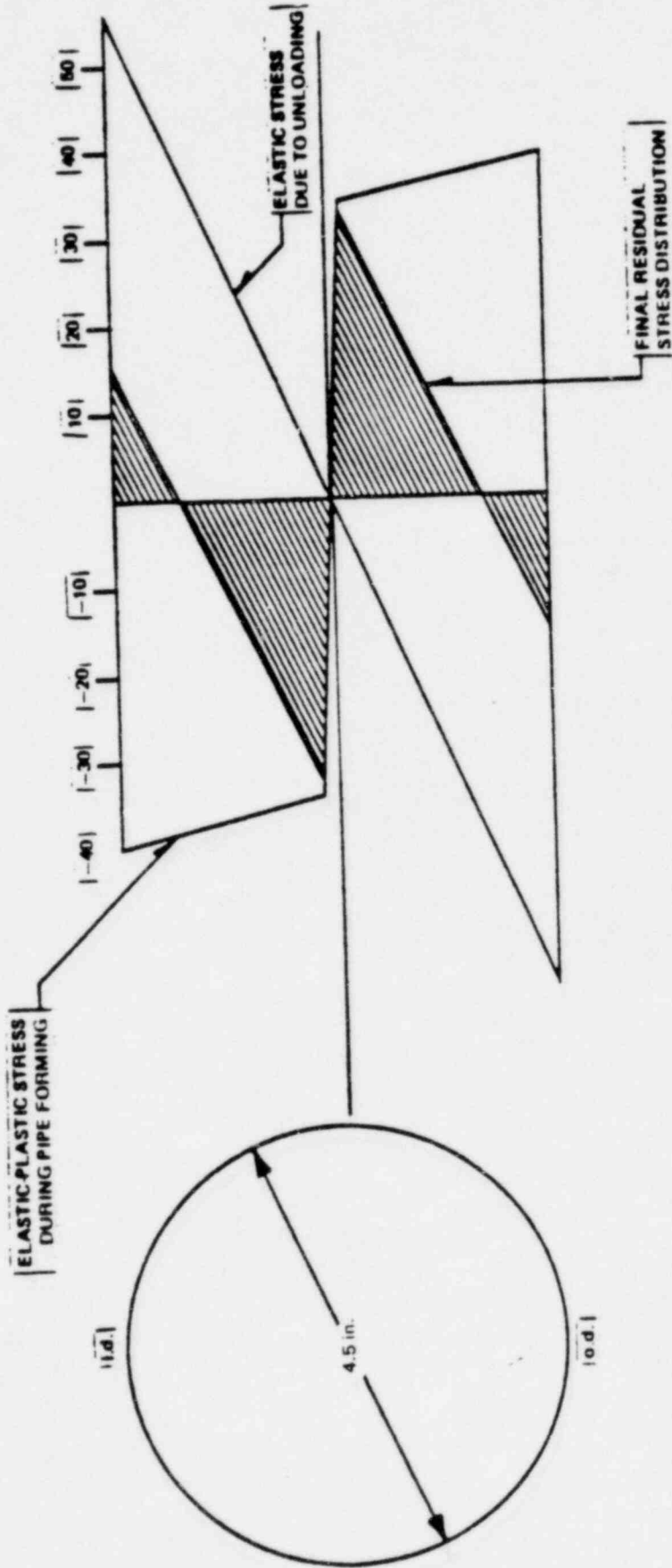
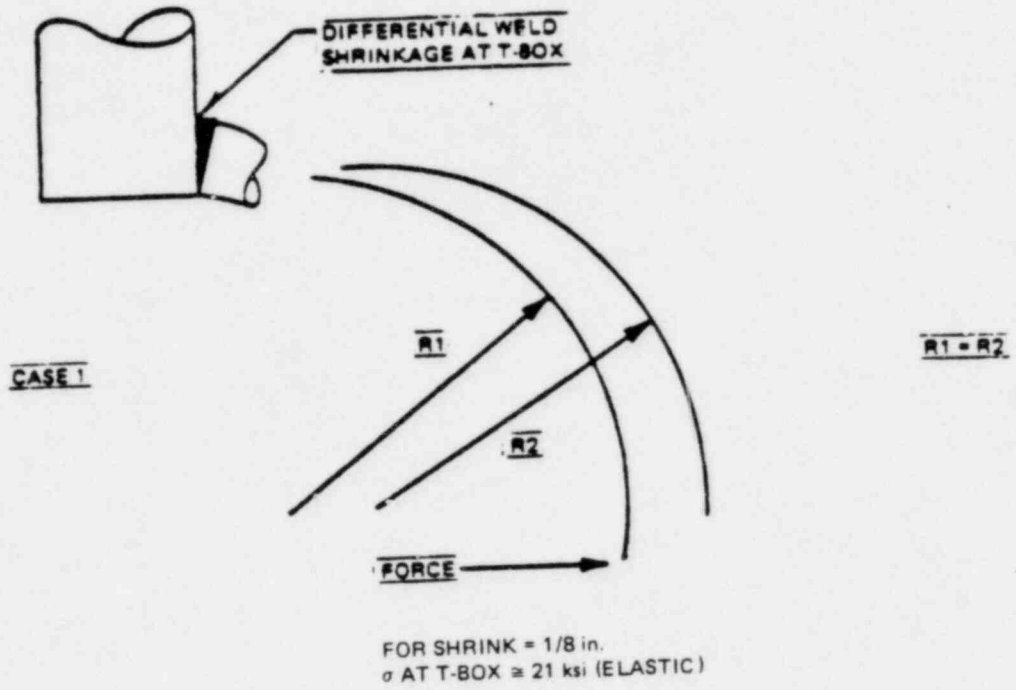


Figure 2-11. Resultant Residual Stress Distribution After Fabrication

INSTALLATION-RADIAL MISMATCH



ASSUME  $R1 = 104.75$   
 $R2 = 105.75$   
UNIFORM FORMING  
 $\epsilon \approx 1.0\%$   
 $\sigma \approx 38$  ksi (FROM  $\sigma - \epsilon$  CURVE)

CASE 2

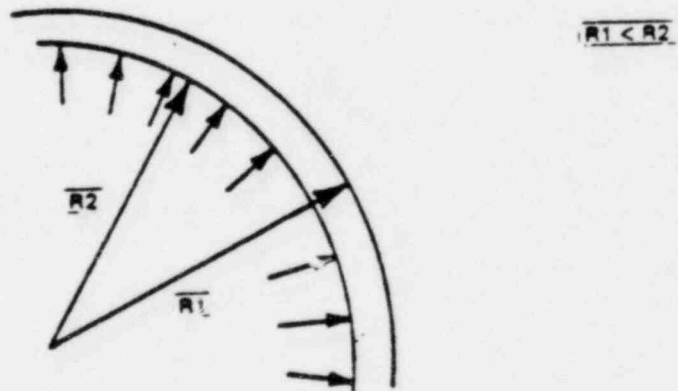


Figure 2-12. Postulated Installation Stresses

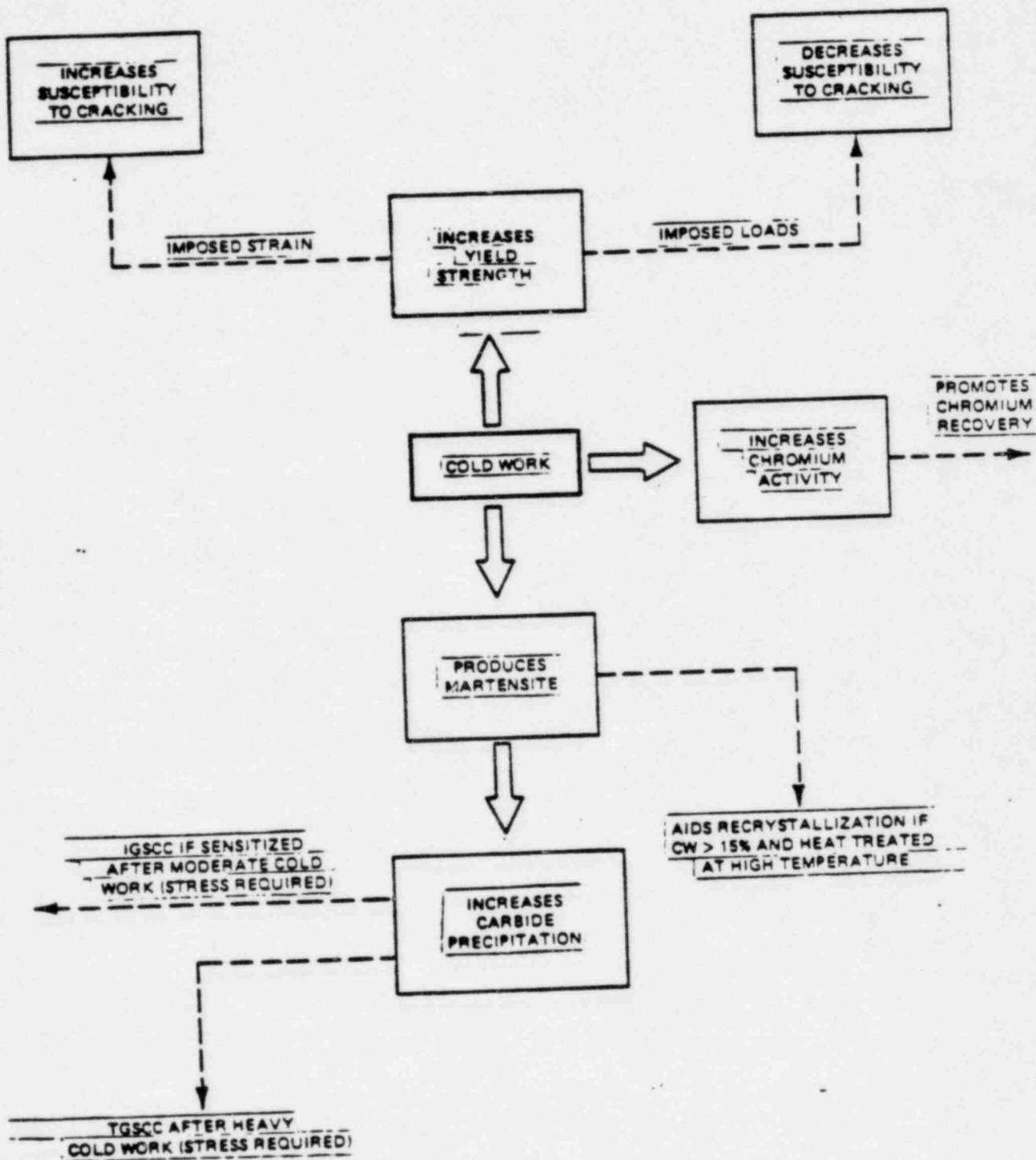


Figure 2-13. Effects of Cold Work on ICSCC of Type-304 Stainless Steel

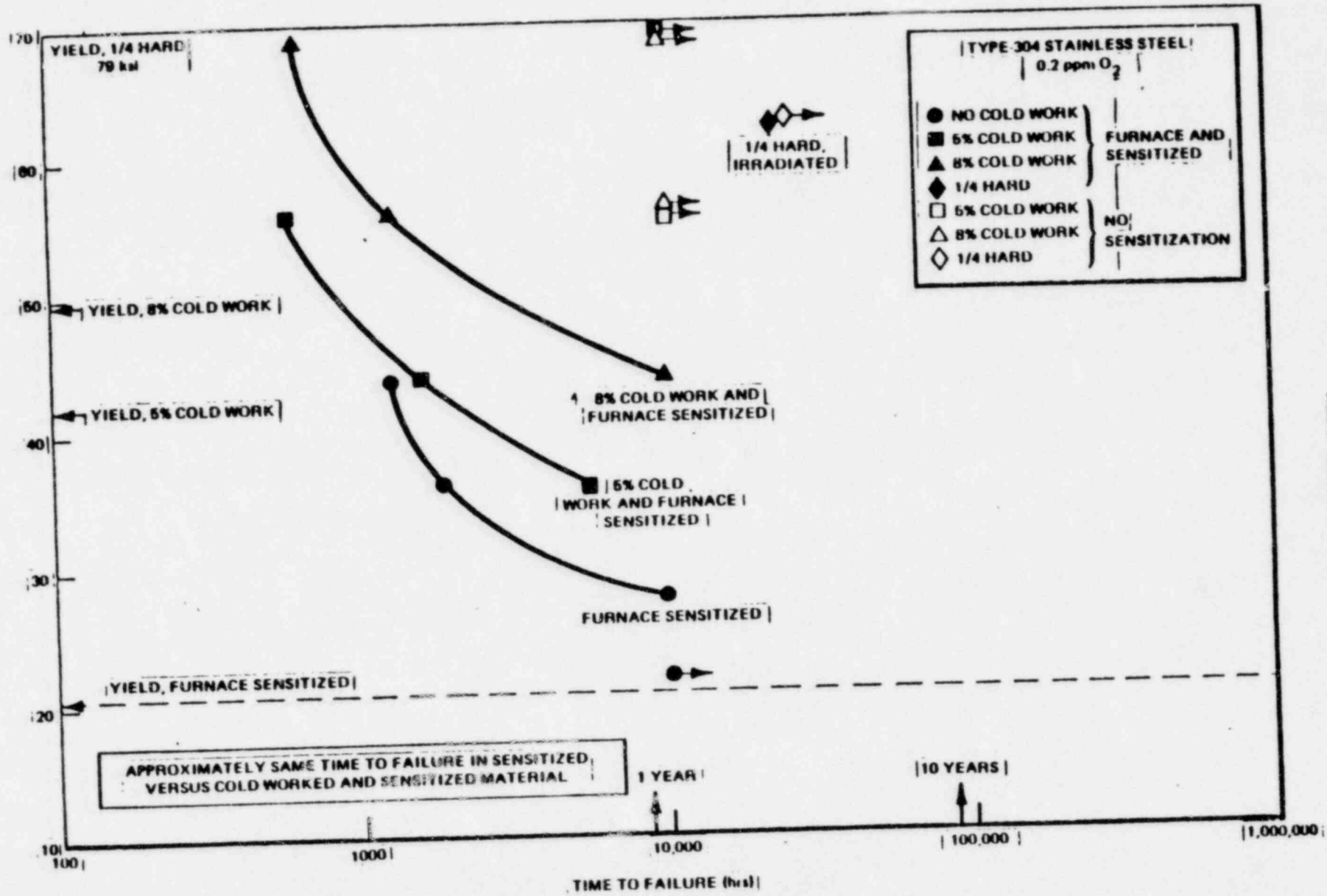


Figure 2-14. Effects of Cold Work on IGSCC

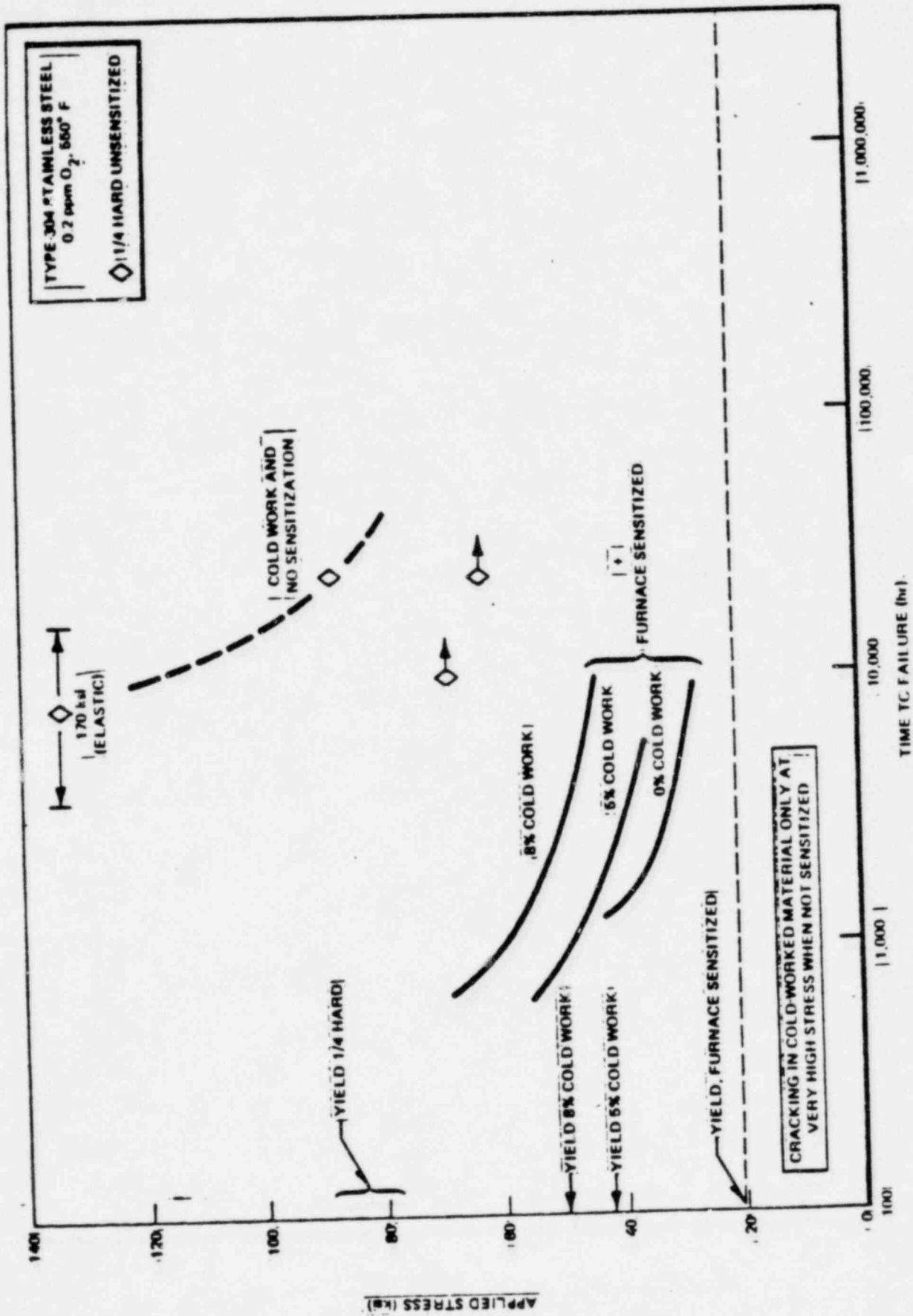


Figure 2-15. Effects of Cold Work on IGSCC

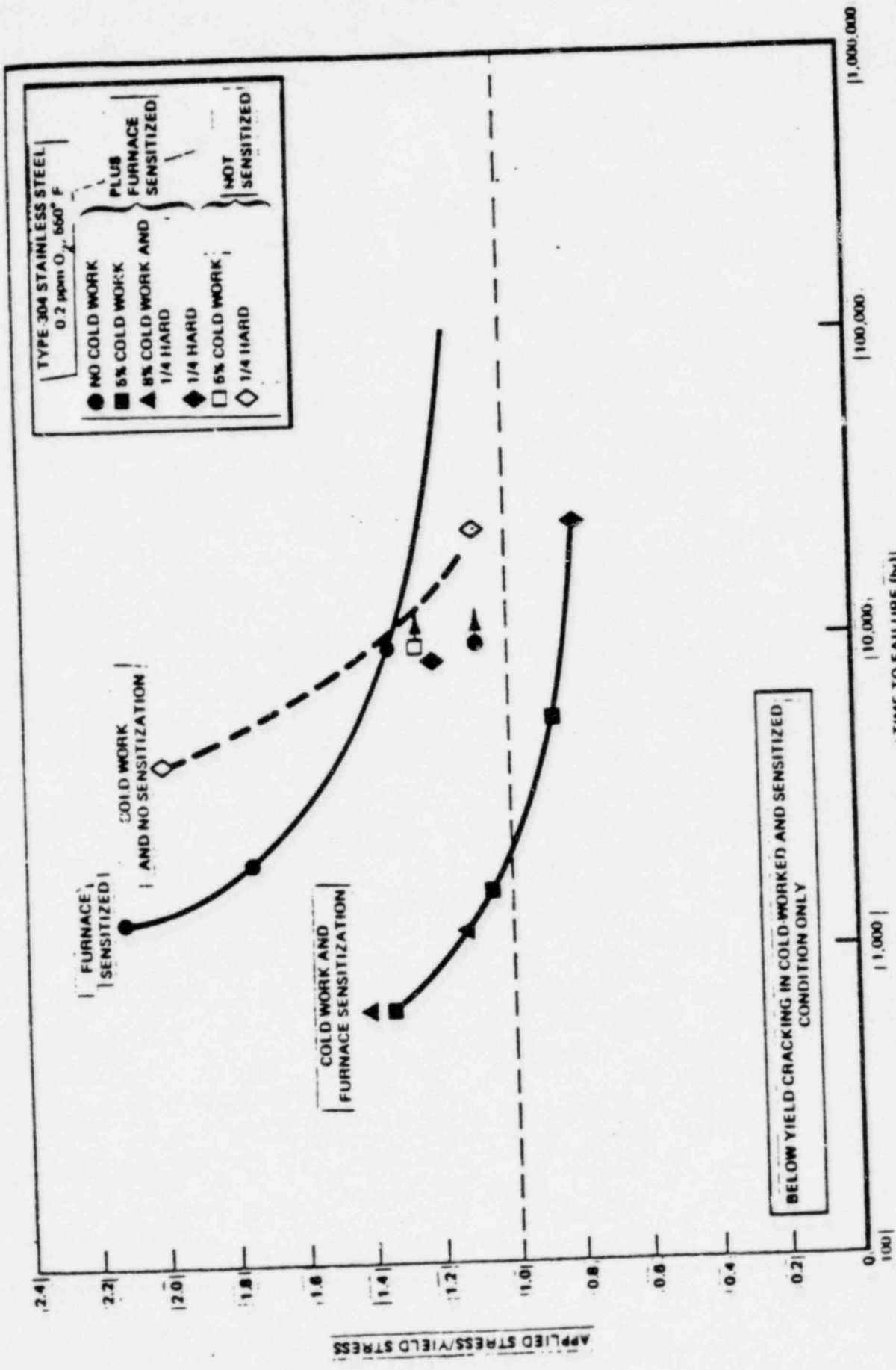


Figure 2-16. Effects of Cold Work on IGSCC

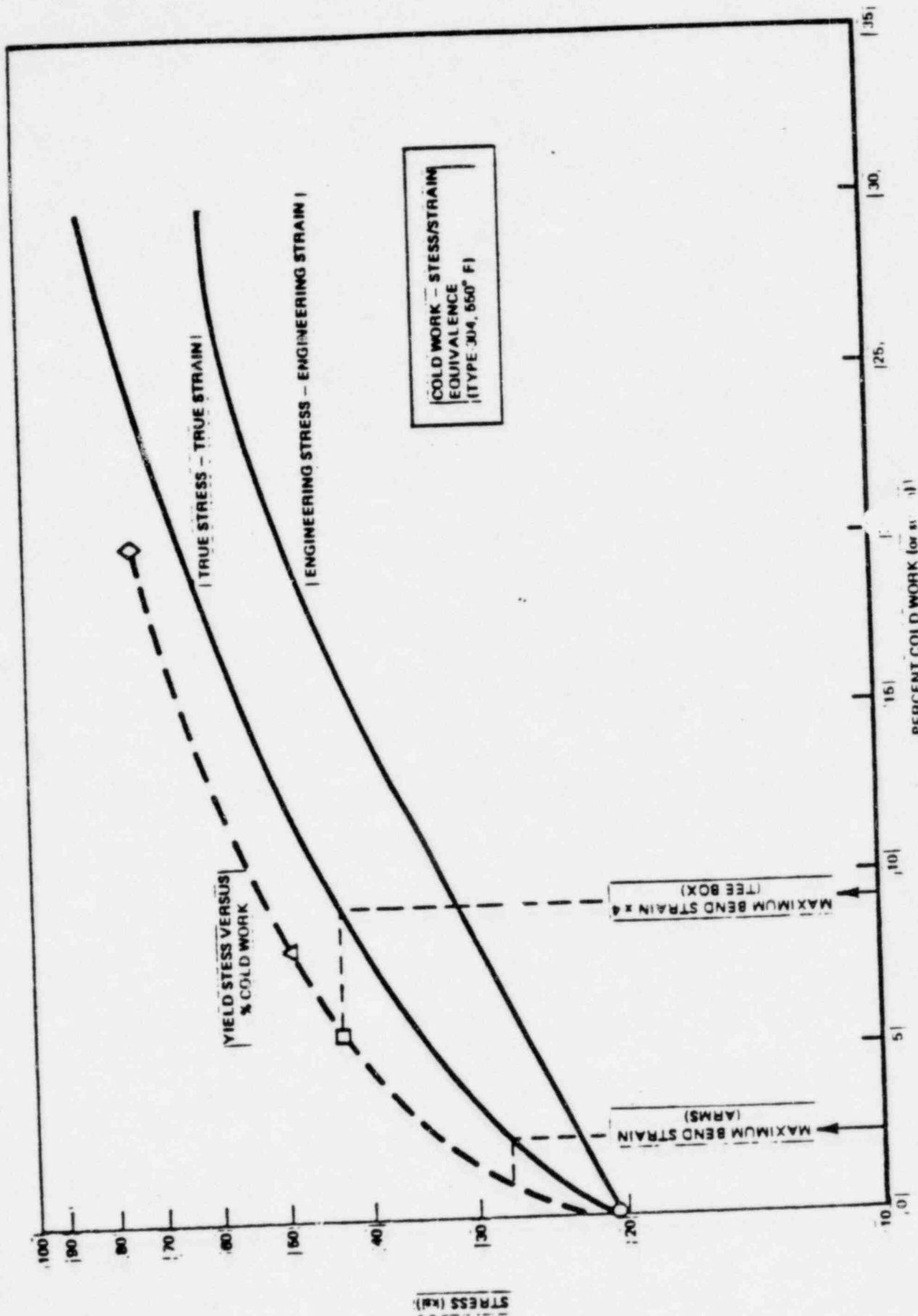


Figure 2-17. Stress Versus Percent Cold Work

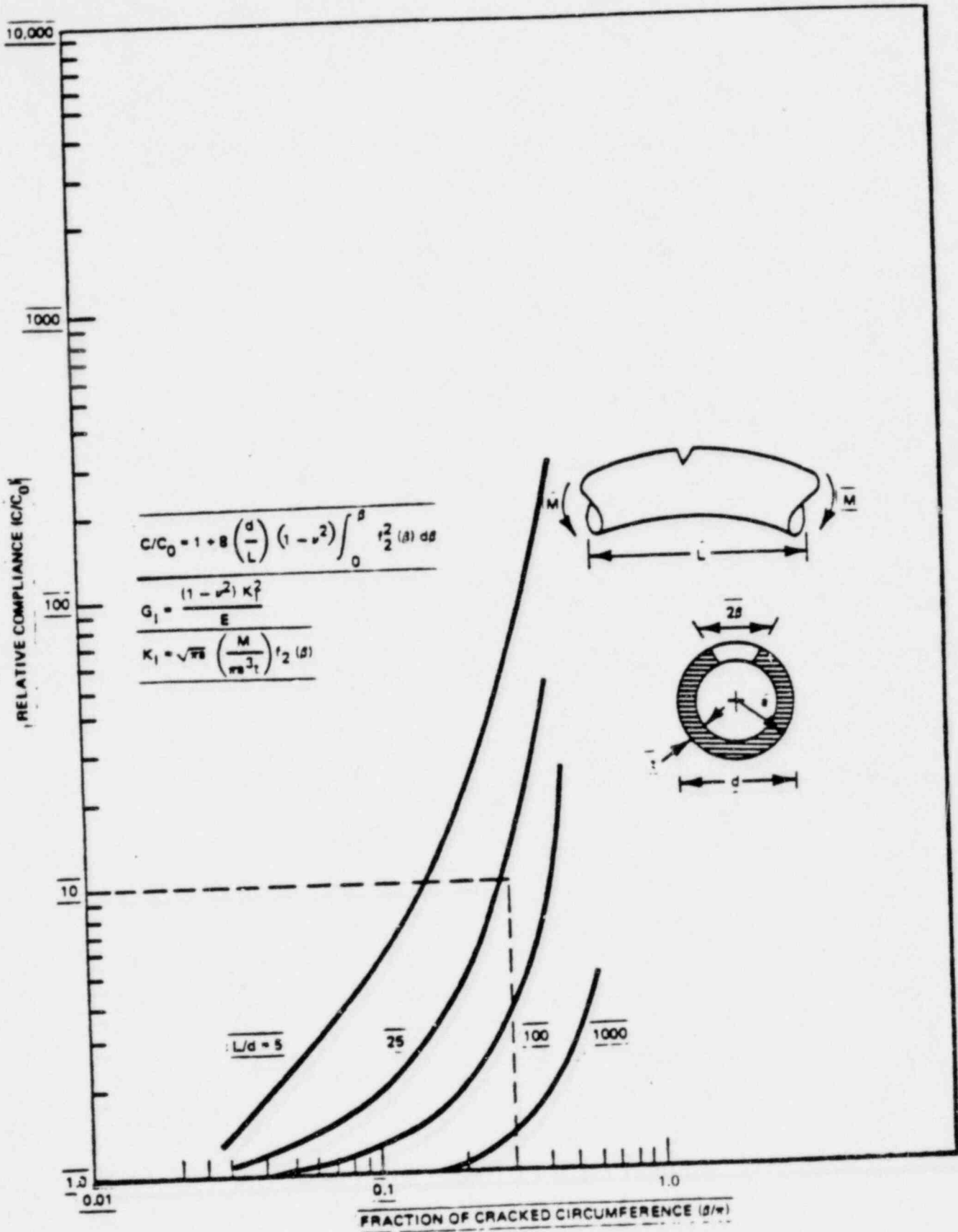


Figure 2-18. Compliance Change, Cracked Pipe

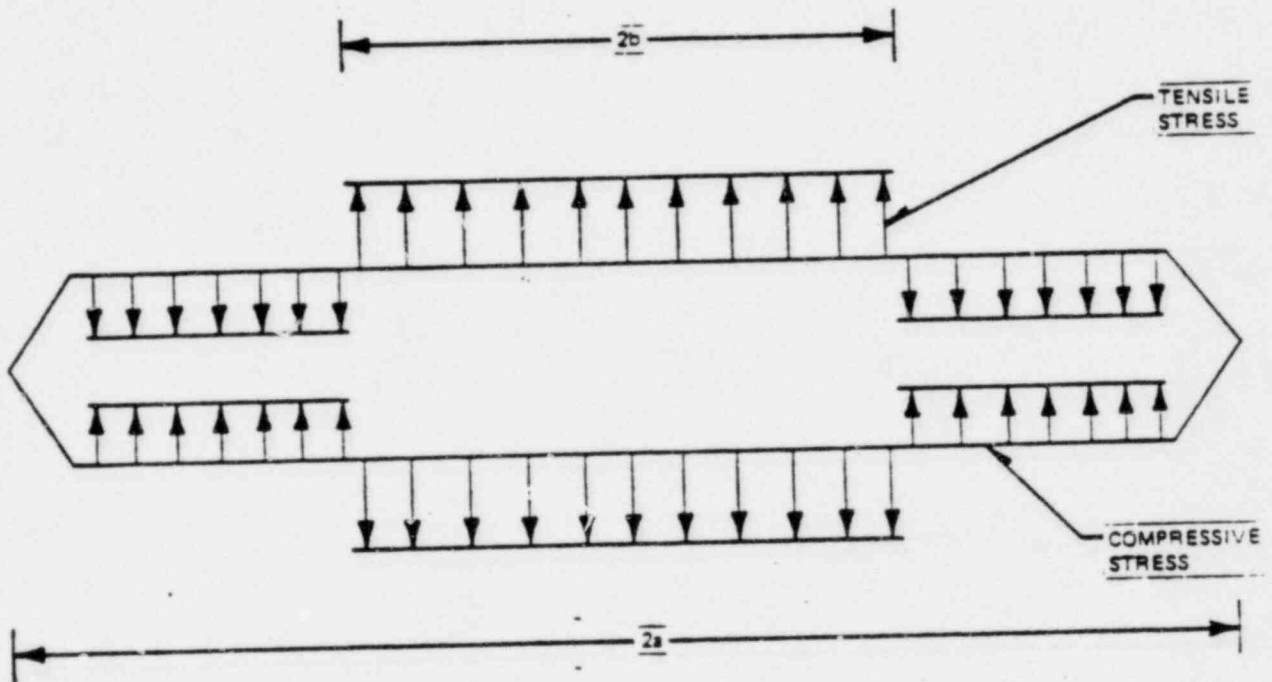


Figure 2-19. Assumed Stress Distribution on the Crack Face

### 3. LOST PARTS ANALYSIS

#### 3.1 INTRODUCTION

Based on the structural analysis given in Section 2, it is expected that the Peach Bottom core spray sparger will not break and result in loose pieces in the reactor. However, an evaluation of the possible consequences of a potential loose piece is presented in this section.

#### 3.2 LOOSE PIECE DESCRIPTION

Since a piece has not been lost, it cannot be uniquely described. Three different types of loose pieces are postulated in Section 3.4.2: (1) a section of sparger pipe; (2) an outlet nozzle; and (3) a small piece of the sparger. The entire sparger is fabricated of Type-304 stainless steel.

#### 3.3 SAFETY CONCERN

The following safety concerns are addressed in this safety analysis:

1. Potential for corrosion or other chemical reaction to reactor materials.
2. Potential for fuel bundle flow blockage and subsequent fuel damage.
3. Potential for interference with control rod operation.

#### 3.4 SAFETY EVALUATION

The above safety concerns for the postulated loose pieces are addressed in this section. The effect of these concerns on safe reactor operation is also addressed.

##### 3.4.1 General Description

The core spray spargers are attached to the inside of the core shroud (Figure 3-1) in the upper plenum. For a piece of the sparger to reach and

potentially block the inlet of a fuel assembly, it would have to be carried out of the upper plenum and pass down into the lower plenum. To accomplish this, it would have to be carried by the fluid flow in the upper plenum up through the steam separators then outward to the downcomer annulus, then through the jet pump nozzle into the lower plenum, then make a 180° turn and be carried upward to the fuel assembly inlet orifices. A part of the sparger cannot reach the fuel assembly inlet orifices by falling down inside the core shroud as the core support plate and the loaded core will prevent this. For a part of the core spray sparger to reach a control rod, it must first traverse the upper plenum from the outer region of the shroud toward the center, which is unlikely, then fall through the restrictive passage between two fuel channels.

Since all parts of the core spray sparger are designed for in-reactor service, there is no possibility that any loose part will cause any corrosion or other chemical reaction to any reactor material.

### 3.4.2 Postulated Loose Pieces

#### 3.4.2.1 Sparger Pipe

The sparger pipe is 4-in. Schedule 40 pipe and is attached to the core shroud at six locations (T-box plus five brackets). The maximum span between supports is about 38-1/2", which corresponds to approximately 71 inches. In order to generate a loose piece of pipe, two throughwall cracks would have to propagate 360° around the sparger. The weight of the largest pipe segment would be approximately 90 lb.

A pipe segment could come to rest in any of three locations: (1) the top surface of the top guide outboard of the fuel assemblies; (2) the top surface of the fuel assembly handles; or (3) in an unlikely event, the top surface of the core plate. In all three of these locations, the flow velocity is low and insufficient to lift a segment of the pipe. Therefore, it will remain at one of these locations (see Appendix C for flow velocity calculations).

A 90-lb piece of pipe which falls from the core spray sparger will not harm the core plate, top guide or fuel assembly handles, since these components are designed for much larger loads.

Since the pipe cannot be lifted by the flow and since the pipe cannot fit through either the steam separator or the jet pump, it will not cause any flow blockage at the fuel inlet orifice. Since the pipe is too large to fit between fuel channels, it will not cause any interference with control rod operations.

#### 3.4.2.2 Spray Nozzle

Each spray nozzle consists of two 1-in. elbows fabricated of Type-304 stainless steel, which are welded to the sparger. In order to generate a loose nozzle, a throughwall crack would have to propagate 360° around the nozzle. The weight of each nozzle assembly is approximately 1-3/4 lb. A loose nozzle would most likely come to rest on the top surface of the core plate or on the top surface of the top guide. The flow velocities in these regions are insufficient to lift the nozzle, thus, it will remain at one of the above mentioned locations.

Since the nozzle cannot be lifted by the flow and since the nozzle cannot fit through the steam separator, it will not cause any flow blockage at the fuel assembly inlet orifices. The nozzle is too large to fit between two fuel channels; thus, it cannot cause any control rod interferences.

#### 3.4.2.3 Small Pieces

A small piece of the sparger could become loose if both longitudinal and circumferential throughwall cracking occurred. A small piece could be lifted by the flow if it maintained an orientation with its maximum projected area perpendicular to the flow. Due to flow turbulence and nonsymmetry of the loose part, the part will tend to rotate so that the minimum projected area will be perpendicular to the flow. With this orientation, all parts with a length of greater than approximately 0.4 in. will sink (Figure 3-7 of Reference 3-1). Thus, most pieces will not be carried by the flow toward the

steam separator. However, in the unlikely event that a piece reaches the steam separator, it would have to pass through the steam separator turning vane (Figure 3-2). The turning vane has eight curved vanes. The outlet of each vane overlaps the inlet of the adjacent vane. The longest straight piece that can fit through the turning vane is approximately 6 inches long and it must be oriented with the long dimension in the vertical direction. The largest piece that can fit through the turning vane with its long dimension in a horizontal plane is shown in Figure 3-3.

It is very unlikely that the flow velocities would carry either of these maximum sized pieces through the turning vane. After passing through the turning vane, the fluid momentum is reduced as the water is removed. At the separator exit, the fluid is almost entirely steam. A typical water content is 1 weight percent. Thus, it is very unlikely that any piece could be carried out of the separator by the steam. If any piece were carried through the separator by the steam, then it could be carried into the downcomer annulus, through the jet pump and enter the lower plenum. A piece that entered the lower plenum would most likely be driven by jet pump flow to the bottom of the reactor pressure vessel where it would most likely remain. However, per Reference 3-1, a small piece could be carried by the flow up to the flow inlet orifices. The orifice sizes are 1.244, 1.469 and 2.211 inches.

It is extremely unlikely for a piece larger than the 1.244-in. orifice and essentially impossible for a piece larger than the 2.211-in. orifice to be carried through the steam separator. The outside diameter of the sparger is 4.5 in., while the fuel inlet orifices are slightly recessed relative to the surface of the control rod guide tubes (Figure 3-4), which have an outside diameter of 10-7/8 inches. Due to the different radii of curvature, flow would be able to enter the fuel assemblies. Thus, unacceptable flow blockage as defined by Reference 3-1 would require that more than one loose piece be carried to the same inlet orifice. This is based on the size of the piece(s) that, in a highly unlikely circumstance, have the potential of reaching the vessel lower plenum. The probability of unacceptable flow blockage of any fuel orifice is judged to be insignificant.

The flow velocities near the sparger are lower than those above the fuel assemblies. Thus, it is unlikely that a small piece would be carried over the fuel assemblies. If the piece were carried over the fuel assemblies and then rotated so that the flow could no longer carry it, the piece could fall on top of a fuel assembly or between fuel assemblies.

Figure 3-5 shows a typical unit cell of four fuel assemblies and one control rod. The control rod moves in the gap between the fuel channels. The gap between fuel channels is 0.75 inch. The length of the gap between the channel spacer and the channel fastener is 2.3 inches. Thus, any piece larger than 2.3 in. by 0.75 in. cannot cause control rod interference. The control rod thickness is 0.312 in. and the diameter of the control rod rollers is 0.520 inches. Thus, pieces smaller than 0.334 in. will fall past the control rod without causing any interference. A piece of precisely the right size could be in contact with the control rod and one or two fuel channels. Such a piece might be detected during the normal control rod exercising. The rods are inserted one notch and withdrawn one notch each day. It is also possible, though unlikely, that a piece might wedge between two fuel channels above the control rod and thus not be detected by normal control rod operation. If the rod were to be inserted, the control rod mechanism has enough force to lift one fuel assembly with the reactor at normal operating pressure. If the fuel assembly were lifted 1 or 2 inches, it would be able to move horizontally at both the bottom and the top, thus most likely relieving any interference. The rod would then insert and the fuel assembly would fall back into place. Thus, it is very unlikely that any control rod will fail to insert.

One of the licensing bases of the reactor is that the highest worth control rods can be fully stuck out and the reactor can be safely shut down. Thus, unacceptable control rod interference will require multiple precisely-sized pieces interfering simultaneously with control rods that are in close proximity to each other. The probability of this is judged to be insignificant.

### 3.5 CONCLUSION

The probability for unacceptable corrosion or other chemical reaction due to a loose piece is zero. The potential for unacceptable flow blockage of a

fuel assembly is essentially zero. The potential for unacceptable control rod interference is essentially zero.

3.6 REFERENCE

3-1 "Consequences of a Postulated Flow Blockage Incident in a Boiling Water Reactor", October 1977 (NEDO-10174, Rev. 1).

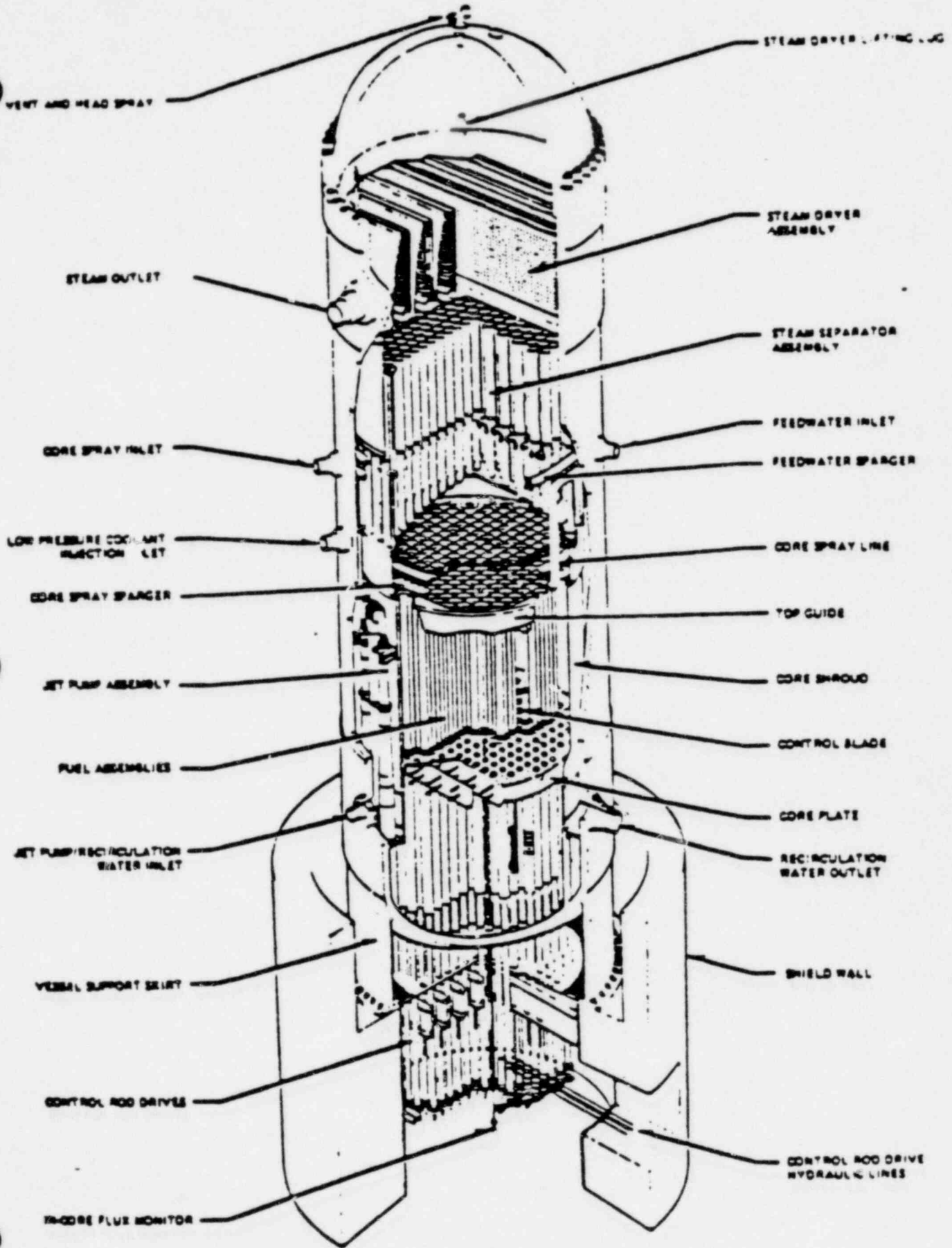


Figure 3-1. Reactor Vessel

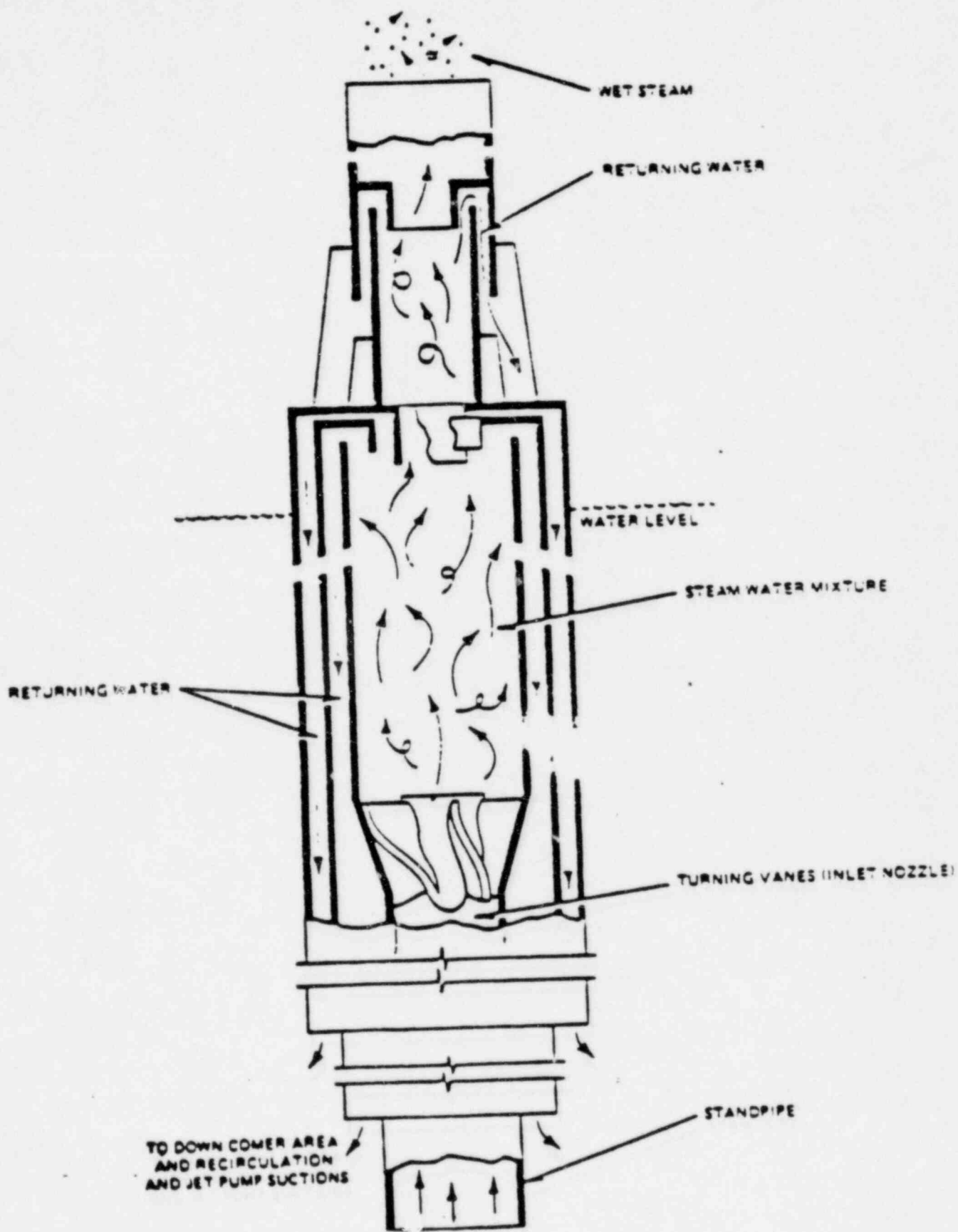


Figure 3-2. Steam Separator

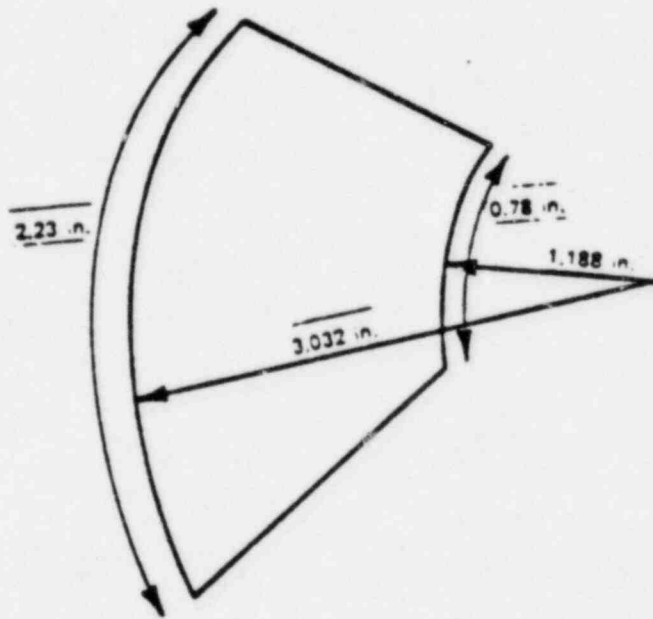


Figure 3-3. Largest Piece That Can Fit Through the Turning Vane with the Long Dimension in a Horizontal Plane

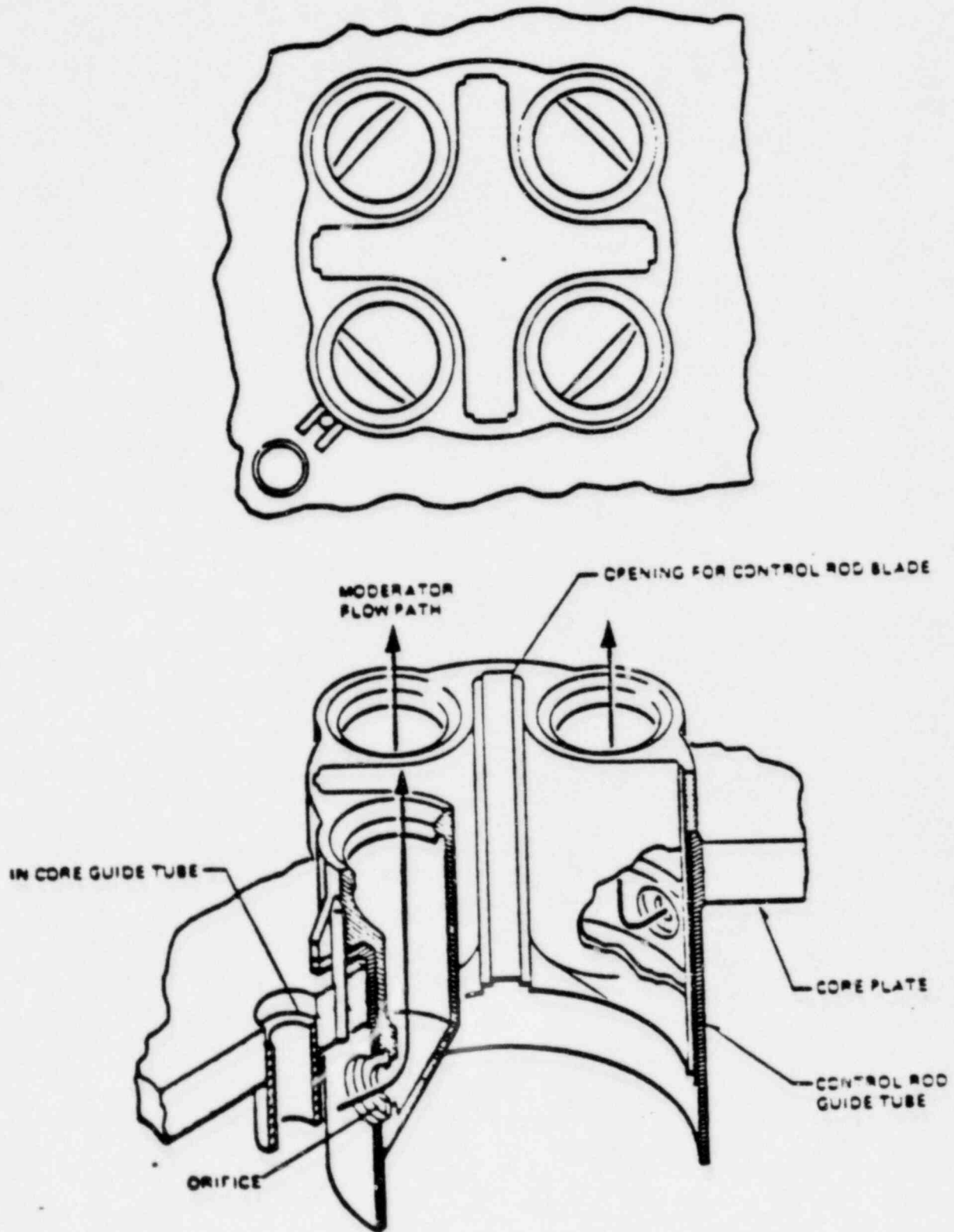
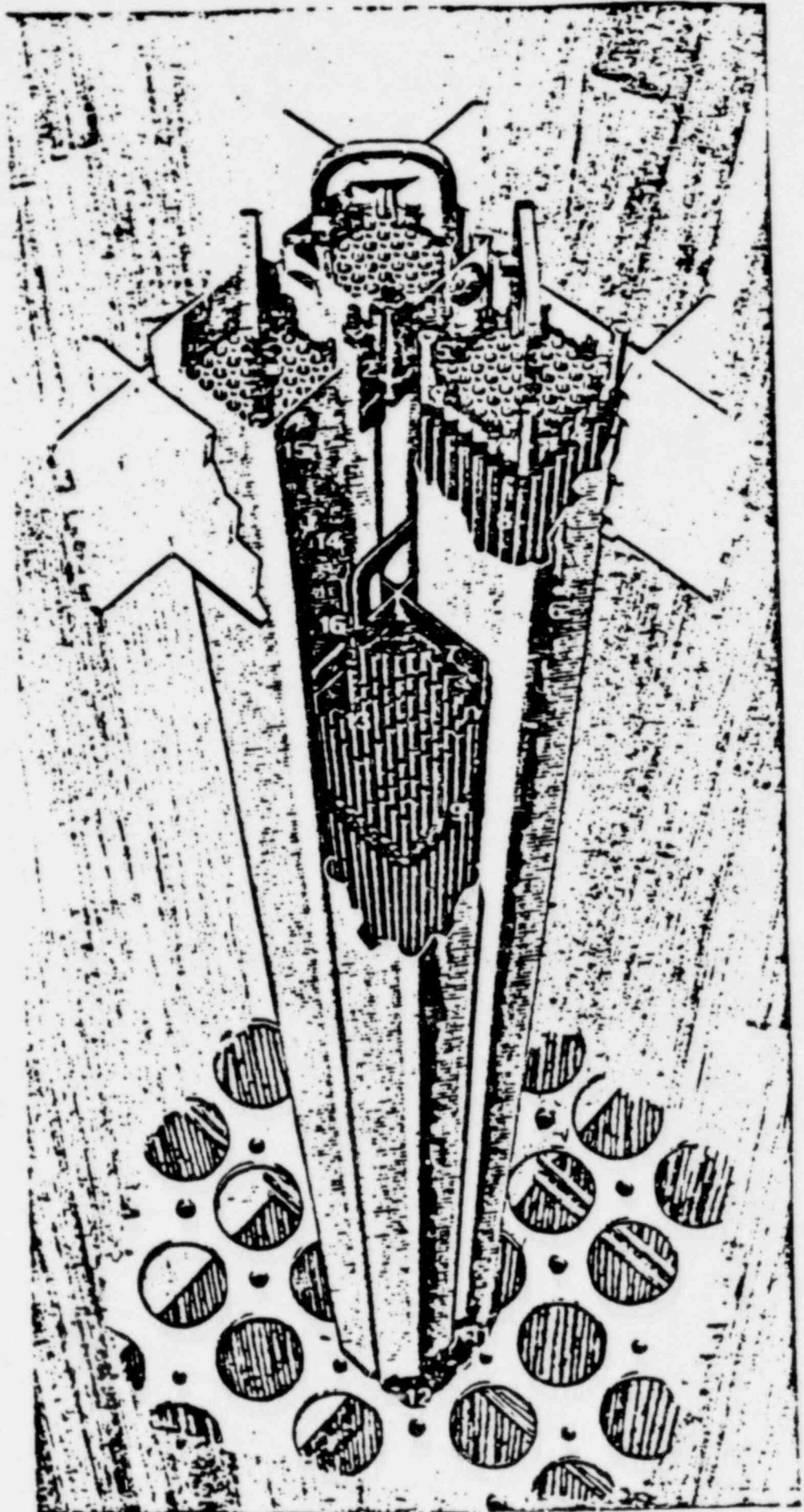


Figure 3-4. Orificed Fuel Support

# FUEL ASSEMBLIES & CONTROL ROD MODULE

- 1.TOP FUEL GUIDE
- 2.CHANNEL FASTENER
- 3.UPPER TIE PLATE
- 4.EXPANSION SPRING
- 5.LOCKING TAB
- 6.CHANNEL
- 7.CONTROL ROD
- 8.FUEL ROD
- 9.SPACER
- 10.CORE PLATE ASSEMBLY
- 11.LOWER TIE PLATE
- 12.FUEL SUPPORT PIECE
- 13.FUEL PELLETS
- 14.END PLUG
- 15.CHANNEL SPACER
- 16.PLENUM SPRING



GENERAL  ELECTRIC

Figure 3-5. Fuel Assemblies and Control Rod Module

#### 4. LOSS-OF-COOLANT ACCIDENT ANALYSIS WITH NONUNIFORM SPRAY IN ONE SPRAY SPARGER

##### 4.1 INTRODUCTION

This section describes the methods used to evaluate the MAPLHGR requirements to meet 10CFR50 Appendix K for the Peach Bottom Reload 5, Cycle 6, assuming no credit for core spray cooling from the cracked core spray sparger. The inputs to the approved 10CFR50 Appendix K computer codes are discussed in Section 4.2; the general sensitivity of the loss-of-coolant accident analysis (LOCA) results to the spray cooling is discussed in Section 4.3; the results of the analysis are given in Section 4.4 and the conclusions are presented in Section 4.5.

##### 4.2 INPUT TO THE LOCA ANALYSIS

The approved versions of SAFE, REFLOOD, and CHASTE codes were used to evaluate the impact of a cracked core spray sparger in Peach Bottom-2.

The potential effects of cracks in one core spray sparger is to cause nonuniform spray distribution from the sparger. If the second sparger is injecting flow (i.e., the other core spray system is operable), the postulated effect could only reduce the amount of spray flow to the hot fuel assembly by the contribution from one sparger. This effect is conservatively modeled by setting the spray heat transfer coefficients in the CHASTE heatup code to one-half of their Appendix K values. This is the same assumption used in standard Appendix K analysis to model a core spray system out of service (Reference 4-1).

If one core spray system is rendered inoperable due to the assumed single failure per Appendix K, the remaining sparger may be assumed to be the one with cracks. The bounding effect (the assumed loss of all spray to the hot fuel assembly) can then be represented by setting the spray heat transfer coefficients in CHASTE to zero.

Therefore, in summary, the effect of cracks in one sparger is represented conservatively in this calculation by setting the spray heat transfer coefficients to zero or to one half their standard value, depending on the single failure analyzed.

This representation is very conservative as discussed in the following paragraphs.

Counter current flow limiting (CCFL) is the phenomenon associated with a steam updraft limiting the downflow of water through a flow path which, in this case, is the fuel assembly. The steam updraft in the fuel assembly (due to flashing during blowdown and to spray evaporation on the fuel rods subsequently) can, under certain conditions, limit the downflow of spray water to an amount smaller than the spray injection rate in the upper plenum. This CCFL is a function of the subcooling of the water in the upper plenum because subcooling can quench the steam updraft and cause the CCFL to "breakdown," eliminating the "holdup" of the coolant downflow.

Currently-approved Appendix K LOCA models assume saturated water CCFL conditions and conservatively ignore the inventory buildup of coolant in the upper plenum. Recent large-scale tests confirm that the CCFL "breakdown" can occur soon after spray initiation, causing downflow of the upper plenum inventory and rapid reflooding of the core. Following this, a residual pool of water remains in the upper plenum, ensuring uniform delivery of coolant to the individual fuel bundles.

The present core reflood time from Appendix K models does not model CCFL breakdown or the residual pool in the upper plenum. The effects of saturated CCFL modeled in the REFLOOD model produce an overly conservative estimate of the core reflooding time. If a crack, or cracks, forms in one sparger to the extent that the flow rate through the spray nozzles is reduced, then more injection will occur at the core periphery which will most likely cause localized subcooling and CCFL breakdown. This would reduce the reflooding time for Peach Bottom-2 up to 100 seconds from the value calculated with the standard Appendix K models resulting in PCTs up to 700°F lower.

On the other hand, if no CCFL breakdown occurs, the upper plenum inventory builds up rapidly and ensures no reduction in coolant delivery from the core spray sparger system to the bundle and subsequently no degradation in cooling heat transfer.

In addition to the above conservatisms, the 1973 ANS + 20% decay heat correlation was used in the analysis per Appendix K. The technical community at this

time recognizes that the subsequent 1979 ANS decay heat correlation provides a more realistic basis for evaluating ECCS performance. This decay heat correlation would further reduce calculated steaming rates and CCFL effects, as well as the core heatup rate, which would reduce the calculated PCT an additional 200° to 400°F.

#### 4.3 SENSITIVITY OF LOCA ANALYSIS TO NON UNIFORM SPRAY

For the Peach Bottom plant, there are no single failures for any break location (other than a core spray line break) that can render both core spray systems inoperable. For core spray line break, there are always at least two low pressure ECCS pumps available, ensuring timely reflooding. For medium and large break sizes (which depressurize relatively fast), the most limiting failures are those that result in the least number of emergency core cooling system (ECCS) pumps remaining operable.

The two single-failure candidates that are potentially limiting for medium to large break sizes are:

- A. Diesel Generator Failure - 1 core spray (LPCS) + 1 Low Pressure Coolant Injection (LPCI) + HPCI + the ADS operable
- B. LPCI Injection Valve Failure - 2 core spray + HPCI + the ADS operable

Since the HPCI (High Pressure Coolant Injection) is steam turbine powered, it is not a significant contributor to mitigating medium to large breaks. Also, since the function of the ADS (Automatic Depressurization System) is to depressurize the reactor as a backup to the HPCI, it contributes little toward mitigating medium and large break LOCAs.

Therefore, failure candidates A and B each results in a dependence on only two ECCS.

Per the Reload 5 analysis, failure candidate B (LPCI Injection valve failure) is limiting because of the conservative modeling of CCFL at the fuel assembly upper tie plates, which limits the downflow from the core spray systems and prolongs reactor reflooding.

These two single-failure candidates were re-examined for larger breaks assuming a cracked spray sparger as described in Section 4.2. The limiting single failure, break size and location does not change, since the calculated core uncover and recovery times and the reactor depressurization rates do not change with the methods described in Section 4.2.

For smaller break sizes, the limiting single failure is the high-pressure ECCS (HPCI), since the LOCA transient is a high pressure transient that is limited by the time required to either reflood the reactor with the high pressure system or the time to depressurize the reactor so that the low pressure systems become effective. Furthermore, the effects of CCFL in limiting coolant delivery to the core are not as large at higher reactor pressures. The small break LOCA transient is therefore insensitive to spray cooling and reflooding occurs very rapidly once any one or two of the six low pressure ECCS begin injecting coolant into the reactor vessel.

Only medium and large break LOCAs are significantly affected by core spray sparger cracking, and the effect is only significant with the conservative assumption of no CCFL breakdown in the peripheral bundles coupled with an assumed nonuniform spray distribution.

#### 4.4 ANALYSIS RESULTS

The most limiting fuel type and exposure combination for the limiting LOCA per the Reload 5 analysis results is a calculated PCT of 1965°F. This is for prepressurized 8x8R fuel at an exposure of 20,000 MWd/t and a MAPLHGR of 12.3 kW/ft.

A reanalysis of this limiting case with the unrealistically conservative assumptions discussed in Section 4.2 results in a calculated PCT of 2075°F. Therefore, a maximum increase in PCT of 110°F bounds the effect of a cracked spray sparger for all fuel types and exposures.

A calculation of the maximum PCT for the limiting break with a single failure of a diesel generator using the cracked sparger assumptions of Section 4.2 results in a PCT of less than 1700°F.

## 4.5 CONCLUSIONS

A conservative analysis of the effect of one cracked core spray sparger in the Peach Bottom-2 BWR results in a maximum increase in PCT of 110°F.

Since the Reload 5 analysis shows a minimum margin of 235°F to the 10CFR50 Appendix K limit of 2200°F, the maximum increase in PCT of 110°F can be accommodated with no change in MAPLHGR limit.

Thus, with cracks in one core spray sparger and with the MAPLHGR limits unchanged, Peach Bottom-2 retains a minimum of 125°F margin to the 2200°F PCT limit. This PCT margin is still in excess of the PCT margin taken credit for in the generic study on the effect of increased fission gas at higher exposures (References 4-2 and 4-3).

## 4.6 REFERENCES

- 4-1 SER, O.D. Parr (NRC) to G. G. Sherwood (GE), "Review of General Electric Topical Report NEDO-20566, Amendment 3," June 13, 1978.
- 4-2 R. E. Engel (GE) to T. A. Ippolito (NRC), "Extension of ECCS Performance Limits," MFN-077-81, May 6, 1981.
- 4-3 R. E. Engel (GE) to T. A. Ippolito (NRC), "Additional Information Regarding Extension of ECCS Performance Limits, MFN-102-81, May 28, 1981.

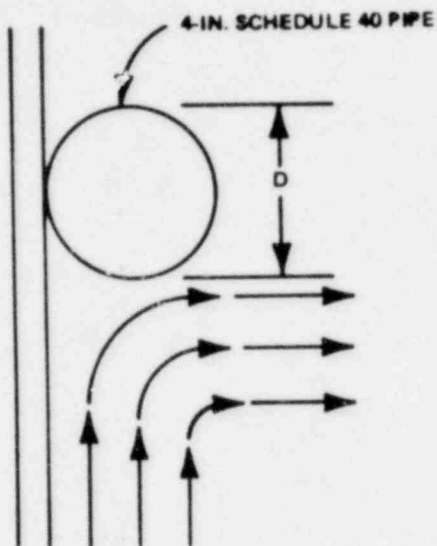
APPENDIX A  
STRUCTURAL ANALYSIS  
OF THE  
PEACH BOTTOM 2 CORE SPRAY SPARGER

Summary

		<u>Stress</u> <u>(lb/in.<sup>2</sup>)</u>
1.	Sparger Pipe	
	Bending - Seismic	853
	(No Break) - Impingement	698
	Bending - Seismic	901
	(Break) - Impingement	737
	Bending - Thermal Mismatch	2980
2.	Nozzle	
	Normal (Weld)	5460
	Shear (Weld)	5700
3.	Bracket (Lower)	
	Normal	5140
	Shear	1502
	Normal (Weld)	3540
	Shear (weld)	633
4.	Bracket (Middle)	
	Normal	9030
	Shear	201
	Normal (Weld)	2233
	Shear (Weld)	215

A.1 DESIGN LOADS

A.1.1 Impingement Loads (to deflect flow 90°)



$$F = P A = \frac{\rho V^2 DL}{g_c}$$

$$\frac{F}{L} = \frac{\rho V^2 D}{g_c}$$

$$\rho = 45.87 \text{ lb/ft}^3 @ 550^\circ\text{F}$$

$$D = \frac{4.5}{12}$$

$$V = 10.0 \text{ ft/sec}^*$$

$$\frac{F}{L} = \frac{45.87 (10.0)^2 (4.5/12)}{32.2}$$

$$\frac{F}{L} = 53.4 \text{ lb/ft} = \underline{\underline{4.45}} \text{ lb/in.}$$

A.1.2 Pressure/Flow Loads

Maximum Flow = 8000 gpm\*\* (Rated Flow = 6250 gpm)

$$Q = 8000 \text{ gal/min} \times \frac{1 \text{ min}}{60 \text{ sec}} \times \frac{\text{ft}^3}{7.48 \text{ gal}}$$

$$= 17.83 \text{ ft}^3/\text{sec}$$

\*Very conservative - more realistic value is ~2 ft/sec.  
 \*\*See page B-5, Appendix B.

- Maximum pressure in sparger arm

$$\Delta P_{\text{meas}} = 29 \text{ psig @ } 6068 \text{ gpm}$$

$$\Delta P_{\text{max}} = 29 \left( \frac{8000}{6068} \right)^2 = \underline{50.4} \text{ psig}$$

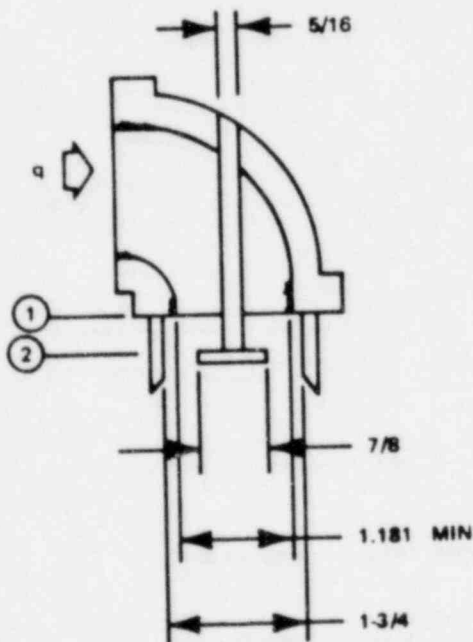
- Pressure load on sparger segment

$$F = \Delta P A \quad A = \frac{\pi}{4} d_i^2 = \frac{\pi}{4} (4.026)^2 = 12.73 \text{ in.}^2$$

$$F_{\text{max}} = 50.4 (12.73) = \underline{642} \text{ lb}$$

- Maximum nozzle flow

The 1-in. VNC nozzle has the highest flow rate and will produce the maximum nozzle thrust.



$$A_1 = \frac{\pi}{4} (1.181^2 - 0.313^2) = 1.018 \text{ in.}^2 \text{ (min.)}$$

$$A_2 = \frac{\pi}{4} (1.75 - 0.375^2) = 1.804 \text{ in.}^2$$

$$\rho = 62.2 \text{ lb/ft}^3 \text{ @ } 80^\circ\text{F}$$

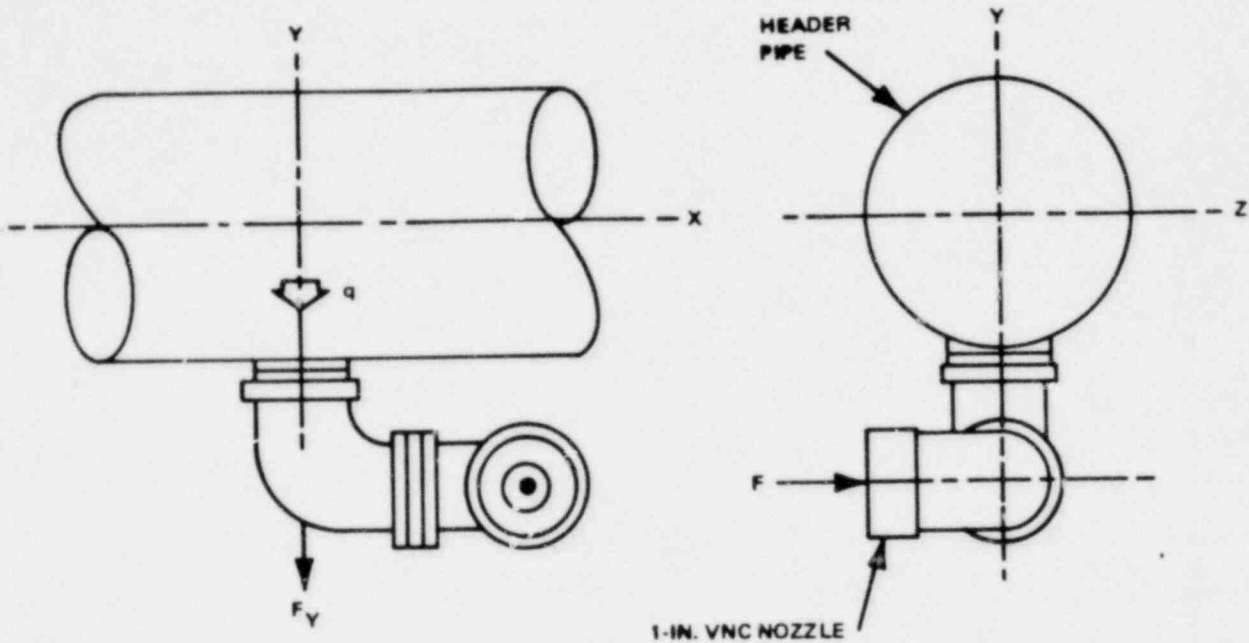
$$q_{\text{max}} = 72 \text{ gpm @ } 6068 \text{ gpm test flow}$$

$$q_{\text{max}} = 72 \left( \frac{8000}{6068} \right) = 95 \text{ gpm}$$

$$W_{\text{max}} = \frac{95(62.2)}{60(7.48)} = \underline{13.2} \text{ lb/sec}$$

$$V_{\text{max}} = \frac{W_{\text{max}}}{\rho A} = \frac{13.2(144)}{62.2(1.018)} = \underline{30} \text{ ft/sec @ nozzle exit}$$

A.1.3 Nozzle Thrust



$$F_y = \Delta P A + \frac{\rho V^2 A}{g}$$

$\Delta P = 25$  psi @ 6068 gpm test flow

$$\Delta P = 25 \left( \frac{8000}{6086} \right)^2 = 43.5 \text{ psi @ runout}$$

$A = \frac{\pi}{4} d^2$ , where  $d = 1.181$  in. (the minor dia. of 1-in. straight internal threads)

$$A = \frac{\pi}{4} (1.181)^2 = 1.095 \text{ in.}^2$$

$$V = \frac{W_{\max}}{\rho A} = \frac{13.2(144)}{62.2(1.095)} = 28 \text{ ft/sec @ exit from header}$$

$$F_y = 43.5(1.095) + \frac{62.2(28)^2(1.095)}{32.2(144)} = \underline{\underline{60}} \text{ lb}$$

$$F_z = \frac{\rho V^2 A}{g} + \Delta P A \quad V = 30 \text{ ft/sec (see Section A.1.2)}$$

$$F_z = \frac{62.2(30)^2(1.018)}{32.2(144)} = \underline{\underline{12.3 \text{ lb}}}$$

A.1.4 Weight

4-in. Schedule 40 pipe

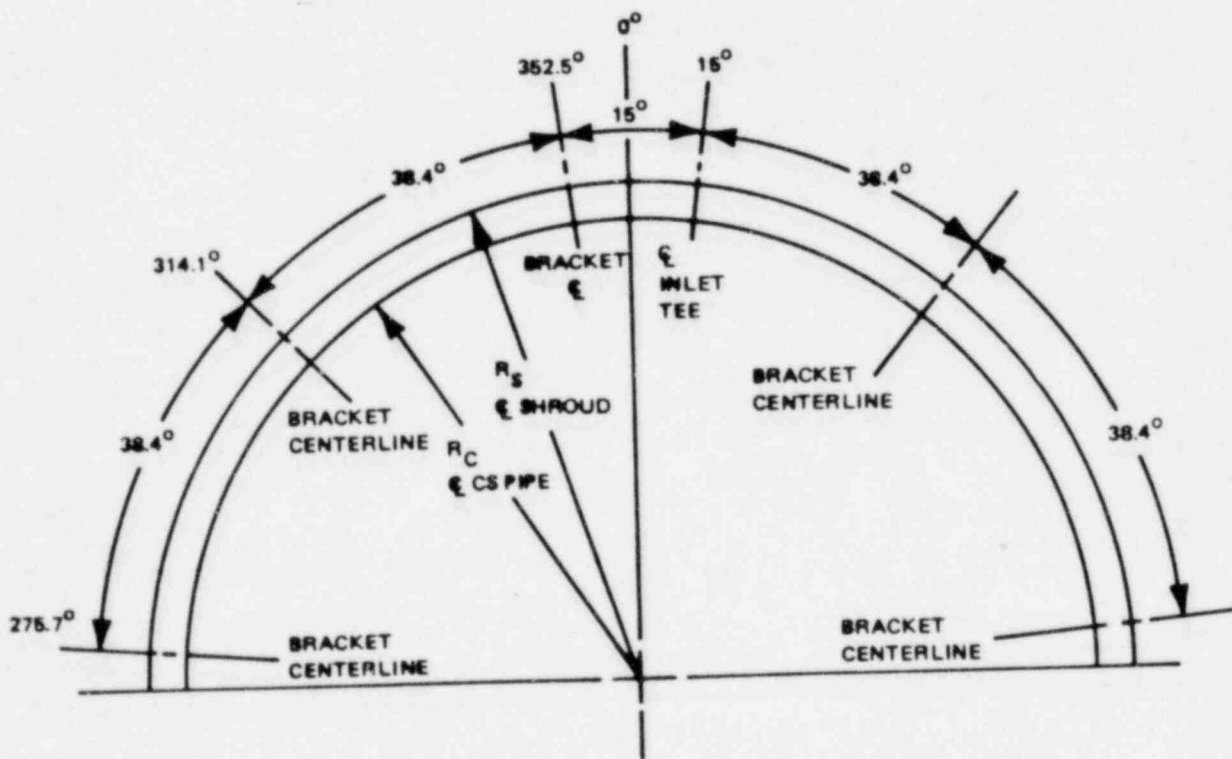
$$W_{\text{pipe}} = 10.8 \text{ lb/ft}$$

$$W_{\text{water}} = 5.5 \text{ lb/ft}$$

$$W = 10.8 + 5.5 = 16.3 \text{ lb/ft}$$

$$= \frac{16.3}{12} = \underline{\underline{1.36 \text{ lb/in.}}}$$

A.1.5 Mismatch Due to Thermal Expansion



$$R_s = \frac{216}{2} + \frac{1.5}{2} = 108.75 \text{ in.}$$

$$R_c = \frac{216}{2} - \frac{4.5}{2} = 105.75 \text{ in.}$$

$$\left. \begin{array}{l} \text{Shroud} = 550^\circ\text{F} \\ \text{CS Pipe} = 198^\circ\text{F} \\ \hline \Delta T = 352^\circ\text{F} \end{array} \right\} \text{ (See page B-2, Appendix B)}$$

$$\Delta R = \alpha R \Delta T \quad \alpha = 9.6 \times 10^{-6} \text{ in./in.}^\circ\text{F for SST}$$

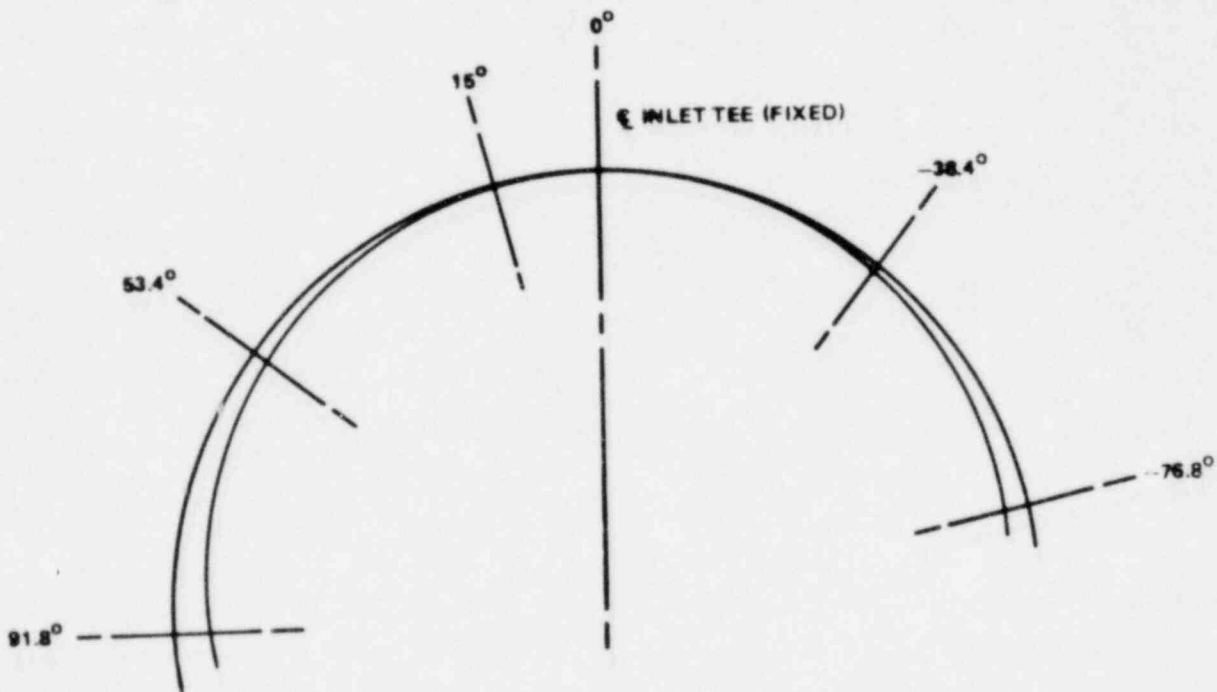
$$R = \frac{216}{2} = 108 \text{ in. at shroud-to-pipe interface}$$

For 90° arc . . .

$$\Delta R_{90^\circ} = 9.6 \times 10^{-6} (108)(352) = 0.365 \text{ in.}$$

For segment assume . . .

$$\Delta R = \Delta R_{90^\circ} (1 - \cos\theta) = 0.365 (1 - \cos\theta)$$



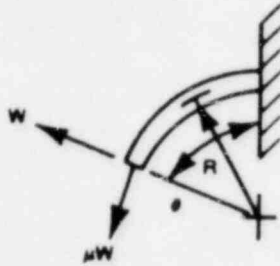
$$\Delta R_{15^\circ} = 0.365 (1 - \cos 15^\circ) = 0.0124 \text{ in.}$$

$$\Delta R_{53.4^\circ} = 0.365 (1 - \cos 53.4^\circ) = 0.1474 \text{ in.}$$

$$\Delta R_{91.8^\circ} = 0.365 (1 - \cos 91.8^\circ) = 0.3765 \text{ in.}$$

$$\Delta R_{-38.4^\circ} = 0.365 (1 - \cos 38.4^\circ) = 0.0790 \text{ in.}$$

$$\Delta R_{-76.8^\circ} = 0.365 (1 - \cos 76.8^\circ) = 0.2817 \text{ in.}$$



Assume the  $\Delta R$  is resisted only by each bracket support in turn:

$$\Delta R = \frac{WR^3}{4EI} (2\theta - \sin 2\theta) - \frac{\mu WR^3}{4EI} (\cos 2\theta - 4 \cos \theta + 3)$$

$$W = \frac{4EI\Delta R}{R^3 (2\theta - \sin 2\theta - \mu \cos 2\theta + 4 \mu \cos \theta - 3\mu)}$$

$$E = 28 \times 10^6 \text{ lb/in.}^2 \quad R = R_c = 105.75 \text{ in.}$$

$$I = \frac{\pi}{64} (4.5^4 - 4.026^4) = 7.23 \text{ in.}^4$$

$$\mu = 0.2 \text{ (coefficient of friction)}$$

$$W = \frac{4(28 \times 10^6)(7.23)\Delta R}{(105.75)^3 (2\theta - \sin 2\theta - 0.2 \cos 2\theta + 0.8 \cos \theta - 0.6)}$$

$$W = \frac{684.7 \Delta R}{(2\theta - \sin 2\theta - 0.2 \cos 2\theta + 0.8 \cos \theta - 0.6)}$$

$$W_{15^\circ} = \frac{684.7(0.0124)}{\left(2\pi \times \frac{15}{180} - \sin 30^\circ - 0.2 \cos 30^\circ + 0.8 \cos 15^\circ - 0.6\right)} = \underline{367 \text{ lb}}$$

$$W_{53.4^\circ} = \frac{684.7(0.1474)}{\left(2\pi \times \frac{53.4}{180} - \sin 106.8^\circ - 0.2 \cos 106.8^\circ + 0.8 \cos 53.4^\circ - 0.6\right)}$$

$$= \underline{120 \text{ lb}}$$

$$W_{91.8^\circ} = \frac{684.7(0.3765)}{\left(2\pi \times \frac{91.8}{180} - \sin 183.6^\circ - 0.2 \cos 183.6^\circ + 0.8 \cos 91.8^\circ - 0.6\right)}$$

$$= \underline{91 \text{ lb}}$$

$$W_{-38.4^\circ} = \frac{684.7(0.0790)}{\left(2\pi \times \frac{38.4}{180} - \sin 76.8^\circ - 0.2 \cos 76.8^\circ + 0.8 \cos 38.4^\circ - 0.6\right)}$$

$$= \underline{155 \text{ lb}}$$

$$W_{-76.8^\circ} = \frac{684.7(0.2817)}{\left(2\pi \times \frac{76.8}{180} - \sin 153.6^\circ - 0.2 \cos 153.6^\circ + 0.8 \cos 76.8^\circ - 0.6\right)}$$

$$= \underline{96 \text{ lb}}$$

#### A.1.6 Flow-Induced Vibration - Natural Frequency

The vortex shedding frequency,  $f_n$ , is given by:

$$\frac{f_v D}{V} = 0.21$$

$V =$  velocity past the shroud wall = 10 ft/sec\*

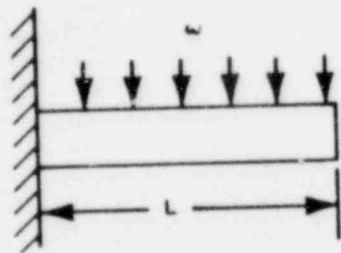
$D =$  sparger pipe diameter =  $\frac{4.5}{12}$  ft

$$f_v = \frac{0.21(10)}{4.5/12} = 5.6 \text{ Hz}$$

General Electric design basis requires natural frequency:

$$f_n \geq 3 f_v$$

Calculate the natural frequency of the unsupported sparger segment. Assume the segment acts as a cantilever and has a uniform load,  $\omega$  (lbs per unit length):



$$f_n = \frac{K_n}{2\pi} \sqrt{\frac{EIg}{\omega L^4}}$$

$$K_n = 3.52$$

$$E = 25.75 \times 10^6 \text{ lb/in.}^2 \quad I = 7.23 \text{ in.}^4 \quad g = 32.2 \text{ ft/sec}^2$$

$$L = \frac{15}{180} \times \pi \times 105.75 = 28 \text{ in. (distance from crack to nearest support bracket)}$$

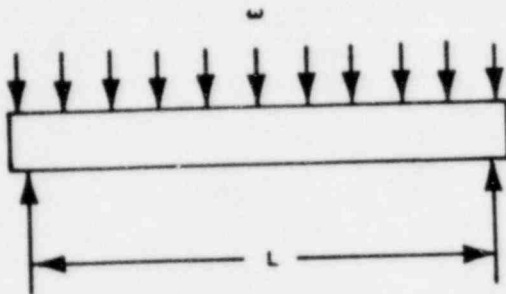
$$\omega = 1.36 \text{ lb/in. (Section A.1.4)}$$

$$f_n = \frac{3.52}{2\pi} \sqrt{\frac{25.75 \times 10^6 (7.23) (32.2) (12)}{1.36 (28)^4}} = 167 \text{ Hz}$$

$$\text{Ratio} = \frac{f_n}{f_v} = \frac{167}{5.6} > 3$$

\*Very conservative - more realistic value is ~2 ft/sec.

Calculate the natural frequency of the sparger by examining the longest segment between support brackets. Assume this section has a uniform load,  $\omega$ , and both ends are simply supported:



$$f_n = \frac{K_n}{2\pi} \sqrt{\frac{EIg}{\omega L^4}}$$

$$K_n = 9.87$$

$$I = 7.23 \text{ in.}^4$$

$$E = 25.75 \times 10^6 \text{ lb/in.}^2 \quad g = 32.2 \text{ ft/sec}^2$$

$$L = \frac{38.4}{180} \times \pi \times 105.75 = 71 \text{ in.}$$

$$\omega = 1.36 \text{ lb/in.}$$

$$f_n = \frac{9.87}{2\pi} \sqrt{\frac{25.75 \times 10^6 (7.23) (32.2) (12)}{1.36 (71)^4}} = 72 \text{ Hz}$$

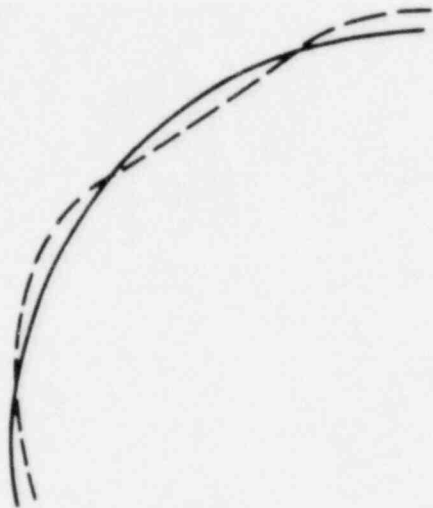
$$\text{Ratio} = \frac{f_n}{f_v} = \frac{72}{5.6} > 3$$

Calculate the natural frequency of the sparger by examining the longest segment between support brackets ignoring an intermediate support. This case is the same as the above case except that  $L = 2 \times 71 = 142$  inches.

$$f_n = \frac{72}{2^2} = 18 \text{ Hz}$$

$$\text{Ratio} = \frac{f_n}{f_v} = \frac{18}{5.6} > 3$$

Calculate the natural frequency of the sparger by considering the sparger arm as a "free-free" beam (or floating ship). Assume the arm has a uniform load,  $\omega$ , and is free to rotate at the three support brackets as shown below:



$$f_n = \frac{K_n}{2\pi} \sqrt{\frac{EIg}{\omega L^4}}$$

$$K_n = K_2 = 61.7$$

$$E = 25.75 \times 10^6 \text{ lb/in.}^2$$

$$I = 7.23 \text{ in.}^4 \quad g = 32.2 \text{ ft/sec}^2$$

$$\omega = 1.36 \text{ lb/in.}$$

$$L = \frac{97.5}{180} \times \pi \times 105.75 = 180 \text{ in.}$$

$$f_n = \frac{61.7}{2\pi} \sqrt{\frac{25.75 \times 10^6 (7.23) (32.2) (12)}{1.36 (180)^4}} = 70 \text{ Hz}$$

$$\text{Ratio} = \frac{f_n}{f_v} = \frac{70}{5.6} > 3$$

## A.2 STRESSES DURING NORMAL OPERATION AND DURING CORE SPRAY INJECTION

### A.2.1 Sparger Pipe

#### A.2.1.1 Impingement Load and Seismic

##### Impingement Only

$$\omega_i = -4.45 \text{ lb/in. (upward) (Section A.1.1)}$$

Seismic Only - Assume 3g (Very Conservative)

$$\omega_s = \omega \pm 3\omega \quad \omega = 1.36 \text{ lb/in. (Section A.1.4)}$$

$$\omega_s = 1.36 - 3(1.36) = -2.72 \text{ lb/in. (upward)}$$

$$\omega_s = 1.36 + 3(1.36) = 5.44 \text{ lb/in. (downward)}$$

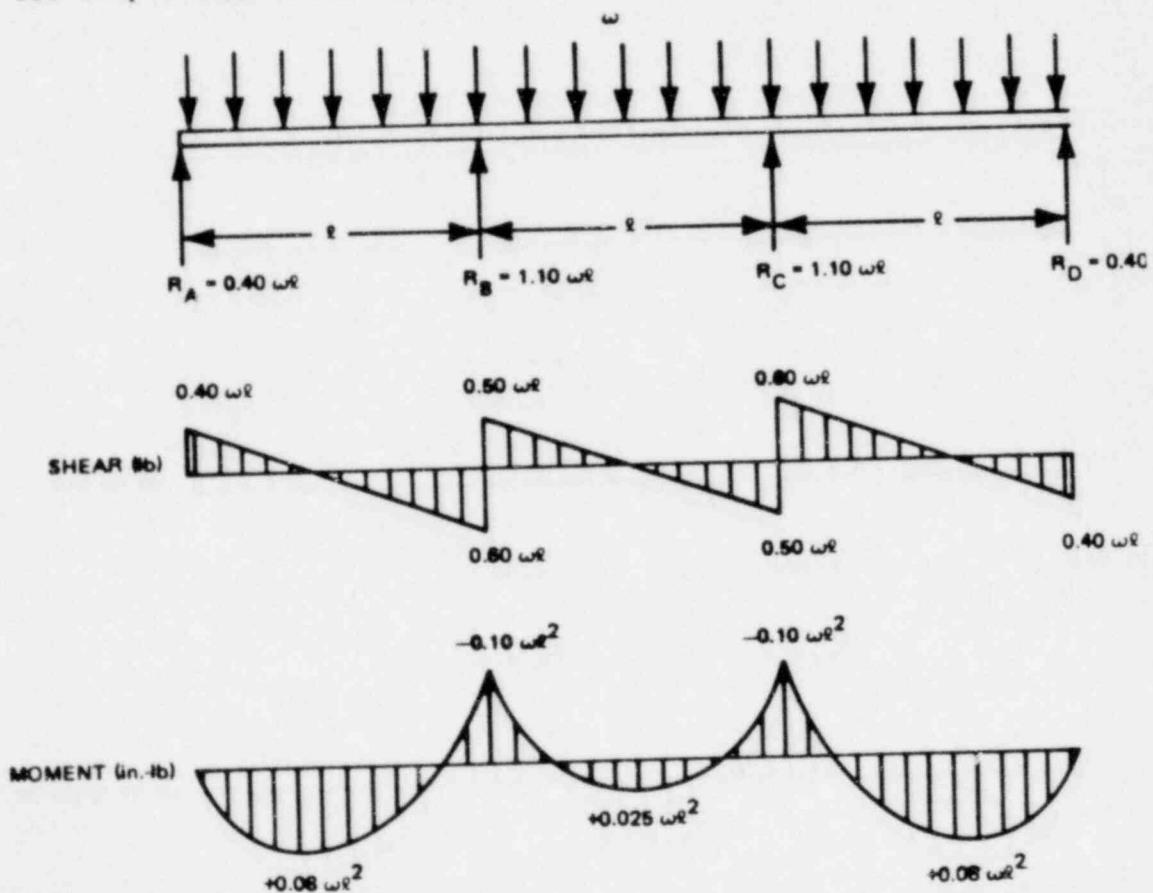
Impingement + Seismic

$$\omega_T = -4.45 - 2.72 = -7.17 \text{ lb/in. (upward)}$$

$$\omega_T = -4.45 + 5.44 = 0.99 \text{ lb/in. (downward)}$$

Assume No Break

For simplicity, assume continuous beam - three equal spans.



$$\ell = \frac{38.4}{180} \times \pi \times 105.75 = 71 \text{ in.}$$

$$M_{\max} = 0.10(5.44)(71)^2 = 2742 \text{ in.-lb}$$

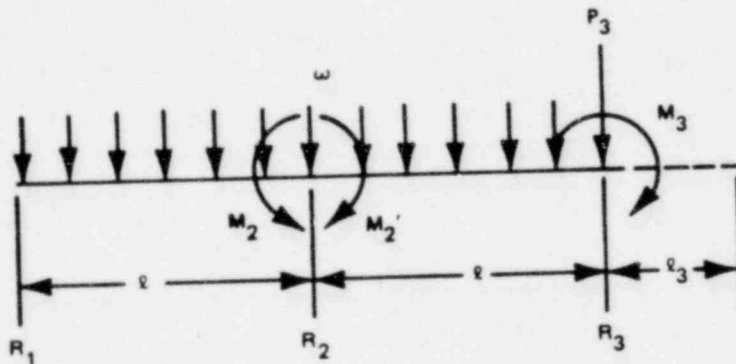
$$\sigma = \frac{Mc}{I} \quad I = 7.23 \text{ in.}^4 \quad c = \frac{4.5}{2} = 2.25 \text{ in.}$$

$$\sigma_{\max} = \frac{2742(2.25)}{7.23} = \underline{\underline{853}} \text{ lb/in.}^2 \text{ (Seismic)}$$

$$\sigma_{\max} = 853 \left( \frac{4.45}{5.44} \right) = \underline{\underline{698}} \text{ lb/in.}^2 \text{ (Impingement)}$$

Assume Break

Assume two equals spans, uniformly loaded with end moment  $M_3$  and force  $P_3$  at the third support.



From the theorem of three moments . . .

$$\frac{M_1 \ell_1}{I_1} + 2M_2 \left( \frac{\ell_1}{I_1} + \frac{\ell_2}{I_2} \right) + \frac{M_3 \ell_2}{I_2} = \frac{\omega_1 \ell_1^2}{4I_1} + \frac{\omega_2 \ell_2^3}{4I_2}$$

$$M_1 = 0 \quad \ell_1 = \ell_2 \quad I_1 = I_2 \quad \omega_1 = \omega_2$$

$$\frac{4M_2 \ell}{I} + \frac{M_3 \ell}{I} = \frac{\omega \ell^3}{2I}$$

$$M_2 = \frac{\omega \ell^2}{8} - \frac{M_3}{4}$$

$M_3$  is caused by the cantilevered section of pipe between the support bracket and the break:

$$M_3 = \frac{\omega \ell_3^2}{2}$$

Likewise,  $P_3$  is caused by the cantilevered section:

$$P_3 = \omega \ell_3$$

For Seismic . . .

$$\omega = 5.44 \text{ lb/in.} \quad \ell_3 = 28 \text{ in.} \quad \ell = 71 \text{ in.}$$

$$P_3 = 5.44(28) = 152 \text{ lb}$$

$$M_3 = \frac{5.44(28)^2}{2} = 2132 \text{ in.-lb}$$

$$M_2 = \frac{5.44(71)^2}{8} - \frac{2132}{4} = 2895 \text{ in.-lb (max)}$$

$$\sigma = \frac{Mc}{I} \quad I = 7.23 \text{ in.}^4 \quad c = \frac{4.5}{2} = 2.25 \text{ in.}$$

$$\sigma_{\text{max}} = \frac{2895(2.25)}{7.23} = 901 \text{ lb/in.}^2$$

For Impingement . . .

$$\omega = |-4.45| = 4.45 \text{ lb/in.}$$

$$P_3 = 152 \left( \frac{4.45}{5.44} \right) = 125 \text{ lb}$$

$$M_3 = 2132 \left( \frac{4.45}{5.44} \right) = 1744 \text{ in.-lb}$$

$$M_2 = 2895 \left( \frac{4.45}{5.44} \right) = 2368 \text{ in.-lb}$$

$$\sigma_{\max} = 2368 \left( \frac{2.25}{7.23} \right) = 737 \text{ lb/in.}^2$$

Determine reaction loads for seismic + impingement:

$$\omega = 7.17 \text{ lb/in.}$$

$$R_3 = P_3 + \frac{\omega \ell}{2} + \frac{M_3}{\ell} - \frac{M_2}{\ell} = 201 + \frac{7.17(71)}{2} + \frac{2811}{71} - \frac{3815}{71} = 441 \text{ lb}$$

$$R_1 = \frac{\omega \ell}{2} - \frac{M_2}{\ell} = \frac{7.17(71)}{2} - \frac{3815}{71} = 201 \text{ lb}$$

$$R_2 = \omega \ell + 2 \frac{M_2}{\ell} - \frac{M_3}{\ell} \quad (M_2' = M_2) = 7.17(71) + 2 \frac{3815}{71} - \frac{2811}{71} = 577 \text{ lb}$$

$$\left. \begin{array}{l} R_1 + R_2 + R_3 = 1219 \text{ lb} \\ \omega (2\ell + \ell_3) = 1219 \text{ lb} \end{array} \right\} \text{ checks}$$

#### A.2.1.2 Differential Pressure

$$\Delta P_{\max} = 50.4 \text{ psi}$$

$$R_o = 4.5/2 = 2.25 \text{ in.}$$

$$R_i = 4.026/2 = 2.013 \text{ in.}$$

$$t_{\text{nom.}} = 0.237$$

$$t_{\text{min.}} = 0.237 - 2[0.003 \text{ (corrosion allowance)}] = 0.231 \text{ in.}$$

- Hoop Stress

$$\sigma = \frac{PR_i}{t} = \frac{50.4(2.013)}{0.231} = 440 \text{ lb/in.}^2$$

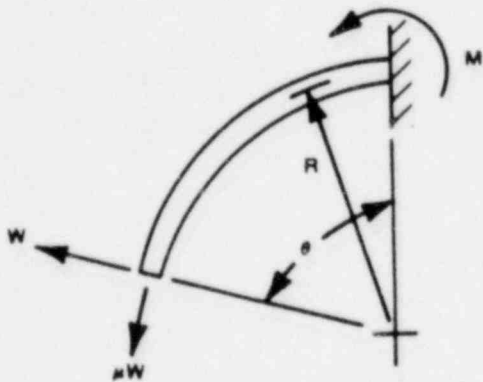
- Axial Stress

$$\sigma = \frac{PR_i}{2t} = \frac{440}{2} = 220 \text{ lb/in.}^2$$

### A.2.1.3 Mismatch Due to Thermal Expansion

$$M = WR \sin\theta - \mu WR (1 - \cos\theta)$$

$$= WR [\sin\theta - \mu(1 - \cos\theta)]$$



Assume  $\mu = 0.2$  (Coefficient of friction)

$$R = 105.75 \text{ in.}$$

See Section A.1.5 for loads at each bracket:

- 15° Bracket

$$M_{15^\circ} = 360(105.75) [\sin 15^\circ - 0.2(1 - \cos 15^\circ)]$$

$$= \underline{9590} \text{ in.-lb (Maximum)}$$

- 53.4° Bracket

$$M_{53.4} = 111(105.75) [\sin 53.4^\circ - 0.2(1 - \cos 53.4^\circ)]$$

$$= 8580 \text{ in.-lb}$$

- 91.8° Bracket

$$M_{91.8^\circ} = 79(105.75) [\sin 91.8^\circ - 0.2(1 - \cos 91.8^\circ)]$$

$$= 6630 \text{ in.-lb}$$

- -38.4° Bracket

$$M_{-38.4^\circ} = 147(105.75) [\sin 38.4 - 0.2(1 - \cos 38.4^\circ)]$$

$$= 8980 \text{ in.-lb}$$

- -76.8° Bracket

$$M_{-76.8^\circ} = 86(105.75) [\sin 76.8^\circ - 0.2(1 - \cos 76.8^\circ)]$$

$$= 7450 \text{ in.-lb}$$

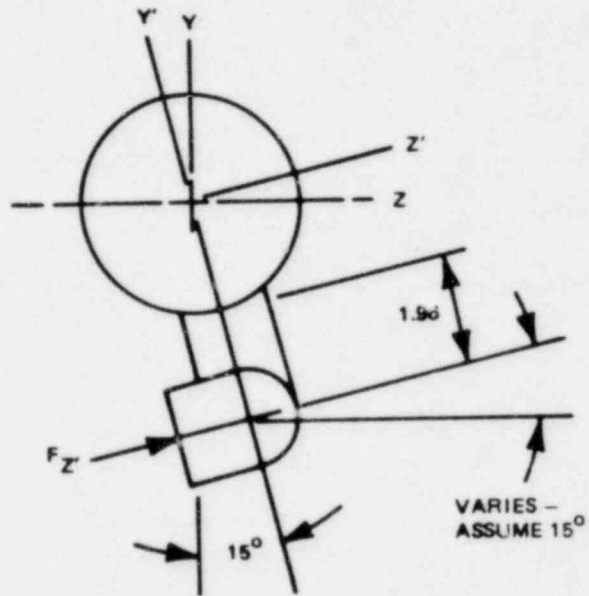
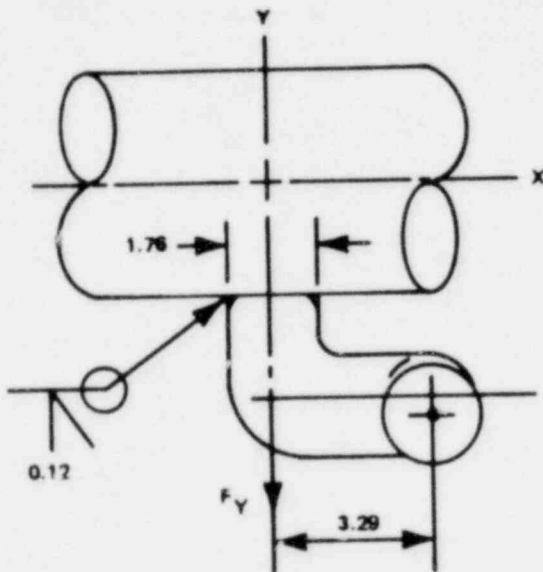
$$\sigma_{\max} = \frac{Mc}{I} \quad c = \frac{4.5}{2} = 2.25 \text{ in.}$$

$$I = 7.23 \text{ in.}^4$$

$$\sigma_{\max} = \frac{9590(2.25)}{7.23} = \underline{2980} \text{ lb/in.}^2$$

A.2.2 Nozzles

A.2.2.1 Nozzle Thrust



Weld properties:

$$I = \frac{\pi}{64} (1.76^4 - 1.52^4) = 0.209 \text{ in.}^4$$

$$K = \frac{\pi}{32} (1.76^4 - 1.52^4) = 0.418 \text{ in.}^4$$

$$A = \frac{\pi}{4} (1.76^2 - 1.52^2) = 0.618 \text{ in.}^2$$

$$c = \frac{1.76}{2} = 0.88 \text{ in.} \quad t = 0.12 \text{ in.} \quad r = \frac{1.76}{2} = 0.88 \text{ in.}$$

Loads:

$$F_y = 60 \text{ lb} \quad f_z = 12.3 \text{ lb} \quad (\text{See Section A.1.3})$$

$$P = 43.5 \text{ psi}$$

The resulting loads at the weld are . . .

$$F_{\text{axial}} = F_y = 60 \text{ lb}$$

$$F_{\text{shear}} = F_z' = 12.3 \text{ lb}$$

$$T_{\text{torsion}} = 3.29 F_z' = 3.29(12.3) = 40.5 \text{ in.-lb}$$

$$M_{\text{moment}} = 1.96 F_z' = 1.96(12.3) = 24.1 \text{ in.-lb}$$

The stresses are conservatively calculated as . . .

$$\sigma_y = \pm \frac{M_m c}{I} + \frac{F_a}{A} + \frac{Pr}{2t} = \pm \frac{24.1(0.88)}{0.209} + \frac{60}{0.618} + \frac{4.35(0.88)}{2(0.12)}$$

$$= \pm 101 + 97 + 160 \text{ lb/in.}^2$$

$$\sigma_y = \underline{358} \text{ lb/in.}^2, 156 \text{ lb/in.}^2$$

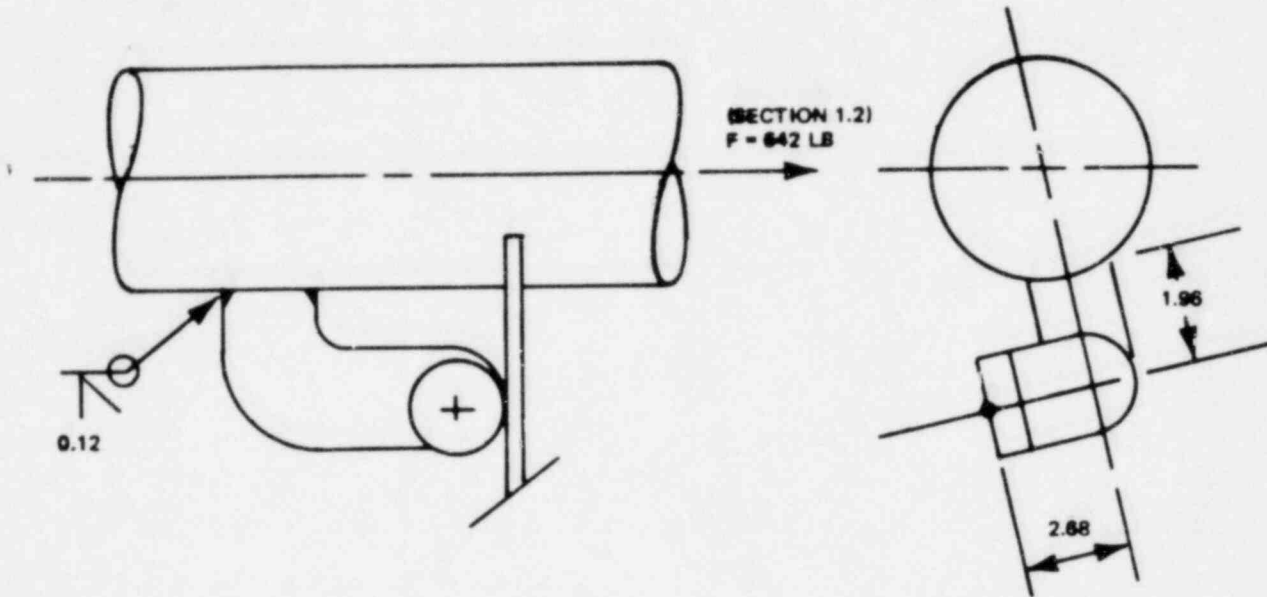
$$\tau_{xy} = \frac{T_t c}{K} + \alpha \frac{F_s}{A} \quad \alpha = 2 \text{ (thin wall cyl.)}$$

$$= \frac{40.5(0.88)}{0.418} + 2 \frac{12.3}{0.618} = 85 + 40$$

$$\tau_{xy} = \underline{125} \text{ lb/in.}^2$$

A.2.2.2 Differential Pressure

Assume 360° break, nozzle loaded by bracket.



The resulting loads at the weld are . . .

$$F_{\text{shear}} = F = 642 \text{ lb}$$

$$T_{\text{torsion}} = 2.68F = 2.68(642) = 1720 \text{ in.-lb}$$

$$M_{\text{moment}} = 1.96F = 1.96(642) = 1260 \text{ in.-lb}$$

The stresses are conservatively calculated as . . .

$$\sigma_y = \pm \frac{M_m c}{I} + \frac{Pr}{2t} = \pm \frac{1260(0.88)}{0.209} + \frac{43.8(0.88)}{2(0.12)} = \pm 5300 + 160$$

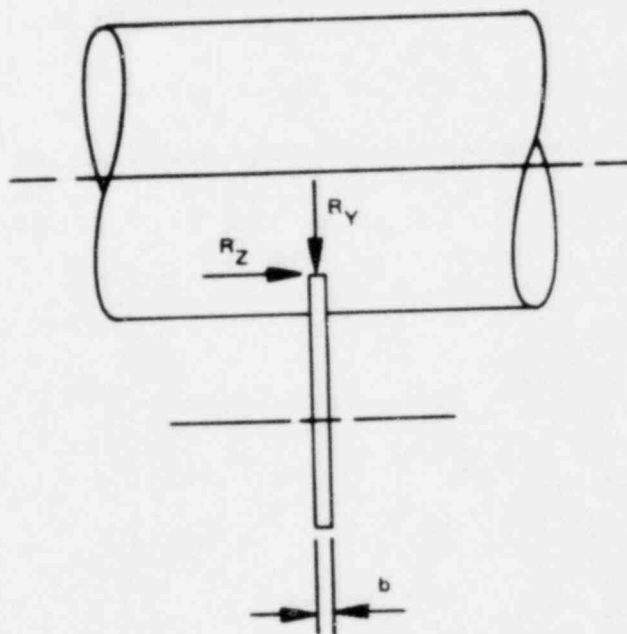
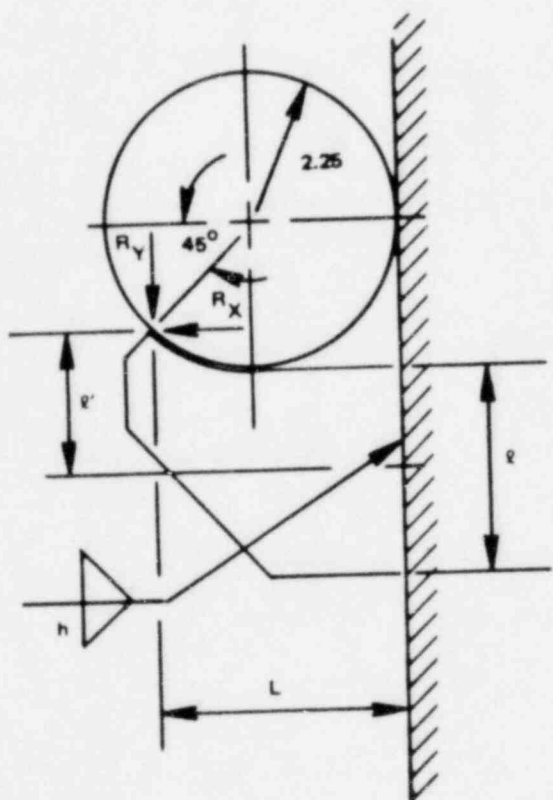
$$\sigma_y = -5,140 \text{ lb/in.}^2, \underline{5,460} \text{ lb/in.}^2$$

$$\tau_{xy} = \frac{T_t c}{K} + \alpha \frac{F_s}{A} \quad \alpha = 2.0$$

$$= \frac{1720(0.88)}{0.418} + 2 \frac{642}{0.618} = 3,620 + 2,080$$

$$\tau_{xy} = \underline{\underline{5,700}} \text{ lb/in.}^2$$

A.2.3 Bracket (Lower)



LOWER BRACKET

$$r = 3.26 \text{ in} \quad L = (1 + \cos 45^\circ)(2.25) = 3.84 \text{ in.}$$

$$r' = \frac{3.26}{2} + (1 - \sin 45^\circ)(2.25) = 2.29 \text{ in.}$$

$$b = 0.38 \text{ in} \quad h = 0.25 \text{ in.}$$

## A.2.3.1 Seismic and Impingement

$$R_y = 577 \text{ lb} \quad R_x = 0 \quad R_z = 0 \quad (\text{Section A.2.1.1})$$

(Conservatism - Uses highest bracket load at weakest bracket and assumes seismic and impingement downward.)

Maximum stresses in the fillet weld . . .

$$\tau_{\text{Avg}} = \frac{\sqrt{2}}{2} \frac{R_y}{h\ell} = \frac{\sqrt{2}}{2} \frac{(577)}{0.25(3.26)} = \underline{\underline{501}} \text{ lb/in.}^2$$

$$\sigma_{\text{Bending}} = \frac{3\sqrt{2} M}{h \ell^2} = \frac{3\sqrt{2} L R_y}{h \ell^2} = \frac{3\sqrt{2} (3.84)(577)}{0.25(3.26)^2} = \underline{\underline{3540}} \text{ lb/in.}^2$$

## A.2.3.2 Mismatch Due to Thermal Expansion

$$\left. \begin{array}{l} R_x = 367 \text{ lb} \\ R_y = 0 \\ R_z = \mu R_x = 0.2(367) = 73.4 \text{ lb} \end{array} \right\} (\text{Section A.1.5})$$

Maximum shear stress in the fillet weld is . . .

$$\tau = \frac{\sqrt{2}}{2} \frac{R_x + R_z}{h\ell} + \frac{\sqrt{2}}{2} \frac{M}{(b+h)(\ell-h)h}$$

where

$$M = \ell R_z$$

$$\tau = \frac{\sqrt{2}}{2} \frac{(367 + 73.4)}{0.25(3.26)} + \frac{\sqrt{2}}{2} \frac{2.29(73.4)}{(0.38 + 0.25)(3.26 - 0.25)(0.25)}$$

$$\pi = 382 + 251 = \underline{\underline{633}} \text{ lb/in.}^2$$

Maximum normal stress in weld is . . .

$$\sigma_{\max} = \frac{\sqrt{2} R_x}{2 h \ell} + \frac{R_z}{h \ell (b + h)} \sqrt{2L^2 + \frac{(b + h)^2}{2}} + \frac{3\sqrt{2} M}{h \ell^2}$$

where

$$M = \ell' R_x$$

$$\sigma_{\max} = \frac{\sqrt{2}}{2} \frac{(367)}{0.25(3.26)} + \frac{3\sqrt{2} (2.29)(367)}{0.25(3.26)^2} + \frac{73.4}{0.25(3.26)(0.38 + 0.25)} \sqrt{2(3.84)^2 + \frac{(0.38 + 0.25)^2}{2}}$$

$$\sigma_{\max} = 318 + 1342 + 779 = \underline{\underline{2439}} \text{ lb/in.}^2$$

Maximum normal stress in the plate is . . .

$$\sigma_{\max} = \frac{R_x}{A} + \frac{\ell' R_x C_{xy}}{I_{xy}} + \frac{LR_z C_{zx}}{I_{zx}}$$

$$A = 0.38(3.26) = 1.24 \text{ in.}^2$$

$$I_{xy} = \frac{b \ell^3}{12} = \frac{0.38(3.26)^3}{12} = 1.097 \text{ in.}^4$$

$$C_{xy} = \frac{3.26}{2} = 1.63 \text{ in.}$$

$$I_{zx} = \frac{\ell b^3}{12} = \frac{3.26(0.38)^3}{12} = 0.01491 \text{ in.}^4$$

$$C_{zx} = \frac{0.38}{2} = 0.19$$

$$\sigma_{\max} = \frac{367}{1.24} + \frac{2.29(367)(1.63)}{1.097} + \frac{3.84(73.4)(0.19)}{0.01491} = 300 + 1250 + 3590$$

$$\sigma_{\max} = \underline{\underline{5140}} \text{ lb/in.}^2$$

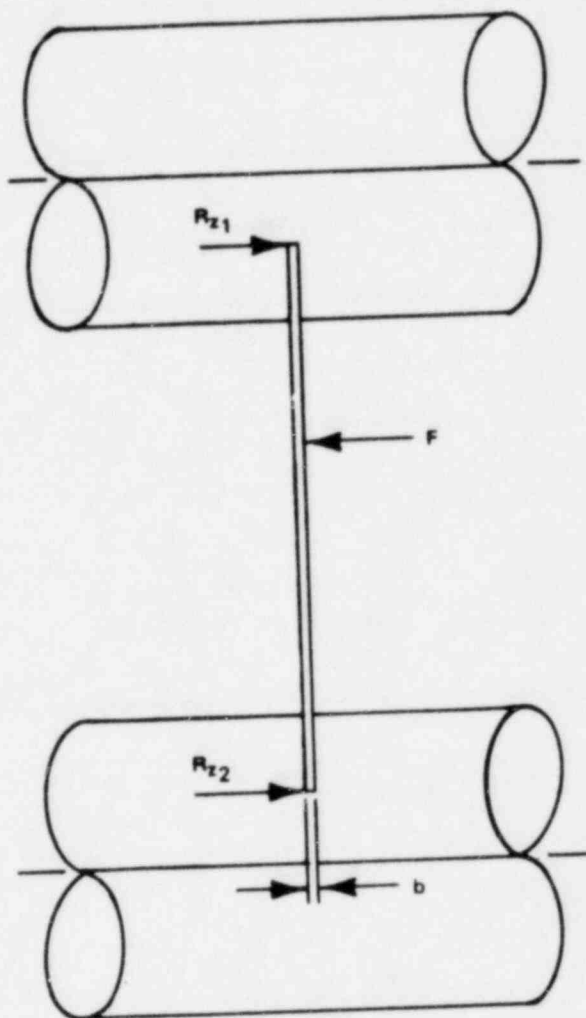
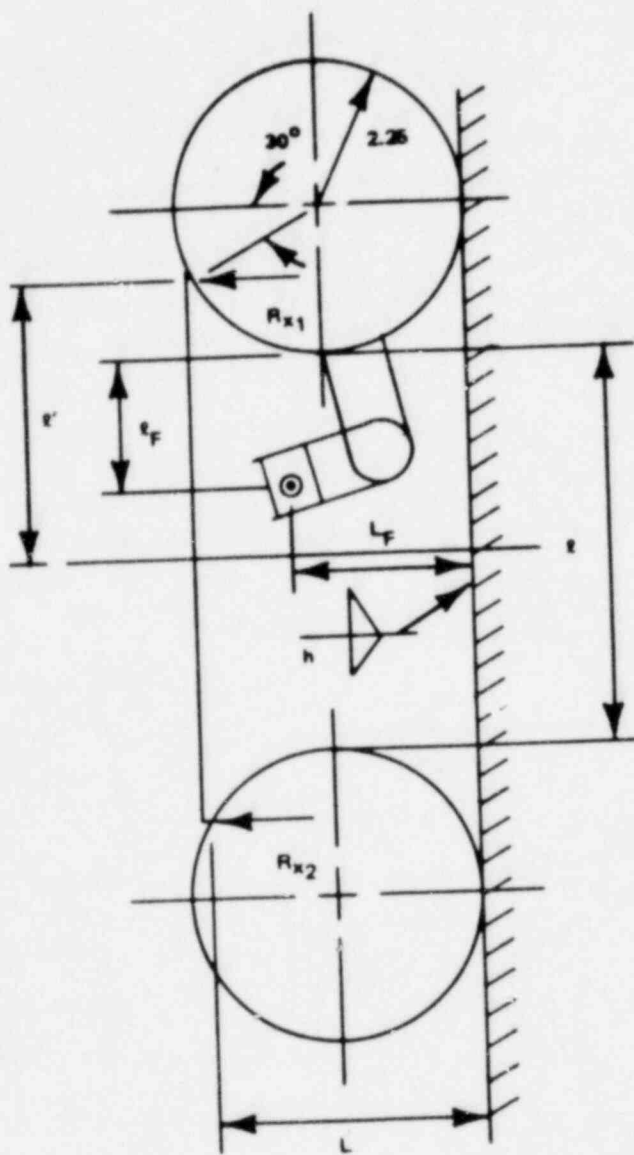
Maximum shear stress in plate is . . .

$$\tau = \frac{R_x + R_z}{bl} + \frac{l^2 R_z (3l + 1.8b)}{l^2 b^2} = \frac{367 + 73.4}{0.38(3.26)}$$

$$+ \frac{2.29(73.4)(3 \times 3.26 + 1.8 \times 0.38)}{(3.26)^2(0.38)^2}$$

$$\tau = 356 + 1146 = \underline{\underline{1502}} \text{ lb/in.}^2$$

A.2.4 Bracket (Middle)



$$l = 12.12 - 2(2.25) = 7.62 \text{ in.} \quad b = 0.38 \text{ in.}$$

$$r' = \frac{7.62}{2} + (1 - \sin 30^\circ)(2.25) = 4.94 \text{ in.} \quad h = 0.25 \text{ in.}$$

$$L = (1 + \cos 30^\circ)(2.25) = 4.20 \text{ in.}$$

$$l_F = (2.25 + 1.96) \cos 15^\circ + (1.50 + 1.18) \sin 15^\circ - 2.25 = 2.51 \text{ in.}$$

$$L_F = 2.25 - (2.25 + 1.96) \sin 15^\circ + \left(1.50 + \frac{1.18}{2}\right) \cos 15^\circ$$

$$L_F = 3.18 \text{ in.}$$

## A.2.4.1 Pressure Load Only

$$F = 642 \text{ lb} \quad (\text{Section A.1.2})$$

Shear Stress (Neglect torsion - small)

$$\tau_{\text{Avg}} = \frac{\sqrt{2} F}{2 h \ell} = \frac{\sqrt{2} (642)}{2 (0.25)(7.62)} = 238 \text{ lb/in.}^2 \text{ (Weld)}$$

$$\tau_{\text{Avg}} = \frac{F}{b \ell} = \frac{642}{0.38(7.62)} = 222 \text{ lb/in.}^2 \text{ (Bracket)}$$

Stress Due to Bending

$$\begin{aligned} \sigma_{\text{max}} &= \frac{F}{h \ell (b + h)} \sqrt{2L_F^2 + \frac{(b + h)^2}{2}} \\ &= \frac{642}{0.25(7.62)(0.38 + 0.25)} \sqrt{2(3.18)^2 + \frac{(0.38 + 0.25)^2}{2}} \end{aligned}$$

$$\sigma_{\text{max}} = 2420 \text{ lb/in.}^2 \text{ (Weld)}$$

$$\sigma_{\text{max}} = \frac{Mc}{I} \quad c = \frac{0.38}{2} = 0.19 \text{ in.}$$

$$I = \frac{\ell b^3}{12} = \frac{7.62(0.38)^3}{12} = 0.03484 \text{ in.}^4$$

$$M = (L_F - h) F$$

$$\sigma_{\max} = \frac{(3.18 - 0.25)(642)(0.19)}{0.03484} = \underline{10,260} \text{ lb/in.}^2 \text{ (Bracket)}$$

#### A.2.4.2 Mismatch Due to Thermal Expansion Only

Assume:

$$R_{x_1} = R_{x_2} = 155 \text{ lb (Section A.1.5)}$$

$$R_{z_1} = R_{z_2} = 0.2(155) = 31 \text{ lb}$$

Shear Stress

$$\pi_{\text{avg}} = \frac{\sqrt{2}}{2} \frac{(R_{z_1} + R_{z_2})}{h\ell} = \frac{\sqrt{2}}{2} \frac{62}{(0.25)(7.62)}$$

$$\pi_{\text{avg}} = \underline{23} \text{ lb/in.}^2 \text{ (Weld)}$$

$$\pi_{\text{avg}} = \frac{(R_{z_1} + R_{z_2})}{b\ell} = \frac{62}{0.38(7.62)}$$

$$\pi_{\text{avg}} = \underline{21} \text{ lb/in.}^2 \text{ (Bracket)}$$

Normal Stress

$$\sigma = \frac{\sqrt{2}}{2} \frac{R_{x_1} + R_{x_2}}{h\ell} \pm \frac{R_{z_1} + R_{z_2}}{h\ell(b+h)} \sqrt{2L^2 + \frac{(b+h)^2}{2}}$$

$$\sigma = \frac{\sqrt{2}}{2} \frac{310}{0.25(7.62)} \pm \frac{61}{0.25(7.62)(0.38 + 0.25)} \times \sqrt{2(4.20)^2 + \frac{(0.38 + 0.25)^2}{2}}$$

$$= 115 \pm 302 = 445 \text{ lb/in.}^2, \underline{-187} \text{ lb/in.}^2 \text{ (Weld)}$$

$$\sigma = \frac{R_{x_1} + R_{x_2}}{bl} \pm \frac{(L - h)(R_{z_1} - R_{z_2})c}{I}$$

$$c = 0.19 \text{ in.} \quad I = 0.0348 \text{ in.}^4$$

$$\sigma = \frac{310}{0.38(7.62)} \pm \frac{(4.20 - 0.25)(62)(0.19)}{0.0348} = 110 \pm 1340$$

$$\sigma = 1450 \text{ lb/in.}^2, \quad \underline{-1230} \text{ lb/in.}^2 \text{ (Bracket)}$$

#### A.2.4.3 Combined Stresses During CS Injection

##### Shear Stress

$$\tau_{\text{Avg}} = 238 - 23 = \underline{215} \text{ lb/in.}^2 \text{ (Weld)}$$

$$\tau_{\text{Avg}} = 222 - 21 = \underline{201} \text{ lb/in.}^2 \text{ (Bracket)}$$

##### Normal Stress

$$\sigma = 2420 - 187 = \underline{2233} \text{ lb/in.}^2 \text{ (Weld)}$$

$$\sigma = 10,260 - 1230 = \underline{9030} \text{ lb/in.}^2 \text{ (Bracket)}$$

#### A.3 REFERENCES

GE Drawing 731E779, "Core Spray Sparger."

GE Drawing 761E506, "Core Spray Sparger."

Roark, R. J., "Formulas for Stress and Strain," McGraw Hill, Fourth Edition, 1965.

Hopkins, R. B., "Design Analysis of Shafts and Beams," McGraw Hill.

"Machine Design Handbook," The Industrial Press, 16th Edition, 1959.

Blevins, R. D., "Flow-Induced Vibration," Van Nostrand Reinhold Co., 1977.

Shields, C. M., Wade, G. E., "Core Spray Distribution No. 17, 251 Standard Plant," NEDE-13006-4, December 1, 1970.

APPENDIX B  
SPARGER TEMPERATURE CALCULATIONS

B.1 SPARGER TEMPERATURE

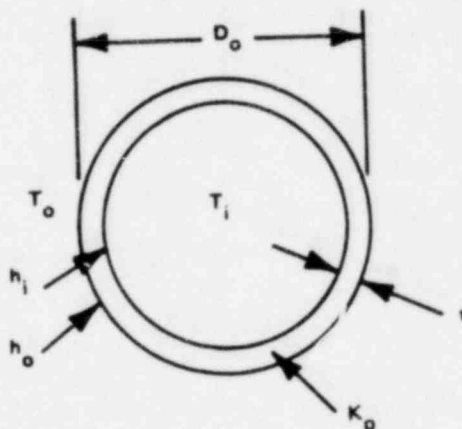
Heat transfer coefficients for inadvertent spray injection are from pages B-3 and B-4.

$$h_i = 5037 \text{ Btu/hr} - \text{ft}^2 - ^\circ\text{F}$$

$$h_o = 365 \text{ Btu/hr} - \text{ft}^2 - ^\circ\text{F}$$

$$K = 10 \text{ Btu/hr} - \text{ft} - ^\circ\text{F}$$

(304 sst @ 200°F)



$$D_o = 4.5 \text{ in.} \quad t = 0.237 \text{ in.} \quad D_i = 4.026 \text{ in.}$$

$$T_i = \text{water in sparger} = 80^\circ\text{F}$$

$$T_o = \text{water outside} = 550^\circ\text{F}$$

$$A_i = \pi \left( \frac{4.026}{12} \right)^2 \cdot 1 = 1.054 \text{ ft}^2 \text{ (1 ft long section)}$$

$$A_o = \pi \left( \frac{4.5}{12} \right)^2 \cdot 1 = 1.178 \text{ ft}^2 \text{ (1 ft long section)}$$

$$A_p = \pi \left( \frac{4.026 + 4.5}{2(12)} \right)^2 \cdot 1 = 1.116 \text{ ft}^2 \text{ (1 ft long section)}$$

The thermal resistance, R, is:

$$\frac{1}{R} = \frac{1}{\frac{1}{A_i h_i} + \frac{1}{A_o h_o} + \frac{t}{A_p K}}$$

$$Q = \frac{T_o - T_i}{\frac{1}{A_i h_i} + \frac{1}{A_o h_o} + \frac{t}{A_p K}}$$

$$\Delta T_{\text{film outside}} = Q \frac{1}{A_o h_o} = \frac{\frac{1}{A_o h_o} (T_o - T_i)}{\frac{1}{A_i h_i} + \frac{1}{A_o h_o} + \frac{1}{A_p K}}$$

$$\Delta T_{\text{film inside}} = \frac{\frac{1}{A_i h_i} (T_o - T_i)}{\frac{1}{A_i h_i} + \frac{1}{A_o h_o} + \frac{t}{A_p K}}$$

$$x = \frac{1}{A_i h_i} + \frac{1}{A_o h_o} + \frac{t}{A_p K}$$

$$x = \frac{1}{1.054 (5037)} + \frac{1}{1.178 (365)} + \frac{0.237/12}{1.116 (10)}$$

$$x = 0.000188 + 0.002326 + 0.001770 = 0.004284$$

$$\Delta T_{\text{film outside}} = \frac{0.002326 (550 - 80)}{0.004284} = 255^\circ\text{F}$$

$$\text{Outside metal temperature} = 550 - 255 = \underline{295^\circ\text{F}}$$

$$\Delta T_{\text{film inside}} = \frac{0.000188 (550 - 80)}{0.004284} = 21^\circ$$

$$\text{Inside metal temperature} = 80 + 21 = \underline{101^\circ\text{F}}$$

$$\text{Average sparger (pipe) temperature} = \frac{285 + 101}{2} = \underline{\underline{198^\circ\text{F}}}$$

$$\Delta T_{\text{Bracket to pipe}} = 550 - 198 = \underline{\underline{352^\circ\text{F}}}$$

In practice, the core spray pumping system cannot inject into the reactor until the pressure reaches 300 psia, where  $T_{\text{sat}} = 417^\circ\text{F}$ . In this case, the  $\Delta T_{\text{Bracket to Pipe}}$  is less than  $337^\circ\text{F}$  ( $417 - 80$ )\*. Thus, the above calculation bounds the inadvertent injection case. It also bounds the case of core spray operation during LOCA for the same reason.

## B.2 CONSERVATISMS

1. Bounding for reason described above.
2. Assumes steady-state conditions ( $Q_o = Q_p = Q_i$ ).
3. Neglects heat conduction from pipe.
4. Assumes runout flow.

## B.3 REFERENCES

1. Kreith, "Principles of Heat Transfer", International, 1969.
2. Welty, et.al., "Fundamentals of Momentum, Heat and Mass Transfer", John Wiley, 1969.

## B.4 HEAT TRANSFER COEFFICIENTS

### B.4.1 Inside Sparger Arm (Near T-Box on Long Side)

Assume average film temperature =  $90^\circ\text{F}$

$$D_o = 4.026/12 \text{ ft} \quad A_{\text{flow}} = \frac{\pi}{4} \left( \frac{4.026}{12} \right)^2 = 0.0884 \text{ ft}^2$$

$$\rho = 62.1 \text{ lb/ft}^3 @ 90^\circ\text{F}$$

---

\* $\Delta T_{\text{film inside}}$  and  $\Delta T_{\text{pipe}}$  are ignored.

$$v = 0.833 (10^{-5}) \text{ ft}^2/\text{sec}$$

$$W_{\text{Total}} = 7980 \text{ gpm} = 1102 \text{ lb/sec}$$

$$W_{\text{Arm}} = 1102 \left( \frac{97.5}{360} \right) = 298.5 \text{ lb/sec}$$

$$V = \frac{W}{A\rho} = \frac{298.5}{0.0884 (62.1)} = 54.4 \text{ ft/sec}$$

$$N_{\mu} = 0.023 R_e^{0.8} P_r^{1/3}$$

$$R_e = \frac{DV}{\mu}$$

$$R_e = \frac{4.026}{12} \left( \frac{54.4}{0.833 (10^{-5})} \right) = 2.19 \times 10^6$$

$$P_r = 5.20 @ 90^\circ\text{F}$$

$$N_{\mu} = 0.023 \left( 2.19 \times 10^6 \right)^{0.8} (5.20)^{1/3} = 4,707$$

$$\frac{hD}{K} = N_{\mu} \quad D = \frac{4.020}{12} \text{ ft}$$

$$K = 0.359 \text{ Btu/hr} - \text{ft} - ^\circ\text{F} @ 90^\circ\text{F}$$

$$h_1 = \frac{4,707 (0.359)}{4,026/12} = \underline{5037} \text{ Btu/hr} - \text{ft}^2 - ^\circ\text{F}$$

#### B.4.2 Outside of Sparger Arm

1. Assume average water velocity is  $\sqrt{2}$  ft/sec.
2. Assume average film temperature =  $420^\circ\text{F}$ .
3. Assume that heat transfer is like a cylinder in cross flow.

$$v = 0.169 \times 10^{-5} \text{ ft}^2/\text{sec} @ 420^\circ\text{F}$$

$$K = 0.375 \text{ Btu/ft} \cdot \text{hr} \cdot ^\circ\text{F}$$

$$P_r = 0.932$$

$$\frac{h_c D_o}{K} = \left[ 0.35 + 0.56 (R_e)^{0.5} \right] P_r^{0.31}$$

$$D_o = \frac{4.5}{12} \text{ ft}$$

$$R_e = \frac{2(4.5)}{12 (0.169 \times 10^{-5})} = 4.438 \times 10^5$$

$$h_o = \frac{0.375}{4.5/12} \left[ 0.35 + 0.56 \left( 4.438 \times 10^5 \right)^{0.5} \right] 0.932^{0.31}$$

$$h_o = \underline{365} \text{ Btu/hr} \cdot \text{ft}^2 \cdot ^\circ\text{F}$$

### B.5 PUMP HEAD/RUNOUT

$$\text{Shutoff Head} = 300 \text{ psia } (Q = 0)$$

$$Q_{\text{Rated}} = 6250 \text{ gpm @ } 125 \text{ psia}$$

$$P = P_{\text{SH}} - C Q^2$$

where  $P_{\text{SH}}$  = shutoff head

$$125 = 300 - C (6250)^2$$

$$C = \frac{300 - 125}{6250^2} = 4.48 (10^{-6}) \text{ psi/gpm}^2$$

@ P = 14.7 psia (Runout)

$$Q_{\text{Runout}} = \sqrt{\frac{P_{\text{SH}} - P}{C}} = \sqrt{\frac{300 - 14.7}{4.48(10^{-6})}} = 7980 \text{ gpm} \approx 8000 \text{ gpm}$$

$$W_{\text{Runout}} = \frac{7980 (62)}{60 (7.48)} = 1102 \text{ lb/sec}$$

APPENDIX C  
FLOW VELOCITY CALCULATIONS

This appendix describes the calculations for the flow velocities supporting statements in Section 3.4.2.1 of the text.

## C.1 FLOW VELOCITY IN BYPASS REGION

## Assumptions:

1. The plant is operating at rated power (3293 MWt) and flow  $102.5 \times 10^6$  lb/hr.
2. The flow in the bypass regions is homogeneous.
3. The bypass flow fraction is 12% ( $12.3 \times 10^6$  lb/hr).
4. The water in the bypass regions is saturated.
5. There is no down flow in the bypass region. This assumption is discussed later.

There are two parallel flow paths in the bypass region--one is between the fuel channels, and the other is between the core shroud and the outermost fuel assemblies. The flow areas for these paths are shown schematically in Figure C-1. The simple analysis that follows will give an estimate of the relative flow velocity in the neighborhood of the spray sparger.

Path 1 is between the core shroud and the outermost fuel channels. The flow area along path 1 changes from  $A_1$ , between the bottom and top of the active fuel, to  $A_5$  at the top guide to  $A_6$  immediately above the top guide:

$$A_1 = 5261 \text{ in.}^2, A_5 = 3720 \text{ in.}^2, A_6 = 9144 \text{ in.}^2$$

Path 2 is between the fuel channels. The flow area along path 2 changes from  $A_2$  to  $A_3$  at the top guide to  $A_4$  above the fuel channels:

$$A_2 = 3918 \text{ in.}^2, A_3 = 2028 \text{ in.}^2, A_4 = 27504 \text{ in.}^2$$

From the geometry and the flow areas,  $K$  for path 1 is approximately 0.3 and  $K$  for path 2 is approximately 1.0:

$$(K_1 W_1^2) / A_5^2 = K_2 W_2^2 / A_3^2$$

$$\frac{(0.3) W_1^2}{3720} = \frac{(1.0) W_2^2}{2028}$$

$$W_1 = 2.5 W_2$$

$$0.40 W_1 = W_2$$

$$1.40 W_1 = 12.3 \times 10^6$$

$$W_1 = 8.8 \times 10^6 \text{ lb/hr}$$

The velocity in the bypass region between the core spray sparger and the fuel assemblies is then:

$$v = W_1 / \rho A_5 = 8.8 \times 10^6 / [3600 \times 45.8 \times (3720/144)] = 2.1 \text{ ft/sec}$$

The fluid in this region is primarily saturated liquid.

The fluid velocity in the periphery of the core bypass region was conservatively estimated at 2.1 ft/sec. In actuality, there probably is downflow in this region. The total pressure drop across the top guide is predominantly due to the elevation head. In some portions near the top of the core bypass region, boiling may occur, reducing the elevation pressure drop. Because

there are no heat sources in the non-fueled peripheral regions of the core bypass, boiling would not be expected in the vicinity of the shroud. Thus, some downflow or crossflow in the peripheral regions toward the central region would be anticipated to balance the density differences.

### C.2 FLOW VELOCITY AT TOP SURFACE OF CORE PLATE

$$V = (W_{\text{Total Bypass}}) / \rho A$$

$$\text{Since } W_{\text{Total Bypass}} = 12.3 \times 10^6 \text{ lb/hr}$$

$$A = \pi/4 (D^2 - Nd)^2$$

$$D = \text{inside diameter of shroud} = 204 \text{ in.}$$

$$N = \text{number of control rod guide tubes} = 185$$

$$d = \text{outside diameter of control rod guide tube} = 10.875 \text{ in.}$$

$$\rho = \text{density} = 45.8 \text{ lb/ft}^3$$

Then

$$V = (12.3 \times 10^6) / (3600 \times 45.8 \times \pi (204^2 - 185(10.875)^2) / (4 \times 144))$$

$$V = 0.69 \text{ ft/sec}$$

### C.3 FLOW VELOCITY AT THE TOP OF THE FUEL ASSEMBLY HANDLES

$$W_{\text{Total}} = 102.5 \times 10^6 - 12.3 \times 10^6 = 90.2 \times 10^6 \text{ lb/hr}$$

$$A = na$$

$$n = \text{number of fuel assemblies} = 764$$

$$a = \text{area associated with each fuel assembly} = (6)^2 = 36 \text{ in.}^2$$

The equivalent single phase velocity is:

$$V = (W_{\text{Total}}) / \rho A$$

Then

$$V = (90.2 \times 10^6) / (3600 \times 45.8 (764 \times 36/144)) = 2.86 \text{ ft/sec}$$

At this location, the fluid is a mixture of steam and water. Therefore, to calculate the lifting force due to the mixture, a two-phase friction multiplier must be used:

$$\phi^2 m = 1 + x (\rho_f / \rho_g - 1)$$

$$x = \text{quality} = \frac{\text{mass flow rate of steam}}{\text{total mass flow rate}}$$

$$= (13.4 \times 10^6) / (102.5 \times 10^6) = 0.131$$

$$\rho_f = 45.8 \text{ lb/ft}^3$$

$$\rho_g = 2.35 \text{ lb/ft}^3$$

$$\phi^2 = 1 + 0.131(45.8/2.35 - 1) = 3.42$$

The lifting force on a section of core spray pipe per unit length is:

$$F = C_D A \rho_f \phi^2 V^2 / (2g)$$

where

$$C_D = \text{drag coefficient} = 1.2$$

$$A = \text{area} = (4.5 \text{ in.} \times 1(\text{ft}/\text{ft}))/12 (\text{in.}/\text{ft}) = 0.375 \text{ ft}^2/\text{ft}$$

Then:

$$F = 1.2 \times 0.375 \times 45.8 \times 3.42 \times (2.86)^2 / (2 \times 32.2) = 9.0 \text{ lb}/\text{ft}$$

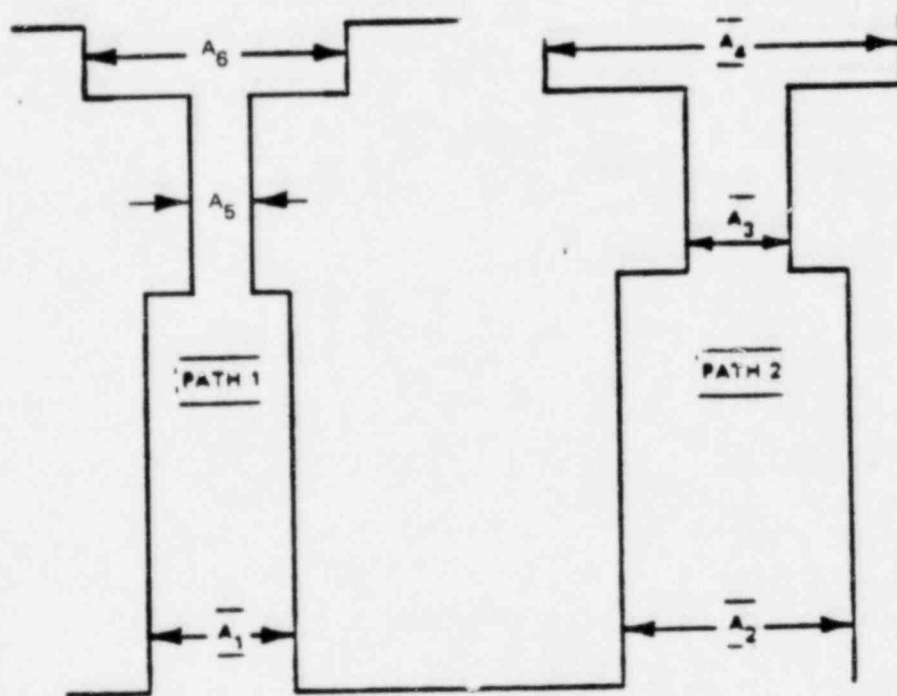


Figure C-1. Flow Paths